Supplemental Appendix

The Dawn of Civilization
Metal Trade and the Rise of Hierarchy

Matthias Flückiger, Mario Larch, Markus Ludwig, and Luigi Pascali

Contents

A Data **1**

A.1 Data sources and variable construction . . . 1

A.1.1 The Urban Revolution . . . 1

A.1.2 Bilateral trade flows . . . 6

A.1.3 Cropland and productive land . . . 7

A.1.4 Metal mines and deposits . . . 8

A.1.5 Additional data . . . 8

A.2 Tables raw data . . . 14

A.3 Figures raw data . . . 17

B Bronze Age transit regions **27**

B.1 Measures of centrality . . . 27

B.1.1 Metal transit indices . . . 27

B.1.2 Other measures of centrality and proximity . . . 28

B.2 Maps centrality measures . . . 30

C Descriptive analysis **32**

C.1 Summary statistics . . . 32

C.2 Metal transit trade and cities . . . 33

D Additional analysis and robustness checks **34**

D.1 Additional analysis and robustness checks urban settlements . . . 34

D.1.1 Point estimates control variables . . . 35

D.1.2 Reduced-form estimates . . . 38

D.1.3 The transition from arsenic bronze to tin bronze . . . 39

D.1.4 Endogeneity of relative transport costs . . . 41

D.1.5 Exploiting Data on Megasites . . . 43

D.1.6 Digging deeper into the metal transit index measure . . . 48

D.1.7 Land productivity and agriculture . . . 51

D.1.8 Heterogeneities . . . 53

D.1.9 Standard error clustering . . . 55

D.1.10 Other robustness checks . . . 57

D.2 Additional analysis and robustness checks archaeological sites . . . 64

D.2.1 Reduced-form estimates . . . 64

D.2.2 Endogeneity of relative transport costs . . . 68

D.2.3 Standard error clustering . . . 68

D.2.4 Other robustness checks . . . 71

D.3 Additional analysis and robustness checks China . . . 75

D.3.1 Reduced-form estimates . . . 75
D.3.2 Other robustness checks . . . 77
D.4 Metal-unrelated trade . . . 79
D.4.1 Generic natural transit trade potential . . . 79
D.4.2 Natural obsidian transit trade potential . . . 82
D.5 Warfare . . . 86
D.6 Europe . . . 93
D.7 Shapley decomposition . . . 102
D.8 Appropriability mechanism . . . 105
D.8.1 Theoretical Model . . . 105
D.8.2 Blockage cost . . . 112
D.8.3 Metal transit trade and blockage cost . . . 113

E Additional case studies **116**
E.1 The Harappan civilization in the Indus Valley (2600-1900 BC) . . . 116
E.2 The city of Mari (2600-1760 BC) . . . 117
E.3 The Bronze Age Aegean . . . 118
E.4 The Bronze Age in China and the Erlitou period (1900-1500 BC) . . . 120

List of Tables

A.1 References for database of copper mine locations . . . 14
A.2 References for database of tin mine locations . . . 15
A.3 References for database of Bronze Age metals exchange (provided by Flückiger et al. (2022)) . . . 16
C.1 Summary statistics of key variables . . . 32
D.1 Metal transit trade and Bronze Age cities. Regressions of Table 1, Panel A, with coefficients of controls reported. . . . 36
D.2 Metal transit trade and Bronze Age cities. Regressions of Table 1, Panel B, with coefficients of controls reported. . . . 37
D.3 Reduced-form estimates corresponding to Table 1 . . . 38
D.4 Robustness endogeneity α_{BA}: Metal transit trade and Bronze Age cities . . . 42
D.5 Neolithic: Transit trade, cities and citadels (Green et al., 2024) . . . 43
D.6 Difference-in-differences: Transit trade, cities and citadels (Green et al., 2024) . . . 44
D.7 Neolithic: Urban areas and metal transit trade (Lawrence, Hinojosa-Balino and Chelazzi, 2025) . . . 46
D.8 Difference-in-differences: Urban areas and metal transit trade (Lawrence, Hinojosa-Balino and Chelazzi, 2025) . . . 47
D.9 Metal transit trade and Bronze Age cities (Green et al., 2024). Disentangling the transit index. . . . 49
D.10 Metal transit trade and Bronze Age cities (Reba, Reitsma and Seto, 2016). Disentangling the transit index. . . . 50
D.11 Robustness check controlling for differences in land fertility: Metal transit trade and Bronze Age cities. . . . 52
D.12 Heterogeneities: Metal transit trade, proximity to croplands, and proximity to mines. 54
D.13 Robustness geographical extent and controls: Metal transit trade and Bronze Age cities . . . 58
D.14 Robustness 0.5×0.5 degree grid cells: Metal transit trade and Bronze Age cities . . . 60
D.15 Robustness IV probit: Metal transit trade and Bronze Age cities . . . 61
D.16 Robustness using HYDE 3.1 data on urban population: Metal transit trade and Bronze Age cities. . . . 63
D.17 Reduced-form estimates corresponding to Table 2 . . . 65
D.18 Robustness endogeneity α_{BA}: Metal transit trade and archaeological sites . . . 69
D.19 Robustness 0.5×0.5 degree grid cells: Metal transit trade and archaeological sites. Difference-in-differences (Stone Age vs Bronze Age) . . . 72
D.20 Robustness 0.5×0.5 degree grid cells: Horse race: Metal transit index vs blockage cost 74
D.21 Reduced-form estimates corresponding to Table 3: Natural metal transit index and archaeological sites in China. Difference-in-differences (Stone Age vs Bronze Age) . . . 75
D.22 Robustness 0.5×0.5 degree grid cells: Metal transit trade and archaeological sites in China. Difference-in-differences (Stone Age vs Bronze Age) . . . 77

D.23 Robustness generic transit trade potential: Metal transit trade and Bronze Age cities 80
D.24 Robustness generic transit trade potential: Metal transit trade and archaeological sites. Difference-in-differences (Stone Age vs Bronze Age) 81
D.25 Robustness obsidian transit trade potential: Metal transit trade and Bronze Age cities 84
D.26 Robustness obsidian transit trade potential: Metal transit trade and archaeological sites. Difference-in-differences (Stone Age vs Bronze Age) 85
D.27 Weapons by museum and period 88
D.28 Museum collection search approach: Stone Age 89
D.29 Museum collection search approach: Bronze Age 90
D.30 Metal transit trade and warfare 92
D.31 Summary statistics of key variables (Europe) 95
D.32 Metal transit trade and elite burials in Europe 96
D.33 Cross-sectional analysis: Metal transit trade and elite burials in Europe 97
D.34 References and number of artifacts per book (Europe) 100
D.35 R-squared and Shapley values 103

List of Figures

A.1 Units of observation . . . 17
A.2 Sites Green et al. (2024) . . . 18
A.3 Cities Reba, Reitsma and Seto (2016) . . . 19
A.4 Sites Bahn (2000) . . . 20
A.5 Sites Pleiades Gazetteer . . . 21
A.6 Correspondence plot Atlas of Chinese Cultural Relics . . . 22
A.7 Sites Atlas of Chinese Cultural Relics . . . 23
A.8 Origins and destinations of artifacts . . . 24
A.9 Mines and croplands . . . 25
A.10 Deposits and NPP . . . 26
B.1 Least-cost paths to mines . . . 30
B.2 Natural metal transit index . . . 31
C.1 Scatterplots of metal transit trade versus city occurrence . . . 33
D.1 Cities and metal transit index over time . . . 39
D.2 Cities and copper transit index over time . . . 40
D.3 Cities and tin transit index over time . . . 40
D.4 Urban areas Lawrence, Hinojosa-Balino and Chelazzi (2025) . . . 45
D.5 Alternative standard error clustering approaches cross-sectional data . . . 56
D.6 Estimated impact of the natural transit index across different types of archaeological finds . . . 66
D.7 Estimated impact of the natural transit index on the spatial location of archaeological sites over time . . . 67
D.8 Alternative standard error clustering approaches panel data . . . 70
D.9 Robustness 0.5×0.5 degree grid cells: Estimated impact of the metal transit index across different types of archaeological finds . . . 71
D.10 Robustness 0.5×0.5 degree grid cells: Estimated impact of the metal transit index on the spatial location of archaeological sites over time . . . 73
D.11 Estimated impact of the natural transit index on the rise of the Urban Revolution in China . . . 76
D.12 Robustness 0.5×0.5 degree grid cells: Estimated impact of the metal transit index on the rise of the Urban Revolution in China . . . 78
D.13 Generic natural transit trade potential . . . 82
D.14 Distribution of volcanoes . . . 83
D.15 Weapon finds . . . 87
D.16 Bronze weapons finds (Europe) . . . 94
D.17 Example entry Prähistorische Bronzefunde . . . 99
D.18 Illustration metal transit index versus blockage cost . . . 114
D.19 Metal transit index versus blockage cost by continent . . . 115

Appendix A: Data

This appendix describes our raw data sources. It also includes maps illustrating the spatial distribution of selected data.

A.1 Data sources and variable construction

This section describes our raw data sources and the construction of the variables used in our analysis. We first present the data and variables discussed in the main body of the paper, and then describe additional materials used in the supplementary analyses. Data are presented in the same order as their discussion in the paper.

The geographical scope of our analysis is the Old World. Our primary unit of analysis is the 1×1 degree grid cell (approximately 110×110 kilometers at the equator), yielding 10,970 individual grid cells. Figure A.1 shows the geographical scope of our analysis along with these grid cells.

A.1.1 The Urban Revolution

Cities and Citadels Data on cities and citadels are sourced from Green et al. (2024) [W1]. Their dataset provides information on the locations of settlements, along with dates indicating the range of their existence and associated cultural affiliations. Settlements are classified into two groups: cities and citadels. A city is defined as a settlement that is markedly larger than contemporaneous villages and typically has a population on the order of tens of thousands. Citadels, by contrast, are defined as "fortified palaces without a substantial surrounding urban settlement", and their populations rarely exceed 10,000. Based on the information on dates and cultural context, we identify the period(s) into which each settlement falls: Neolithic and Bronze Age.[34] For our empirical analysis, we construct a dummy variable indicating whether at least one city or citadel is present in a given 1×1-degree grid cell and period.

Figure A.2 visualizes the spatial distribution of cities and citadels, separately for the Neolithic and the Bronze Age. There are 18 grid cells in the Neolithic period with at least one city or citadel, amounting to 0.16 percent of the observations. In the Bronze Age, this number increases to 53, representing 0.48 percent of the observations. Table C.1 provides more detailed summary statistics for this outcome variable.

Online sources

W1 https://gitlab.com/tcwilkinson/citiesandcitadels-figs/-/raw/master/data/city_citadel_db.csv?ref_type=heads&inline=false, downloaded 11 February 2025.

Cities Data on cities are sourced from Reba, Reitsma and Seto (2016) [W2]. The dataset provides geocoded information on the location and (estimated) size of cities—defined as settlements with more than 10,000 inhabitants—from 3700 BC to 2000 AD. For our empirical analysis, we identify 1×1 degree grid cells for which there is evidence of at least one city prior to 1300 BC and create an indicator variable to capture this. There is evidence of ancient cities in only 0.42 percent of the grid cells. Figure A.3 shows the location of these cities while Table C.1 provides further information on summary statistics.

[34] We assign settlements falling into the Chalcolithic (Copper Age) to the Bronze Age.

Online sources

W2 https://figshare.com/authors/Meredith_Reba/746877, downloaded 22 January 2024

Urban population Information on urban population is sourced from the HYDE 3.1 database (Klein Goldewijk et al., 2011). The raster data are provided at a 5×5 minute resolution and represent the estimated number of urban inhabitants in 2000 BC [W3]. Klein Goldewijk et al. (2011) draw on historical population and urbanization rate estimates from a variety of sources.[35] To allocate population to grid cells, they use combined weighting maps based on various proxies such as soil suitability, slope, distance to water, and case studies from several disciplines (e.g. history, archaeology). For our empirical analysis, we aggregate the data to the 1×1 degree grid cell level and create an indicator variable capturing whether a cell contains any urban population or not.

Online sources

W3 https://geo.public.data.uu.nl/vault-hyde/HYDE%203.1%5B1701183246%5D/original/, downloaded 18 December 2019.

Urban areas Southwest Asia and Egypt We source data on the extent of urban areas in Southwest Asia and Egypt from Lawrence, Hinojosa-Balino and Chelazzi (2025) [W4]. The database contains information on settlement sizes for all settlements that exceeded 10 hectares between 10,000 BP and 1,000 BP—the threshold used in this study to define an urban area.[36] For each 1×1 degree grid cell, we compute the total urban area separately for the Neolithic and the Bronze Age.[37]

Online sources

W4 https://www.brepols.net/products/IS-9782503615639-1, last downloaded 11 December 2025. Data were originally kindly made available to us by Dan Lawrence on 28 January 2025 prior to their publication.

Archaeological sites with global coverage We draw on two data sources to map the global spatial distribution of archaeological sites.

The first source is Bahn (2000)'s Atlas of World Archaeology, a collection of detailed maps and descriptions of the world's most significant archaeological sites. The atlas covers 7,708 sites spanning from the Paleolithic to Classical antiquity. We use the geocoded version of the atlas provided by Schönholzer and François (2023) and extract the sites that fall into the Paleolithic/Mesolithic, Neolithic, and Bronze Age periods [W5]. We identify the ages based on the titles of the maps, descriptions of the individual sites, and the geographical information conveyed by the maps.[38] Sites falling into the Chalcolithic period are assigned to the Bronze Age. This yields a total of 559 sites from the Paleolithic/Mesolithic, 585 from the Neolithic, and 1,512 from the Bronze Age. Figure A.4 depicts the location of these sites, shown separately for the Stone Age (i.e., Paleolithic and Neolithic combined) and the Bronze Age.

Among all the sites, we identify and differentiate the following types: settlements, major settle-

[35] The sources providing population estimates before 1000 BC are: Clark (1977); Grigg (1987); Kremer (1993); Livi-Bacci (2007); McEvedy and Jones (1978); Renfrew and Bahn (1996); Thomlinson (1975)

[36] More details are provided in Appendix D.1.5.

[37] We define the Bronze Age to start in 3300 BC and end in 1300 BC.

[38] For example, some maps differentiate between cultures (or periods) by shading the areas of the cultures (periods) in different colors or assigning sites different symbols.

ments, elite burials, and any burials.[39] For our empirical analysis, we create a dummy variable that captures whether a site of a given type is present in a given 1×1 degree grid cell. Only 4.9 percent of grid cells contain at least one site. Stratified by type, this share is 0.7 percent for settlements, 0.3 percent for major settlements, 0.4 percent for elite burials, and 1.8 percent for any burial.

The second source is the Pleiades Project, an open-source gazetteer of ancient sites (Bagnall, 2022) [w6]. We limit our analysis to sites characterized by the presence of man-made structures and for which the location is precisely known.[40] More specifically, we focus on sites identifiable as settlements, elite burials, or any burials.[41] To assign these sites to a time period, we use two alternative approaches. First, we use the textual descriptions in the Pleiades database to identify pre-Bronze and Bronze Age sites. This yields a total of 866 sites, 213 of which predate the invention of bronze (see Figure A.5 for their geographical location). Alternatively, we use the numeric estimates of the start and end dates for each site, which are also reported in the Pleiades database. Based on these dates, we construct a panel dataset covering the years 7000–1300BC in 1,000-year intervals. [42] For our empirical analysis, we create a dummy variable that indicates whether a site of a given type is present in a 1×1 degree grid cell during a specific time period. Overall, 1.8 percent of grid cell–period observations contain one or more sites. A more detailed summary of the Bahn (2000) and Pleiades data is provided in Table C.1.

`Online sources`

w5 `https://www.davidschonholzer.com/`, downloaded 27 July 2023.

w6 `https://pleiades.stoa.org/downloads`, downloaded 6 April 2022.

Archaeological sites China Our archaeological site data for China are drawn from the Atlas of Chinese Cultural Relics (Zhongguo Wenwu Ditu Ji), an official multi-volume series published under the authority of the State Administration of Cultural Heritage (SACH) of the People's Republic of China. The Atlas represents the most comprehensive official nationwide compilation of known archaeological sites in China and is widely used as a primary source for mapping and digitizing archaeological site locations (e.g., Wagner et al. (2013) and Hosner et al. (2016)). Data quality is ensured by the fact that the underlying archaeological information was systematically compiled and evaluated prior to publication by the archaeological research institutes of the respective provinces or autonomous regions, following national standards set by SACH.

The Atlas is divided into 40 volumes covering 28 Chinese provinces. Each volume provides cartographic maps of site locations together with an indexed catalog of the mapped sites and short textual descriptions. In the atlas, each site is assigned a geographic location, dated, and described in detail. For our analysis, we OCR 31 volumes of the Atlas, corresponding to all volumes that include sites predating the Han dynasty (206 BCE). This yields a dataset of 86,187 geocoded archaeological sites with textual descriptions averaging 58 words in length. For approximately one-tenth of the sample (7,342 sites), we manually coded whether the description references any of the following features: 1) urban settlements, 2) a ruling class exempt from manual labor, 3) monumental buildings, 4) a standardized system of measures and records used in exchange and production, 5) writing, and 6)

[39] Settlements are sites clearly labeled as such; major settlements are sites described as cities, major settlements, or administrative centers; elite burials are burial sites indicative of social stratification; any burials include burial sites of any type.

[40] See Bakker et al. (2021, p. 658) for more details.

[41] Settlements are places labeled as 'settlement' or 'urban' in the database; elite burials are burial sites labeled as 'pyramid' or 'tumulus'; any burials are burial sites of any type.

[42] The time intervals are: [7000, 6000), [6000, 5000), [5000, 4000), [4000, 3000), [3000, 2000), and [2000, 1300].

highly developed art forms. After developing this training sample, we use a naïve Bayesian classifier to categorize all sites in the Atlas according to these six criteria.

Figure A.6 presents a correspondence plot highlighting the words most frequently associated with each classification criterion. For instance, in the top right, we see that words such as "city", "township", "wall", and "village" are disproportionately associated with the criterion "Urban Settlements", while terms like "Han", "dynasty", and "state" are linked to the criterion "Ruling Class". Once each site is classified, we count the number of sites associated with criteria indicative of the Urban Revolution within each 1×1 grid cell during the Paleolithic, Neolithic, and Bronze Age periods. Figure A.7 displays the spatial distribution of these sites, while Table C.1 (Panel C) reports summary statistics for the final dataset.

This is the list of volumes of the Atlas of Chinese Cultural Relics used in the empirical analysis.

1. State Administration of Cultural Heritage. 1989. Zhongguo Wenwu Ditu Ji: Guangdong Sheng [Atlas of Chinese Cultural Relics: Guangdong Province]. Guangzhou: Guangdong Cartographic Publishing House.

2. State Administration of Cultural Heritage. 1991. Zhongguo Wenwu Ditu Ji: Henan Sheng [Atlas of Chinese Cultural Relics: Henan Province]. Beijing: SinoMaps Press.

3. State Administration of Cultural Heritage. 1993. Zhongguo Wenwu Ditu Ji: Jilin Sheng [Atlas of Chinese Cultural Relics: Jilin Province]. Beijing: Cultural Relics Publishing House.

4. State Administration of Cultural Heritage. 1996. Zhongguo Wenwu Ditu Ji: Qinghai Sheng [Atlas of Chinese Cultural Relics: Qinghai Province]. Beijing: SinoMaps Press.

5. State Administration of Cultural Heritage. 1997. Zhongguo Wenwu Ditu Ji: Hunan Sheng [Atlas of Chinese Cultural Relics: Hunan Province]. Changsha: Hunan Cartography Publishing House.

6. State Administration of Cultural Heritage. 1998. Zhongguo Wenwu Ditu Ji: Shaanxi Sheng (Vol. 2). [Atlas of Chinese Cultural Relics: Shaanxi Province]. Xi'an: Xi'an Map Publishing House.

7. State Administration of Cultural Heritage. 2001. Zhongguo Wenwu Ditu Ji: Yunnan Sheng [Atlas of Chinese Cultural Relics: Yunnan Province]. Beijing: Cultural Relics Publishing House.

8. State Administration of Cultural Heritage. 2002. Zhongguo Wenwu Ditu Ji: Hubei Sheng (Vol. 2). [Atlas of Chinese Cultural Relics: Hubei Province]. Xi'an: Xi'an Map Publishing House.

9. State Administration of Cultural Heritage. 2002. Zhongguo Wenwu Ditu Ji: Tianjin Shi [Atlas of Chinese Cultural Relics: Tianjin Municipality]. Beijing: Encyclopedia of China Publishing House.

10. State Administration of Cultural Heritage. 2003. Zhongguo Wenwu Ditu Ji: Nei Mongol Zizhiqu (Vol. 2). [Atlas of Chinese Cultural Relics: Inner Mongolia Autonomous Region]. Beijing: Cultural Relics Publishing House.

11. State Administration of Cultural Heritage. 2006. Zhongguo Wenwu Ditu Ji: Shanxi Sheng (Vol. 2). [Atlas of Chinese Cultural Relics: Shanxi Province]. Beijing: SinoMaps Press.

12. State Administration of Cultural Heritage. 2006. Zhongguo Wenwu Ditu Ji: Shanxi Sheng (Vol. 3). [Atlas of Chinese Cultural Relics: Shanxi Province]. Beijing: SinoMaps Press.

13. State Administration of Cultural Heritage. 2007. Zhongguo Wenwu Ditu Ji: Fujian Sheng (Vol. 2). [Atlas of Chinese Cultural Relics: Fujian Province]. Beijing: Cultural Relics Publishing House.

14. State Administration of Cultural Heritage. 2008. Zhongguo Wenwu Ditu Ji: Beijing Shi (Vol. 2). [Atlas of Chinese Cultural Relics: Beijing Municipality]. Beijing: Cultural Relics Publishing House.

15. State Administration of Cultural Heritage. 2008. Zhongguo Wenwu Ditu Ji: Jiangsu Sheng (Vol. 2). [Atlas of Chinese Cultural Relics: Jiangsu Province]. Beijing: SinoMaps Press.

16. State Administration of Cultural Heritage. 2008. Zhongguo Wenwu Ditu Ji: Shandong Sheng (Vol. 2). [Atlas of Chinese Cultural Relics: Shandong Province]. Beijing: Cultural Relics Publishing House.

17. State Administration of Cultural Heritage. 2009. Zhongguo Wenwu Ditu Ji: Sichuan Sheng (Vol. 2). [Atlas of Chinese Cultural Relics: Sichuan Province]. Beijing: Cultural Relics Publishing House.

18. State Administration of Cultural Heritage. 2009. Zhongguo Wenwu Ditu Ji: Sichuan Sheng (Vol. 3). [Atlas of Chinese Cultural Relics: Sichuan Province]. Beijing: Cultural Relics Publishing House.

19. State Administration of Cultural Heritage. 2009. Zhongguo Wenwu Ditu Ji: Zhejiang Sheng (Vol. 2). [Atlas of Chinese Cultural Relics: Zhejiang Province]. Beijing: Cultural Relics Publishing House.

20. State Administration of Cultural Heritage. 2009. Zhongguo Wenwu Ditu Ji: Liaoning Sheng (Vol. 2). [Atlas of Chinese Cultural Relics: Liaoning Province]. Beijing: Cultural Relics Publishing House.

21. State Administration of Cultural Heritage. 2010. Zhongguo Wenwu Ditu Ji: Chongqing Shi (Vol. 2). [Atlas of Chinese Cultural Relics: Chongqing Municipality]. Beijing: Cultural Relics Publishing House.

22. State Administration of Cultural Heritage. 2010. Zhongguo Wenwu Ditu Ji: Ningxia Huizu Zizhiqu [Atlas of Chinese Cultural Relics: Ningxia Hui Autonomous Region]. Beijing: Cultural Relics Publishing House.

23. State Administration of Cultural Heritage. 2010. Zhongguo Wenwu Ditu Ji: Xizang Zizhiqu [Atlas of Chinese Cultural Relics: Tibet Autonomous Region]. Beijing: Cultural Relics Publishing House.

24. State Administration of Cultural Heritage. 2011. Zhongguo Wenwu Ditu Ji: Gansu Sheng (Vol. 2). [Atlas of Chinese Cultural Relics: Gansu Province]. Beijing: Chinese Map Publishing House of Surveying and Mapping Press.

25. Cultural Relics Publishing House. State Administration of Cultural Heritage. 2012. Zhongguo Wenwu Ditu Ji: Xinjiang Weiwuer Zizhiqu (Vol. 2). [Atlas of Chinese Cultural Relics: Xinjiang Uyghur Autonomous Region]. Beijing: Cultural Relics Publishing House.

26. State Administration of Cultural Heritage. 2013. Zhongguo Wenwu Ditu Ji: Hebei Sheng (Vol. 2) [Atlas of Chinese Cultural Relics: Hebei Province]. Beijing: Cultural Relics Publishing House.

27. State Administration of Cultural Heritage. 2013. Zhongguo Wenwu Ditu Ji: Hebei Sheng (Vol. 3) [Atlas of Chinese Cultural Relics: Hebei Province]. Beijing: Cultural Relics Publishing House.

28. State Administration of Cultural Heritage. 2014. Zhongguo Wenwu Ditu Ji: Anhui Sheng

(Vol. 2). [Atlas of Chinese Cultural Relics: Anhui Province]. Beijing: SinoMaps Press.

29. State Administration of Cultural Heritage. 2015. Zhongguo Wenwu Ditu Ji: Heilongjiang Sheng [Atlas of Chinese Cultural Relics: Heilongjiang Province]. Beijing: Cultural Relics Publishing House.

30. State Administration of Cultural Heritage. 2017. Zhongguo Wenwu Ditu Ji: Shanghai Shi [Atlas of Chinese Cultural Relics: Shanghai Municipality]. Beijing: SinoMaps Press.

31. State Administration of Cultural Heritage. 2021. Zhongguo Wenwu Ditu Ji: Guangxi Sheng (Vol. 2) [Atlas of Chinese Cultural Relics: Guangxi Province]. Beijing: Cultural Relics Publishing House.

Europe (elite burials) Data on elite burials are sourced from the *Prähistorische Bronzefunde* (PBF). This project systematically compiles information on archaeological metal artifacts found across Europe. Since 1966, it has published 186 volumes documenting individual metal finds dating from 3000 to 500 BC. The PBF organizes these into book series, or *Abteilungen* (divisions), by artifact type. We focus on weapons, specifically those classified as "axes and hatchets" and "swords" (*Abteilung IV* and *Abteilung IX*, for a total of 39 volumes). We augment this data with artifacts from the "Bronze und urnenfelderzeitliche Schwerter" database (Hahnekamp, 2011) [W7]. For each artifact in the combined database, we identify three key characteristics: (i) the location of the excavation site, which we manually geocode; (ii) the site's nature (e.g., burial site); and (iii) the artifact's archaeological type or family (e.g., Pădureni axe type). Using (ii), we identify the elite burials, while (iii) allows us to link the burial to specific time periods (Early, Middle, and Late Bronze Age in Central Europe). For our empirical analysis, we identify 1×1 degree grid cells for which there is evidence of at least one elite burial. We do this separately for the periods corresponding to the Central European Early/Middle Bronze Age [3000 BC, 1300 BC) and the Late Bronze Age [1300 BC, 750 BC]. More details on data sources and construction processes are provided in Appendix D.6.

`Online sources`
W7 http://chc.sbg.ac.at/schwerter/map.php, downloaded 31 May 2023.

A.1.2 Bilateral trade flows

Ancient trade flows are reconstructed using archaeological artifacts compiled by Flückiger et al. (2022) [W8]. For each artifact, we treat the excavation site as the destination and the production site as the origin. Figure A.8 illustrates the geographic distribution of artifact origins and destinations: the overwhelming majority of artifacts in the dataset were exchanged within Europe. In their published analysis, Flückiger et al. (2022) focus on intra-European trade flows, even though their underlying dataset also contains observations outside of Europe. We retain these observations and use the full dataset as compiled by the authors. Below, we describe the characteristics of the data, the underlying sources, and the aggregation procedure used to construct grid-cell-pair–level trade flows from artifact-level observations.

Stone Age trade data Stone Age trade flows are derived from two databases. The first is the *Alpine Jade Database*, which was compiled by more than 50 researchers from several European countries as part of the project "JADE: Social Inequalities in Neolithic Europe: The Circulation of

Long Axeheads of Alpine Jades" (Pétrequin et al., 2012). The data were compiled between 2008 and 2018 and focus on long axeheads made from jade (mainly extracted in the Alps). These axes mainly circulated within Europe during the fifth and fourth millennia BC, but some of the objects moved over long distances from the Alps to the Atlantic coast and the Black Sea via extensive exchange networks. To identify the provenance of the axeheads, the researchers used visual analysis and spectroradiometry. For 1,355 axeheads, the database includes information on the origin of the artifacts with sufficient precision for the purpose of our analysis. The jade included in our analysis primarily originates from high-altitude quarries at Monte Viso near Turin and Monte Beigua near Genoa in the Italian Alps. Some of the finds can also be reliably traced back to the Vosges in France or the Pennine Alps in Switzerland.

The second source is Schauer et al. (2020), who provide an extensive database on British axeheads that combines information collected in projects overseen by the Implement Petrology Group (IPG), the Neolithic Axehead Archive, and the Irish Stone Axe Project. The database contains precise information on the find site of axeheads from the Early Neolithic (4100–3400 BC) discovered across England, Wales, and southern Scotland. Provenance of the axeheads is identified via petrological analysis. In total, we have 2,340 artifacts for which the provenance is pinpointed within a radius of less than 50 km in Schauer et al. (2020).

For each artifact coming from these two databases, we first identify which of the 1×1-degree grid cells its origin and destination fall into. We then aggregate this information to the grid-cell-pair level, yielding the number of find sites within cell j that show evidence of trade originating from cell i.

Bronze Age trade data The dataset is compiled from 34 separate publications (listed in Table A.3). Most artifacts are weapons, tools, and jewelry. In total, this database encompasses 3,735 artifacts for which find site and provenance can be determined with sufficient precision. In most cases, the artifacts' provenance was identified based on metal parts, such as copper, silver, tin, or lead, using lead isotope analysis and trace element pattern analysis. In a few cases, provenance was determined by typological similarities. For more details on the methodology behind the data collection process, see Online Appendix E in Flückiger et al. (2022).

For our empirical analysis, we aggregate information of the individual artifacts to the 1×1 degree grid-cell-pair level.

`Online sources`

W8 The find-level data compiled in Flückiger et al. (2022) are available at `github.com/Matthias-Flueckiger/FindLevelDataFlueckigerEtAl2022`.

A.1.3 Cropland and productive land

Croplands Information on cropland areas is sourced from the HYDE 3.1 database (Klein Goldewijk et al., 2011) [W9]. The raster data are provided at a 5×5 minute resolution and represent the estimated share of each grid cell's total area that was occupied by cropland in 3000 BC. For our empirical analysis, we aggregate this information to the 1×1 degree grid cell level.

`Online sources`

W9 `https://geo.public.data.uu.nl/vault-hyde/HYDE%203.1%5B1701183246%5D/original/hyde31_final.zip`, downloaded 18 December 2019.

Net primary productivity Precipitation and temperature data—the key factors influencing net primary productivity (NPP)—are sourced from Karger et al. (2021) [w10]. The data are provided in raster format at a 1×1 kilometer resolution and in 100-year intervals from 20100 BC to 1990 AD. We aggregate the precipitation and temperature data to the 1×1 degree grid cell level and compute net primary productivity using the equations from the original Miami model (Lieth, 1975), applying the updated coefficients from Zaks et al. (2007).[43] We calculate net primary productivity in this way for all available years between 4000 BC and 3000 BC and then take the average across these years.

Online sources

w10 https://envicloud.wsl.ch/#/?bucket=https%3A%2F%2Fos.zhdk.cloud.switch.ch%2Fchelsav1%2F&prefix=chelsa_trace%2F, downloaded 8 February 2022 (version 1.0). All years between 4000BC and 3000BC (files ending in -40 to -30). Temperature: bio01; precipitation: bio12.

A.1.4 Metal mines and deposits

Mines We compile a database on location of copper and tin mines from our own review of the archaeological literature. A prerequisite for the data to be included in our analysis is that (i) the precise location of the mines could be inferred, and (ii) we could ascertain that the mining sites were active during the Bronze Age. In total, we identified 121 copper mines and 46 tin mines that fulfil these criteria. Figure A.9 depicts the location of these mines (along with the croplands), while Tables A.1–A.2, listed at the end of this data appendix, provide the names of the mines along with the sources from which they were retrieved.

Mineral deposits Geocoded information on known metal deposits is sourced from U.S. Geological Survey (2005) [w11]. For the main analysis, we extract information on the location of copper and tin deposits. The location of these deposits, along with the net primary productivity, is shown in Figure A.10. For both types of metal, we identify the 1×1 degree cells containing deposits. Many cells include multiple deposits of the same metal. To speed up the computation of least-cost paths and construction of our instrumental variable (see details below), we retain only one deposit per cell and metal, and set its location to the center of the respective grid cell.

Online sources

w11 https://mrdata.usgs.gov/mrds/mrds-trim.zip, downloaded 24 February 2024.

A.1.5 Additional data

Transport cost surface

To create the transport cost surface, we require data on mountains, inland waterways, and landmasses. The data, along with their respective sources, are described below.

Mountains Data on mountain classes are sourced from UNEP-WCMC (2002) [w12]. These data are provided in raster format at a 1×1 kilometer resolution. We first aggregate the data to 0.25×0.25 degree raster cells (i.e., the resolution of the transport cost surface raster) and define a cell as a 'high mountain cell' if at least 50% of its area has an elevation of 4,500 meters or higher. For the main analysis, we further aggregate the data to the 1×1 degree grid cell level and create a dummy

[43] See Table 3, row 4 in Zaks et al. (2007).

variable, 'mountains', which equals one if any high mountain areas fall within the grid cell.

Online sources

w12 https://datadownload-production.s3.amazonaws.com/Mountains_and_Tree_Cover_in_Mountain_Regions_2002.zip, downloaded 22 April 2024.

Rivers and lakes Vector data on inland waterways are sourced from Natural Earth (rivers [w13], and lakes [w14]). Due to their historical importance, we also include rivers of the Indus River system (Ravi, Jhelum, Beas, Satluj, and Chenab). To account for major historical river shifts, we replace current-day courses of the Euphrates, Tigris, and Yellow River with information on their historical courses. The data on the course of the Euphrates and Tigris are provided by Bätscher (2020) [w15], while the data on the course of the Nile comes from the Harvard WorldMap [w16]. Finally, we digitized and added the historical course of the Ghaggar-Hakra River based on Clift et al. (2012). For our empirical analysis, we combine and rasterize these data at both the 0.25×0.25 and 1×1 degree grid cell level. For the 1×1 degree grid cells, we also create an indicator that captures if a cell is intersected by an inland waterway.

Online sources

w13 https://www.naturalearthdata.com/downloads/10m-physical-vectors/, Version 5.0.0 of `Rivers + lake centerlines`, downloaded 20 April 2024 .

w14 https://www.naturalearthdata.com/downloads/10m-physical-vectors/, Version 3.0.0 of `Lakes`, downloaded 7 May 2020.

w15 https://zenodo.org/api/records/3787265/files-archive, downloaded 24 May 2024.

w16 The data were originally downloaded from worldmap.harvard.edu after registration on 22 March 2018. Since then, the repository has moved to a new platform and is now visualised here: https://www.arcgis.com/apps/mapviewer/index.html?layers=3abd82960bc24c91aa0b5320f135c4d5. Registration is required.

Landmass and sea Vector data on landmasses and seas is sourced from Natural Earth (land [w17], and sea [w18]). We manually re-draw the coastline of the Persian Gulf to reflect its extent during the Bronze Age. We crop the landmass to the Old World and rasterize this data at both the 0.25×0.25 and 1×1 degree grid cell level.[44] We further construct an indicator variable that takes the value of one if a 1×1 degree grid cell is intersected by the coastline.

Online sources

w17 https://www.naturalearthdata.com/downloads/10m-physical-vectors/, Version 5.1.1 of `Land`, downloaded 20 April 2024.

w18 https://www.naturalearthdata.com/downloads/10m-physical-vectors/, Version 5.1.1 of `Ocean`, downloaded 20 April 2024.

Transport cost surface We combine rasterized information—aggregated at a 0.25×0.25 degree resolution—on mountains, inland waterways, and landmasses to construct a transport cost surface. Each grid cell is classified as either a sea, river, land, or mountain cell. By assigning each surface class its corresponding estimate of relative transport costs, the surface captures the cost of movement across space. We do not allow sea transport more than 25 km from the coast or in latitudes greater

[44] We use this map to define the landmass of the Old World: https://en.wikipedia.org/wiki/Old_World#/media/File:LocationAfricaEurasia.png (last accessed 30 July 2023).

than 60° north. Overland transport is not permitted in high mountain areas.[45]

Weapons

Weapons Information on weapons is sourced from the Metropolitan Museum of Art [w19], the University of Pennsylvania Museum of Archaeology and Anthropology [w20], the Phoebe A. Hearst Museum of Anthropology at UC Berkeley [w21], the Smithsonian Institution [w22], the Louvre Museum [w23], and the British Museum [w24]. We extract artifacts that are identifiable as weapons and clearly assignable to either the Stone or Bronze Age. We then manually geocode the find sites of these artifacts. A more detailed description of the data processing procedure is described in Appendix D.5. Finally, we aggregate the data to the 1×1 degree grid cell level and create an indicator variable that captures whether a cell contains any weapons from a given period.

Online sources

w19 https://www.metmuseum.org/art/collection, accessed and downloaded 5 June 2025.
w20 https://www.penn.museum/collections/advanced.php, accessed and downloaded 5 June 2025.
w21 https://portal.hearstmuseum.berkeley.edu/, accessed and downloaded 5 June 2025.
w22 https://www.si.edu/search/images, accessed and downloaded 5 June 2025.
w23 https://collections.louvre.fr/en/recherche, accessed and downloaded 5 June 2025.
w24 https://www.britishmuseum.org/collection/search, accessed and downloaded 5 June 2025.

Additional geographic and environmental data

Additional land productivity measures We use two alternative data sources on land productivity. The first represents global estimates of land suitability for cultivation in the current era, based on climate and soil constraints, developed in Ramankutty et al. (2002) and available in raster format at a 0.5×0.5 degree resolution [w25]. The second is the Caloric Suitability Index developed in Galor and Özak (2015) [w26]. This dataset is provided in raster format at a 5×5 minute resolution and represents estimates of average potential yields within each cell, attainable given the set of crops suitable for cultivation in the pre-1500 period. We aggregate both raster datasets to the 1×1 degree grid cell level.

Online sources

w25 https://sage-public-files.s3.amazonaws.com/atlas/SUIT.ZIP, downloaded 22 August 2023.
w26 https://zenodo.org/records/14714917/files/pre1500AverageCalories.tif?download=1, downloaded 15 May 2024.

Malaria suitability index Information on malaria suitability is sourced from Kiszewski et al. (2004) [w27]. The data are available in raster format at a resolution of 0.5×0.5 degrees, which we aggregate to the 1×1 degree grid cell level.

Online sources

w27 https://www.dropbox.com/scl/fi/t4je3iqo795gdu18v4swr/ME_raster.zip?rlkey=921dnfkahuxh4g4jy0uh8mmdl&e=2&dl=0, downloaded 1 August 2022.

Biomes Biomes are 14 mutually exclusive classes that represent the dominant natural vegetation expected in an area. The vectorized distribution of the biomes is sourced from David M. Olson (2001) [w28]. We assign each 1×1 degree cell to a biome based on the location of its center point.

[45] In practice, we block these cells by assigning them very high relative shipping costs (10,000).

Online sources

W28 https://www.sciencebase.gov/catalog/item/508fece8e4b0a1b43c29ca22, downloaded 15 May 2024.

Growing days Information on the total number of growing period days is extracted from FAO and IIASA (2021) [W29].[46] The data are provided in raster format at a 5×5 minute resolution, which we aggregate to the 1×1 degree cell level.

Online sources

W29 https://s3.eu-west-1.amazonaws.com/data.gaezdev.aws.fao.org/res01/CRUTS32/Hist/lgd_CRUTS32_Hist_0010.tif, downloaded 15 May 2024.

Elevation and ruggedness Elevation data are sourced from the WorldClim database (v.1.4). We download the raster data at a 2.5×2.5 minute resolution [W30]. Using these data, we compute a terrain ruggedness index following Wilson et al. (2007) and then aggregate the index at the 1×1 degree cell level. We also compute the average elevation for each 1×1 degree cell.

Online sources

W30 https://geodata.ucdavis.edu/climate/worldclim/1_4/grid/cur/alt_2-5m_bil.zip, downloaded 18 December 2019.

Precipitation and temperature Precipitation and temperature data are sourced from Karger et al. (2021). The data are provided in raster format at a 1×1 kilometer resolution and in 100-year intervals from 20100 BC to 1990 AD [W31]. We extract data for all available years between 4000 BC and 3000 BC and aggregate it to the 1×1 degree grid cell level. We use the average across these years as explanatory variables in our empirical analysis.

Online sources

W31 https://chelsa-climate.org/paleo-climate/, downloaded 8 February 2022 (version 1.0).

Natural harbors Geocoded information on the location of ports is sourced from NGA (2019) [W32]. For each 1×1 degree cell, we calculate the distance from its center to the nearest natural harbor and define an indicator variable that equals one if this distance is less than 50 km.

Online sources

W32 https://msi.nga.mil/api/publications/download?key=16694622/SFH00000/WPI_Shapefile.zip&type=view, downloaded 29 September 2019.

Continents Continent vector data is sourced from Esri (2023) [W33]. Each 1×1 degree cell is assigned to a continent based on the location of its center point.

Online sources

W33 https://hub.arcgis.com/datasets/CESJ::world-continents/explore, downloaded 20 April 2024 (version dated 1 February 2024).

[46] Estimates are provided for different time periods, both past and future. We select the estimates that represent the long-run historical average number of growing days, 1961–1990.

Environmental circumscription We follow the procedure described in Schönholzer and François (2023) to construct a measure of environmental circumscription. As outlined in detail in Section 3 and Appendix A in Schönholzer and François (2023), this measure captures the difference between the local potential agricultural yield and the potential yield of neighboring cells. Data on potential agricultural yields are from FAO and IIASA (2021). Specifically, we extract yields for the Old World crops used in Schönholzer and François (2023). These are barley [w34], buckwheat [w35], chickpea [w36], foxtail millet [w37], groundnut [w38], oat [w39], pearl millet [w40], rapeseed [w41], rye [w42], sorghum [w43], soybean [w44], wetland rice [w45], and wheat [w46], achievable under irrigation and low-input conditions.[47] The yield data are provided in raster format at a 5×5-minute resolution. We construct the circumscription data at this level of aggregation and then compute the average for each 1×1-degree cell. `Online sources`

w34 https://s3.eu-west-1.amazonaws.com/data.gaezdev.aws.fao.org/res02/CRUTS32/Hist/6190L/barl200a_yld.tif, downloaded 15 May 2025.
w35 https://s3.eu-west-1.amazonaws.com/data.gaezdev.aws.fao.org/res02/CRUTS32/Hist/6190L/bckw200a_yld.tif, downloaded 15 May 2025.
w36 https://s3.eu-west-1.amazonaws.com/data.gaezdev.aws.fao.org/res02/CRUTS32/Hist/6190L/chck200a_yld.tif, downloaded 15 May 2025.
w37 https://s3.eu-west-1.amazonaws.com/data.gaezdev.aws.fao.org/res02/CRUTS32/Hist/6190L/fmlt200a_yld.tif, downloaded 15 May 2025.
w38 https://s3.eu-west-1.amazonaws.com/data.gaezdev.aws.fao.org/res02/CRUTS32/Hist/6190L/grnd200a_yld.tif, downloaded 15 May 2025.
w39 https://s3.eu-west-1.amazonaws.com/data.gaezdev.aws.fao.org/res02/CRUTS32/Hist/6190L/oats200a_yld.tif, downloaded 15 May 2025.
w40 https://s3.eu-west-1.amazonaws.com/data.gaezdev.aws.fao.org/res02/CRUTS32/Hist/6190L/pmlt200a_yld.tif, downloaded 15 May 2025.
w41 https://s3.eu-west-1.amazonaws.com/data.gaezdev.aws.fao.org/res02/CRUTS32/Hist/6190L/rape200a_yld.tif, downloaded 15 May 2025
w42 https://s3.eu-west-1.amazonaws.com/data.gaezdev.aws.fao.org/res02/CRUTS32/Hist/6190L/ryes200a_yld.tif, downloaded 15 May 2025.
w43 https://s3.eu-west-1.amazonaws.com/data.gaezdev.aws.fao.org/res02/CRUTS32/Hist/6190L/sorg200a_yld.tif, downloaded 15 May 2025.
w44 https://s3.eu-west-1.amazonaws.com/data.gaezdev.aws.fao.org/res02/CRUTS32/Hist/6190L/soyb200a_yld.tif, downloaded 15 May 2025.
w45 https://s3.eu-west-1.amazonaws.com/data.gaezdev.aws.fao.org/res02/CRUTS32/Hist/6190L/ricw200a_yld.tif, downloaded 15 May 2025.
w46 https://s3.eu-west-1.amazonaws.com/data.gaezdev.aws.fao.org/res02/CRUTS32/Hist/6190L/whea200b_yld.tif, downloaded 15 May 2025.

Irrigation potential We follow the procedure described in Bentzen, Kaarsen and Wingender (2017) to construct a measure of irrigation potential. As outlined in detail in Section 3.1 of Bentzen, Kaarsen and Wingender (2017), this measure captures the share of a region's agricultural land that is only cultivable if irrigation is available, reflecting the extent to which farming in the area depends on artificial water supply.

Data on agricultural land under different irrigation regimes—originally provided by the Global Agro-Ecological Zones 2002 database of the Food and Agriculture Organization—are sourced from Bentzen, Kaarsen and Wingender (2017)'s replication package [w47]. The data are available in

[47] We select the data that represent the long-run historical averages between 1961–1990.

raster format at a 5×5-minute resolution. For each 1×1-degree cell, we compute the share of total agricultural land that is only cultivable under irrigation.

Online sources

w47 https://www.dropbox.com/scl/fo/p8kphtrjot0ux6tjj2puz/AFoEhGRmaNfcgbfWhPkMmI8?dl=0&e=1&preview=plate47.zip&rlkey=ctb6fs9jl6o3b4rjjpzbrlnti, downloaded 26 February 2025.

Distance to cereal domestication regions Data on distance to cereal domestication regions is sourced from Mayshar, Moav and Pascali (2022) [w48].

Online sources

w48 https://www.journals.uchicago.edu/doi/suppl/10.1086/718372/suppl_file/2018030data.zip, downloaded 26 February 2025.

Countries Administrative boundaries in vector format are sourced from World Food Programme (UN Agency) [w49]. Each 1×1 degree cell is assigned to a country based on the location of its center point.

Online sources

w49 https://public.opendatasoft.com/explore/dataset/world-administrative-boundaries/export/, downloaded 23 June 2023.

Mountain ranges Information on the location of mountain ranges, used in the production of Figure 6 for the case studies, was sourced from Encyclopaedia Britannica [w50].

Online sources

w50 Arvalli range: https://www.britannica.com/place/Aravalli-Range; Taurus mountains: https://www.britannica.com/place/Taurus-Mountains; Zagros mountains: https://www.britannica.com/place/Zagros-Mountains. Downloaded 8 July 2025 and georeferenced manually.

A.2 Tables raw data

Table A.1: References for database of copper mine locations

Name	Country	Source	Name	Country	Source
Kelchalm	Austria	O'Brien (2015)	Nikolaevskoe	Kazakhstan	Stöllner et al. (2011)
Leogang-Shwarzleo	Austria	O'Brien (2015)	Orlovskoe	Kazakhstan	Stöllner et al. (2011)
Mauken	Austria	Schibler et al. (2011)	Vilabouly Complex	Laos	Cadet et al. (2019)
Mitterberg	Austria	O'Brien (2015)	Al-Moyassar	Oman	Giardino (2019)
Obersteiermark	Austria	O'Brien (2015)	Batin	Oman	Giardino (2019)
Schwaz-Brixlegg	Austria	O'Brien (2015)	Bilad Al-Maidin	Oman	Giardino (2019)
St. Veit	Austria	O'Brien (2015)	Gebel Saleli	Oman	Giardino (2019)
Viehofen-Wirtsalm	Austria	O'Brien (2015)	Huqain	Oman	Giardino (2019)
Ai Bunar	Bulgaria	O'Brien (2015)	Nujum	Oman	Giardino (2019)
Baishantang	China	Jaang (2015)	Tawi Ubaylah	Oman	Giardino (2019)
Gangxia	China	Liu et al. (2019)	Wadi Miadin	Oman	Giardino (2019)
Jinniudong	China	Reinhardt (1997)	Mociços	Portugal	O'Brien (2015)
Linxi	China	Pollard et al. (2017)	Kargaly	Russia	O'Brien (2015)
Mayang	China	Reinhardt (1997)	Minussinsk basin	Russia	Stöllner et al. (2011)
Nulasai	China	Wang et al. (2019)	Novonikolayevskiy	Russia	Ankushev et al. (2018)
Tongling	China	Liu et al. (2019)	Novotemirskiy	Russia	Ankushev et al. (2018)
Tonglushan	China	Larreina-García (2017)	Vorovskaya Yama	Russia	Ankushev et al. (2018)
Xichengyi	China	Jaang (2015)	Funtana Raminosa	Sardinia	O'Brien (2015)
Xiquegou	China	Pollard et al. (2017)	Jarmovac	Serbia	Derikonjic, Pernicka and Rehren (2011)
Zhongtiaoshan	China	Liu et al. (2019)	Majdanpek	Serbia	Radivojević et al. (2010)
Cyprus	Cyprus	Constantinou (2012)	Mali Sturak	Serbia	O'Brien (2015)
Wadi Maghara	Egypt	Hauptmann (1997)	Rudna Glava	Serbia	O'Brien (2015)
Alderly Edge	England	National Trust	Zdrelo	Serbia	Radivojević et al. (2010)
Ecton	England	Timberlake and Marshall (2018)	Spania Dolina	Slovakia	O'Brien (2015)
Bouco-Payrol	France	O'Brien (2015)	Cabezo Jure	Spain	O'Brien (2015)
Causiat	France	O'Brien (2015)	Chinflon	Spain	O'Brien (2015)
Clue de Roua	France	O'Brien (2015)	Cuchillares	Spain	O'Brien (2015)
La Roussignole	France	O'Brien (2015)	El Aramo	Spain	O'Brien (2015)
Les Rousses	France	O'Brien (2015)	La Loba	Spain	O'Brien (2015)
Maraval	France	O'Brien (2015)	Las Navas, Berrocal	Spain	O'Brien (2015)
Pioch Farrus	France	O'Brien (2015)	Loma de la Tejeria	Spain	O'Brien (2015)
Saint Veran	France	O'Brien (2015)	Mallorca	Spain	O'Brien (2015)
Vallarade	France	O'Brien (2015)	Mitja Lluna	Spain	Ortiz et al. (2014)
Kythnos	Greece	Catapotis (2007)	Redondilla	Spain	O'Brien (2015)
Lavrion	Greece	Gale et al. (2002)	Sierra de Orihuela	Spain	O'Brien (2015)
Othrys Mountains	Greece	Gale et al. (2002)	El Milagro	Spain	O'Brien (2015)
Seriphos	Greece	O'Brien (2015)	La Profunda	Spain	O'Brien (2015)
Anarak Talmessi	Iran	Nezafati and Stöllner (2018)	Solana del Bepo	Spain	Rafel et al. (2019)
Taknar	Iran	Nezafati and Stöllner (2018)	Khao Sai On	Thailand	Pryce et al. (2011*a*)
Veshnāveh (Ghar Chale)	Iran	Nezafati and Stöllner (2018)	Nil Kham Haeng	Thailand	Higham et al. (2020)
Ballyrisode Hill	Ireland	O'Brien (2015)	Non Pa Wai	Thailand	Pryce et al. (2011*b*)
Canshanavoe	Ireland	O'Brien (2015)	Phu Lon	Thailand	Higham et al. (2020)
Derrycarhoon	Ireland	O'Brien (2015)	Derekutugun	Turkey	Yalcın and Maass (2013)
Mount Gabriel	Ireland	O'Brien (1999)	Ergani Maden	Turkey	Özbal, Adriaens and Earl (1999)
Ross Island	Ireland	Northover, O'Brien and Stos (2001)	Kure	Turkey	Glatz (2020)
Tooreen	Ireland	O'Brien (2015)	Murgul	Turkey	Kaptan (1990)
Boulysallagh	Ireland	O'Brien (2015)	Tokat-Erbaa, Kozlu	Turkey	Lehner and Yener (2013)
Callaros Oughter	Ireland	O'Brien (2015)	Wadi al-Hilo	UAE	Kutterer, Neureiter and Jasim (2013)
Carrigacat	Ireland	O'Brien (2015)	Copa Hill	Wales	Hughes (1981)
Crumpane	Ireland	O'Brien (2015)	Erglodd	Wales	O'Brien (2015)
Nahal 'Amram	Israel	Avner et al. (2018)	Great Orme	Wales	Lewis (1997)
Timna	Israel	Avner (2014)	Llancynfelin	Wales	O'Brien (2015)
Campolungo	Italy	O'Brien (2015)	Nantyrarian	Wales	O'Brien (2015)
Grotta della Monaca	Italy	Quarta et al. (2013)	Nantyreira	Wales	O'Brien (2015)
Libiola	Italy	O'Brien (2015)	Ogof Wyddon	Wales	O'Brien (2015)
Monte Loreto	Italy	O'Brien (2015)	Parys Mountain	Wales	O'Brien (2015)
Trentino	Italy	O'Brien (2015)	Twll-y-mwyn	Wales	O'Brien (2015)
Madsus	Jordan	Hauptmann (2007)	Tyn y fron	Wales	O'Brien (2015)
Qalb Ratiye	Jordan	Hauptmann (2007)			
Umm el-Amad	Jordan	Hauptmann (2007)			
Umm ez-Zuhur	Jordan	Hauptmann (2007)			
Wadi Abiad	Jordan	Hauptmann (2007)			
Wadi Khalid	Jordan	Hauptmann (2007)			

Notes: This table lists the location of copper mines by reference.

Table A.2: References for database of tin mine locations

Name	Country	Source
Ebrahimi	Afghanistan	Cleuziou (1982)
Mes Aynak	Afghanistan	Massoudi (2011)
Misgaran	Afghanistan	Cleuziou (1982)
Sarkar	Afghanistan	Cleuziou (1982); Garner (2014)
Shaida	Afghanistan	Cleuziou (1982)
De'an	China	Liu et al. (2015, 2018, 2019)
Guangxi	China	Liu et al. (2015, 2018)
Jiangxi	China	Liu et al. (2015, 2018)
Qiaomailing	China	Liu et al. (2015, 2018)
Yunnan	China	Liu et al. (2015, 2018)
Brittany	France	Benvenuti et al. (2003); Tolksdorf et al. (2020); Valera and Valera (2003)
Schellerhau	Germany	Tolksdorf et al. (2020)
Tosham	India	Singh and Singh (2016)
Deh Hosein	Iran	Valamoti and Jones (2010)
Askaraly	Kazakhstan	Garner (2014)
Bajmurza	Kazakhstan	Garner (2014)
Čerdojak	Kazakhstan	Garner (2014); Stöllner et al. (2011)
Čudskoje	Kazakhstan	Stöllner et al. (2011)
Delbegetej	Kazakhstan	Stöllner et al. (2011)
Južnyj Bulattau	Kazakhstan	Garner (2014)
Kalai Topkan	Kazakhstan	Garner (2014)
Karagoin	Kazakhstan	Garner (2014)
Mynčunkur	Kazakhstan	Stöllner et al. (2011)
Ubinskoe	Kazakhstan	Garner (2014); Stöllner et al. (2011)
Ulytauskie	Kazakhstan	Garner (2014)
Urunčaj	Kazakhstan	Stöllner et al. (2011)
Mount Cer	Serbia	Huska et al. (2014)
Cerro de San Cristobal	Spain	Benvenuti et al. (2003); Tolksdorf et al. (2020); Valera and Valera (2003)
Džaupai	Tajikistan	Garner (2014)
Mushiston	Tajikistan	Garner (2014, 2015); Valamoti and Jones (2010)
Mušiston	Tajikistan	Garner (2014)
Takfon	Tajikistan	Garner (2014)
Göltepe	Turkey	Garner (2014)
Hisarcik	Turkey	Yener et al. (2015)
Kestel	Turkey	Valamoti and Jones (2010); Yener et al. (1989)
Monte Valerio	Tuscany	Valamoti and Jones (2010); Muhly (1985)
Cornwall	UK	Benvenuti et al. (2003); Tolksdorf et al. (2020); Valera and Valera (2003)
Devon	UK	Benvenuti et al. (2003); Tolksdorf et al. (2020); Valera and Valera (2003)
St Austell	UK	Muhly (1985)
St Eval	UK	Muhly (1985)
Auminza-tau	Uzbekistan	Garner (2014)
Čhangali	Uzbekistan	Garner (2015); Stöllner et al. (2011)
Isfajramsaj	Uzbekistan	Garner (2014)
Karatube	Uzbekistan	Garner (2014)
Karnab	Uzbekistan	Stöllner et al. (2011); Valamoti and Jones (2010)
Lapas	Uzbekistan	Garner (2014); Stöllner et al. (2011)

Notes: This table lists the location of tin mines by reference.

Table A.3: References for database of Bronze Age metals exchange (provided by Flückiger et al. (2022))

Commodity	# Items	# Destinations	# Origins	Source
Bronze axes	2	2	1	Artioli et al. (2020)
Amber jewelry and ornaments	46	1	1	Beck, Fellows and Adams (1970)
Amber jewelry	70	1	1	Beck, Southard and Adams (1972)
Copper ingots	47	6	1	Begemann et al. (2001)
Bronze weapons	7	6	3	Burgess and O'Connor (2008)
Lead utensils	71	12	2	Gale and Stos-Gale (1981)
Lead utensils	40	1	2	Gale, Stos-Gale and Davis (1984)
Copper ingots and lead artifacts	614	7	3	Gale and Stos-Gale (2005)
Copper ingots	79	4	1	Gale (2006)
Copper artifacts	120	1	1	Giumlia-Mair (2005)
Copper artifacts	24	2	1	Hauptmann, Begemann and Schmitt-Strecker (1999)
Bronze axes	3	3	2	Klassen, Cassen and Pétrequin (2012)
Copper ingots	4	1	1	Kristiansen and Suchowska-Ducke (2015)
Bronze weapons	53	35	12	Ling et al. (2014)
Bronze swords	105	80	8	Ling et al. (2019)
Copper ingots and ceramic goods	3	3	2	Lo Schiavo (2005)
Tin artifacts	143	64	2	Mason (2020)
Bronze utensils	1227	21	2	Matthäus (2005)
Bronze weapons and jewelry	67	34	9	Melheim et al. (2018)
Bronze weapons	1	1	1	Montero Ruiz, Martínez Navarrete and Galán (2016)
Bronze weapons and copper utensils	13	1	3	Montero Ruiz et al. (2018)
Amber jewelry	1	1	1	Murillo-Barroso and Martinón-Torres (2012)
Amber jewelry	268	5	1	Murillo-Barroso et al. (2018)
Bronze weapons and utensils	19	19	1	Needham and Giardino (2008)
Bronze weapons	383	7	2	Pernicka, Lutz and Stöllner (2016)
Bronze weapons and jewelry	29	3	4	Pernicka et al. (2016)
Copper ingots	8	1	2	Pinarelli (2004)
Bronze axes and copper ingots	27	4	3	Reguera-Galan et al. (2019)
Bronze weapons and jewelry	3	2	3	Reiter et al. (2019)
Copper ingots and ceramic goods	52	8	9	Sabatini and Lo Schiavo (2020)
Silver coins	12	1	1	Stos-Gale and Gale (2009)
Bronze, tin and silver artifacts	99	20	7	Stos-Gale and Gale (2010)
Copper ingots	17	3	1	Stos-Gale (2011)
Bronze weapons	74	3	1	Williams and Le Carlier de Veslud (2019)

A.3 Figures raw data

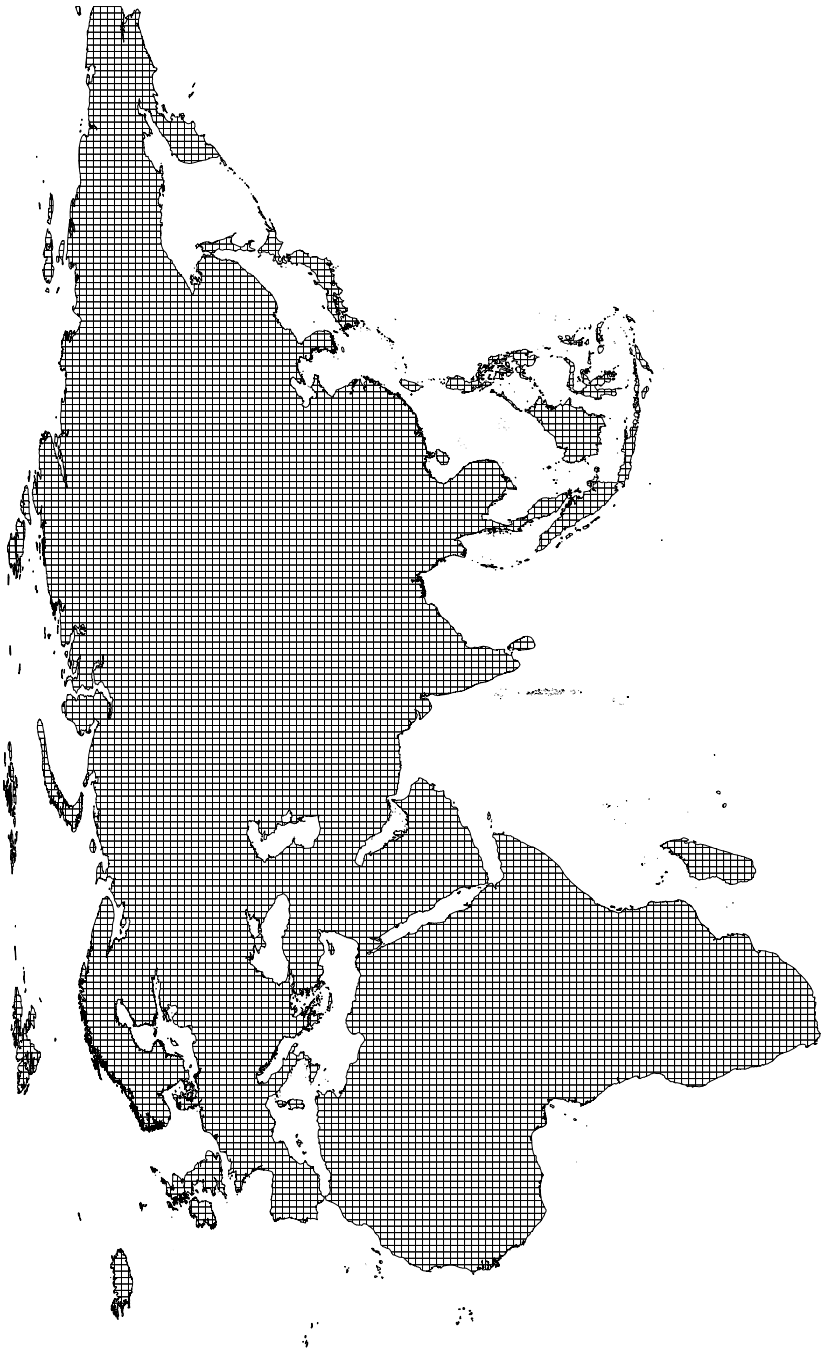


Figure A.1: Units of observation
The figure depicts the geographical scope of our analysis, along with the individual units of observation—the 1×1 degree grid cells—cropped to the landmass using the coastline.

Panel (a)



Panel (b)

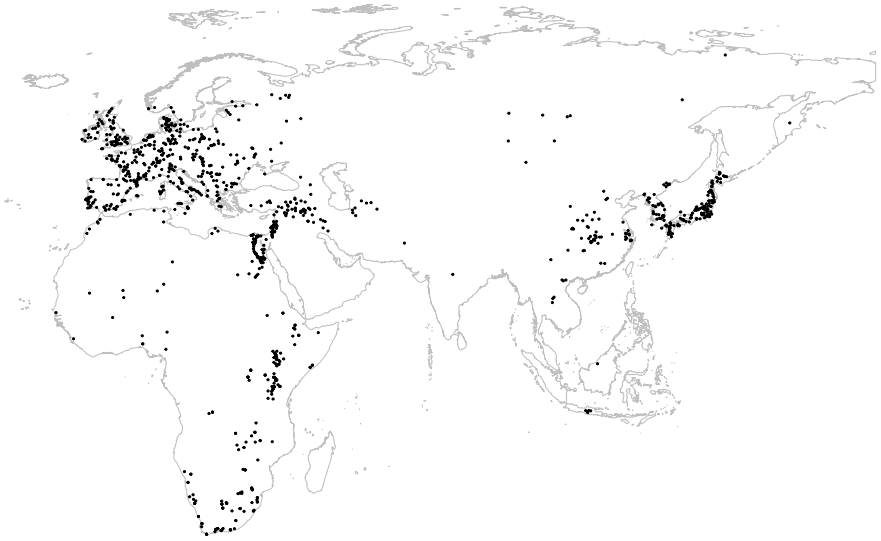


Figure A.2: Sites Green et al. (2024)
Figure depicts the location of cities and citadels from Green et al. (2024). Panel (a) shows sites present in the Stone Age, panel (b) sites present in the Bronze Age.



Figure A.3: Cities Reba, Reitsma and Seto (2016)
Figure depicts the locations of cities in the Reba, Reitsma and Seto (2016) dataset that emerged before 1300 BC.

Panel (a)



Panel (b)

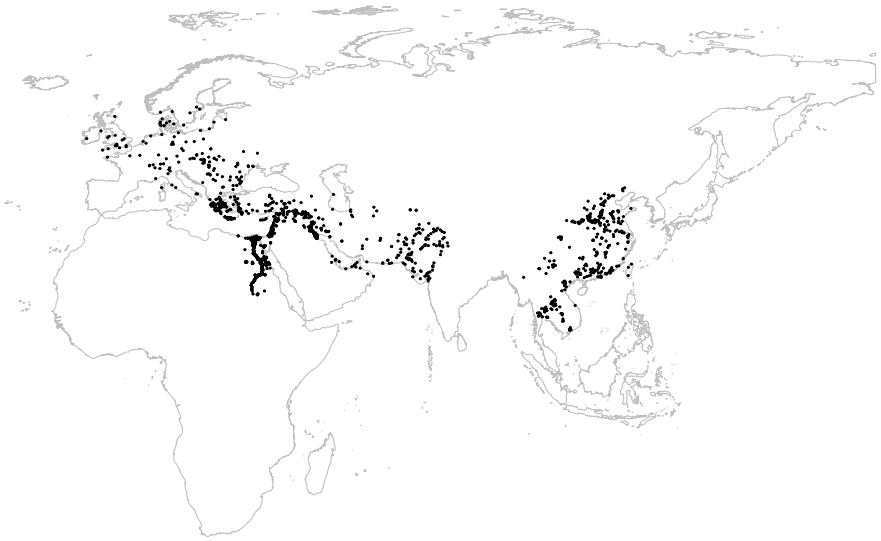


Figure A.4: Sites Bahn (2000)
Figure depicts the location of archaeological sites from Bahn (2000)'s Atlas of World Archaeology. Panel (a) shows sites present in the Stone Age, panel (b) sites present in the Bronze Age.

Panel (a)



Panel (b)

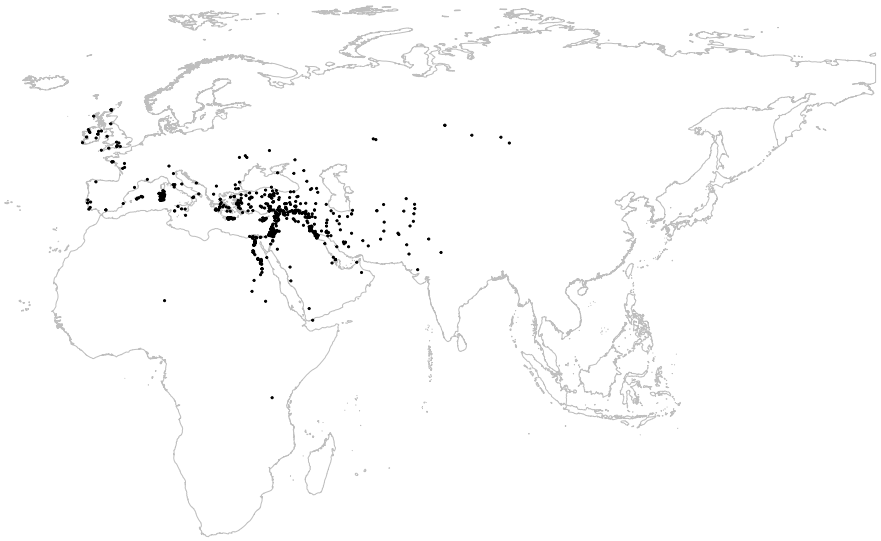


Figure A.5: Sites Pleiades Gazetteer
Figure depicts the location of archaeological sites from the Pleiades Gazetteer Bagnall (2022). Panel (a) shows sites present in the Stone Age, panel (b) sites present in the Bronze Age.

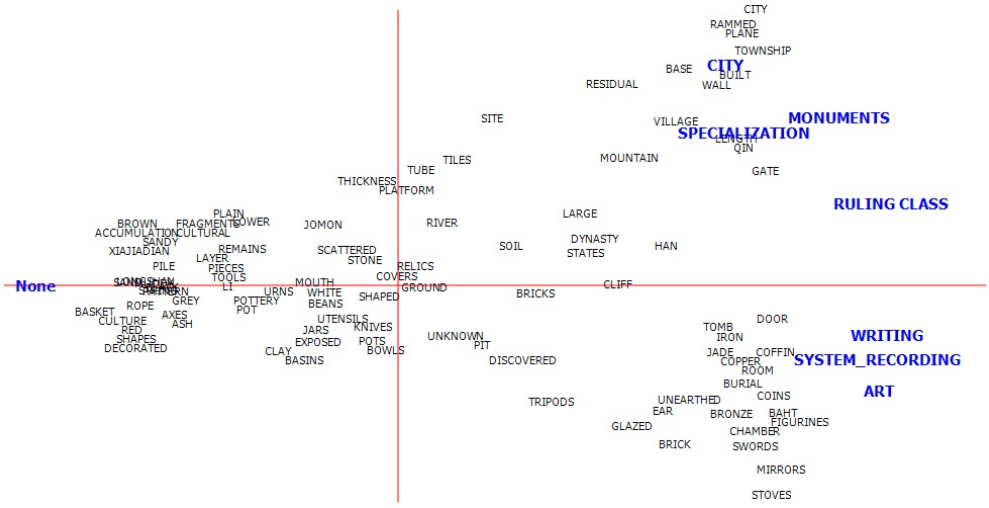


Figure A.6: Correspondence plot Atlas of Chinese Cultural Relics
Figure depicts the correspondence plot between the most frequent 100 words in the Atlas of Chinese Cultural Relics and the criteria indicative of the rise of the Urban Revolution recognized by the classifier.

Panel (a)



Panel (b)



Figure A.7: Atlas of Chinese Cultural Relics
Figure depicts the location of archaeological sites of the Atlas of Chinese Cultural Relics. Data is unavailable for provinces shaded in grey. Panel (a) shows sites present in the Stone Age, panel (b) sites present in the Bronze Age.

(a)



(b)

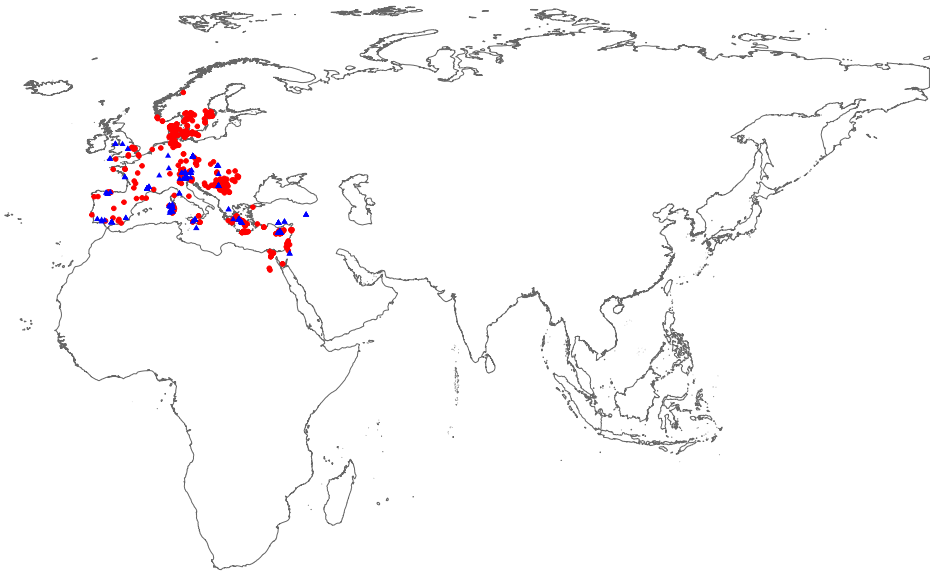


Figure A.8: Origins and destinations of artifacts

Panel (a) depicts origins (blue triangles) and destinations (red dots) of artifacts traded during the Stone Age. Panel (b) depicts origins (blue triangles) and destinations (red dots) of artifacts traded during the Bronze Age.

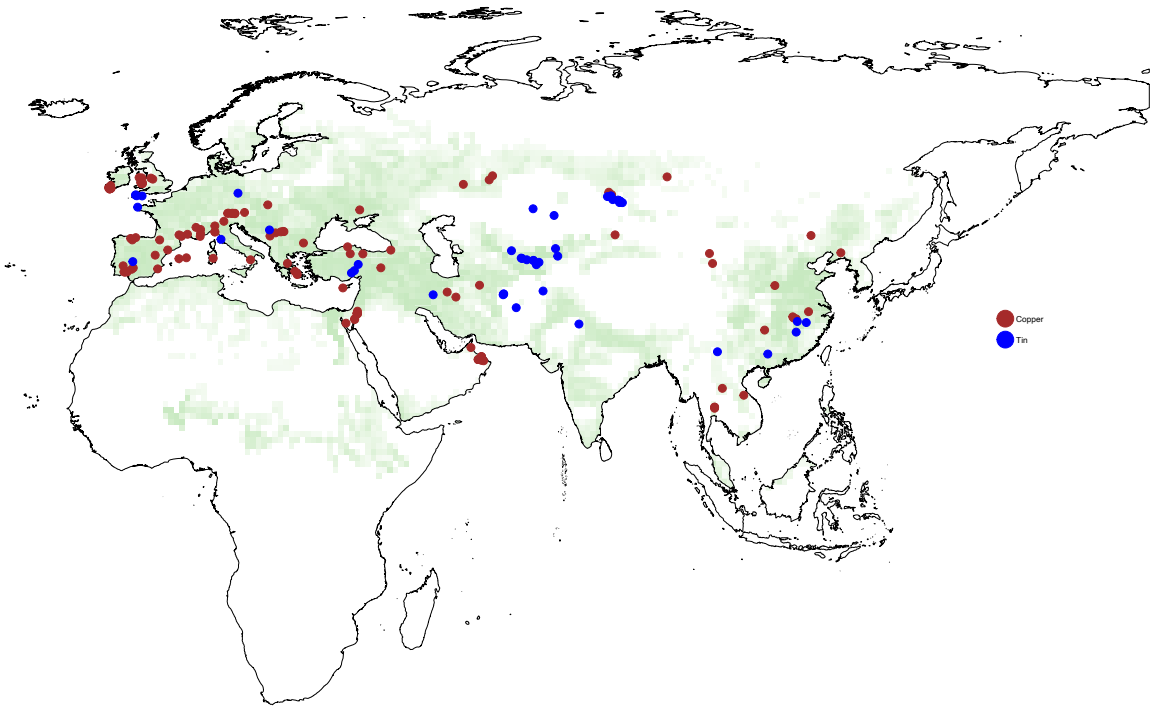


Figure A.9: Mines and croplands

Figure shows the location of mines and croplands. Copper mines are symbolized by red dots, tin mines by blue dots. Croplands are depicted in green.

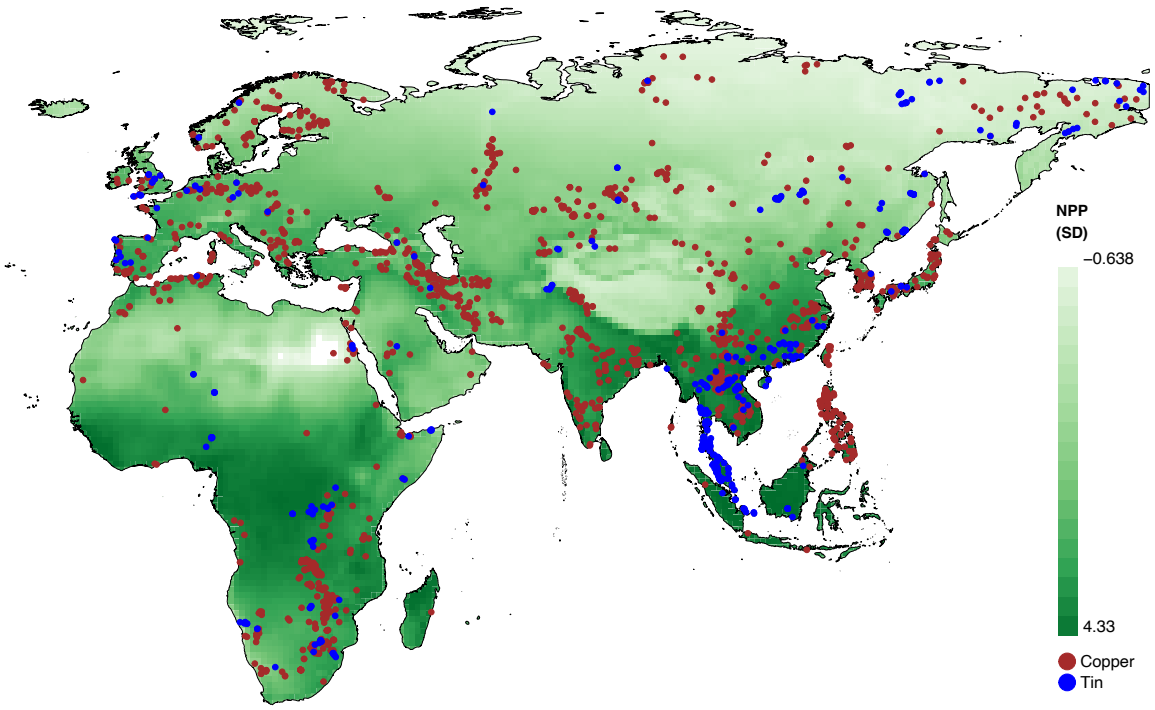


Figure A.10: Deposits and NPP

Figure depicts the spatial distribution of copper deposits (brown dots), tin deposits (blue dots), and NPP (green shadings, where darker shadings imply higher values of NPP).

Appendix B: Bronze Age transit regions

This appendix describes the construction of our metal transit indices, as well as other measures of centrality and proximity.

B.1 Measures of centrality

Having estimated the relative transport costs across the shipping modes available during the Bronze Age, we can now construct a variety of centrality measures within the transport network. The construction processes are described below.

B.1.1 Metal transit indices

Metal transit index We construct the metal transit index by combining the transport cost surface, the estimated relative transport costs for the Bronze Age, cropland areas, and information on the location of copper and tin mines.

We proceed in three steps.

First, using the estimated Bronze Age transport costs ($\widehat{\boldsymbol{\alpha}}$) and the topographic map, we compute the least-cost paths connecting each grid cell with cropland (in 3000 BC) to each Bronze Age tin and copper mine using Dijkstra (1959)'s algorithm. To exclude impractically long routes, we discard paths for which total transport cost exceeds the cost of traveling a distance equivalent to 10,000 kilometers by sea.[48]

Second, for each cropland cell f, we select the tin mine and the copper mine with the lowest transport cost to f. Denote these selected mines by $Sn^\star(f)$ and $Cu^\star(f)$, respectively, and let $P^\star_{Sn^\star(f),\,f}$ and $P^\star_{Cu^\star(f),\,f}$ be the corresponding least-cost paths from these mines to cell f. Figure B.1 shows the full set of these least-cost paths, together with the locations of mines and croplands.

Third, for each grid cell k, we compute a "metal transit index", T_k, as the cropland-weighted count of these selected least-cost paths that traverse k:

$$T_k = \sum_{f \in \mathcal{F} \setminus \{k\}} \left(\mathcal{I}_{P^\star_{Sn^\star(f),\,f}}[k] + \mathcal{I}_{P^\star_{Cu^\star(f),\,f}}[k] \right) \text{Crop}_f \,.$$

where $\mathcal{F}$ is the set of all grid cells with cropland; $\mathcal{I}_{P^\star_{Sn^\star(f),\,f}}[k]$ is an indicator function equal to 1 if $k \in P^\star_{Sn^\star(f),\,f}$; $\mathcal{I}_{P^\star_{Cu^\star(f),\,f}}[k]$ is an indicator function equal to 1 if $k \in P^\star_{Cu^\star(f),\,f}$; $Crop_f$ is the cropland area (measured in square kilometers) in grid cell f in 3000 BC. T_k thus measures the square kilometers of cropland for which the cost-minimizing routes to access tin and copper mines traverse cell k.

Natural metal transit index We compute our instrumental variable, the natural metal transit trade potential, following a procedure analogous to that outlined in the preceding paragraph. The two main differences are that we replace the locations of mines with those of deposits, and we use net primary productivity instead of cropland areas as destination weights. Formally, the instrument is given by:

$$D_k = \sum_{f \in \mathcal{F}} \left(\mathcal{I}_{P^\star_{DSn^\star(f),\,f}}[k] + \mathcal{I}_{P^\star_{DCu^\star(f),\,f}}[k] \right) \text{Prod}_f \,.$$

[48] This threshold has negligible impact on the results.

where $DSn^{\star}(f)$ and $DCu^{\star}(f)$ denote the tin and copper deposits with the lowest transport cost to f; and $Prod_f$ is the net primary production of cell f in 3000 BC.[49]

Figure B.2 visualizes the spatial variation in the natural metal transit index.

Natural metal transit index (Stone Age) We construct an alternative version of our instrumental variable using relative transport costs estimated for the Stone Age, rather than for the Bronze Age.

B.1.2 Other measures of centrality and proximity

Centrality in the natural transport network Based on the transport cost surface, we compute the eigenvector centrality for each 0.25×0.25 degree grid cell. We then assign each 1×1 degree cell the eigenvector value based on the location of its center point.

Proximity to croplands Combining the transport cost surface, estimated relative transport costs during the Bronze Age, and cropland data, we compute our measure of proximity to croplands, defined as the inverse transport costs-weighted sum of cropland areas for each cell. Formally, proximity to croplands, PC_k, is given by:

$$PC_k = \sum_{f \in \mathcal{F} \setminus \{k\}} \frac{1}{LC_{f,k}} \times Crop_f,$$

where $LC_{f,k}$ are the transport cost from grid cell f to cell k and $Crop_f$ is the croplands area of cell f.

Proximity to mines We compute proximity to mines by combining the transport cost surface, estimated relative transport costs during the Bronze Age, and information on the location of copper and tin mines. For each 1×1 cell, we identify the tin and copper mine, respectively, associated with the lowest transport costs. We then use the inverse of the sum of transport costs to these mines as our measure for proximity to mines. Formally, proximity to mines PM_k is defined as:

$$PM_k = \frac{1}{LC_{Sn^{\star}(k),k} + LC_{Cu^{\star}(k),k}},$$

where $LC_{Sn^{\star}(k),k}$ and $LC_{Cu^{\star}(k),k}$ are the transport costs from the cost-minimizing tin and copper mines to grid cell k, $Sn^{\star}(k)$ and $Cu^{\star}(k)$, respectively. That is, the denominator is simply the sum of the shipping costs to the cost-minimizing copper mine and the cost-minimizing tin mine.

Transit paths to croplands Combining the transport cost surface, estimated relative transport costs during the Bronze Age, and cropland areas, we identify the least-cost paths from each 1×1 degree cell to the nearest cropland. For our empirical analysis, we then count the number of least-cost paths that intersect each 1×1 degree cell.

Transit paths to mines Combining the transport cost surface, estimated relative transport costs during the Bronze Age, and the locations of copper and tin mines, we identify the least-cost paths

[49] More precisely, it is the average across the years 4000–3000 BC.

from each 1×1 degree cell to the nearest copper and tin mine. For our empirical analysis, we then count the number of least-cost paths that intersect each 1×1 degree cell.

Metal transit index (distance) We construct the transit index (distance) in analogy to our main transit index. The only difference is that we use geographical distance to measure transport costs, rather than the Bronze Age and mode-specific relative transport costs.

Transit paths to NPP Combining the transport cost surface, estimated relative transport costs during the Bronze Age, and NPP, we identify the least-cost paths from each 1×1 degree cell to the nearest cell with NPP. For our empirical analysis, we then count the number of least-cost paths that intersect each 1×1 degree cell.

Transit paths to deposits Combining the transport cost surface, estimated relative transport costs during the Bronze Age, and the locations of copper and tin deposits, we identify the least-cost paths from each 1×1 degree cell to the nearest copper and tin deposit. For our empirical analysis, we then count the number of least-cost paths that intersect each 1×1 degree cell.

Natural metal transit index (distance) We construct the IV transit index (distance) in analogy to our main instrumental variable. The only difference is that we use geographical distance to measure transport costs, rather than the Bronze Age and mode-specific relative transport costs.

B.2 Maps centrality measures

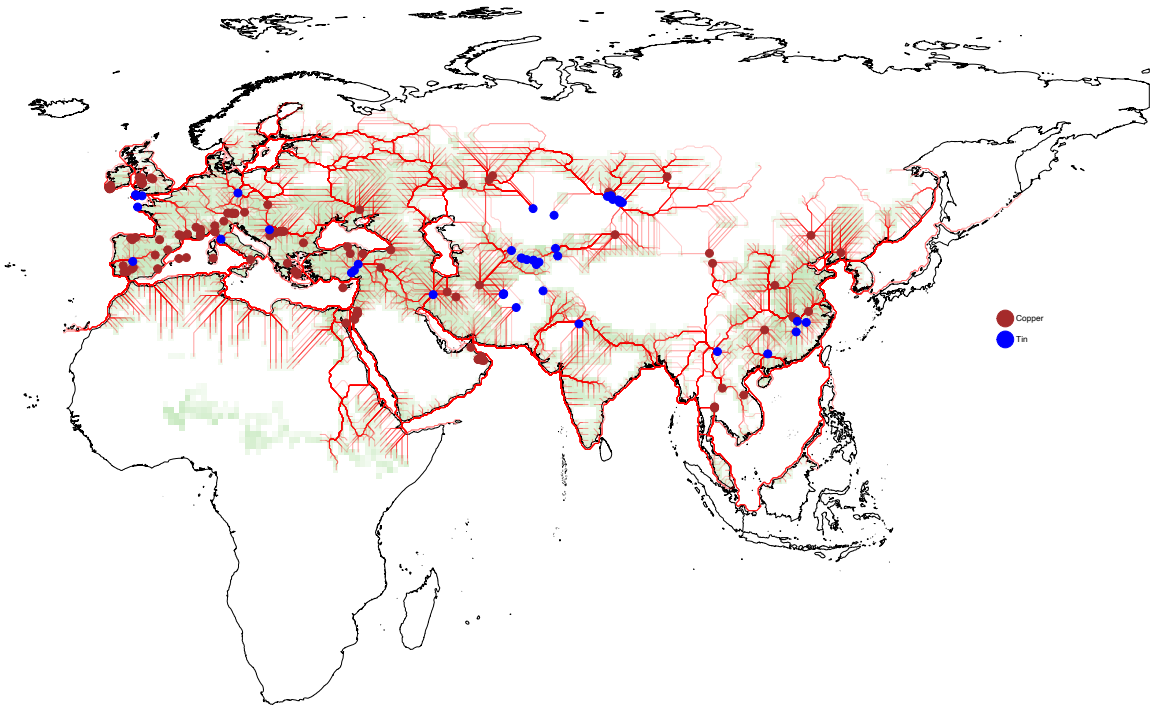


Figure B.1: Least-cost paths to mines
This figure shows the location of mines and croplands and the least-cost paths connecting each cropland cell to its least-cost copper and tin mine. Copper mines are shown as red dots and tin mines as blue dots. Least-cost paths are shown in red.

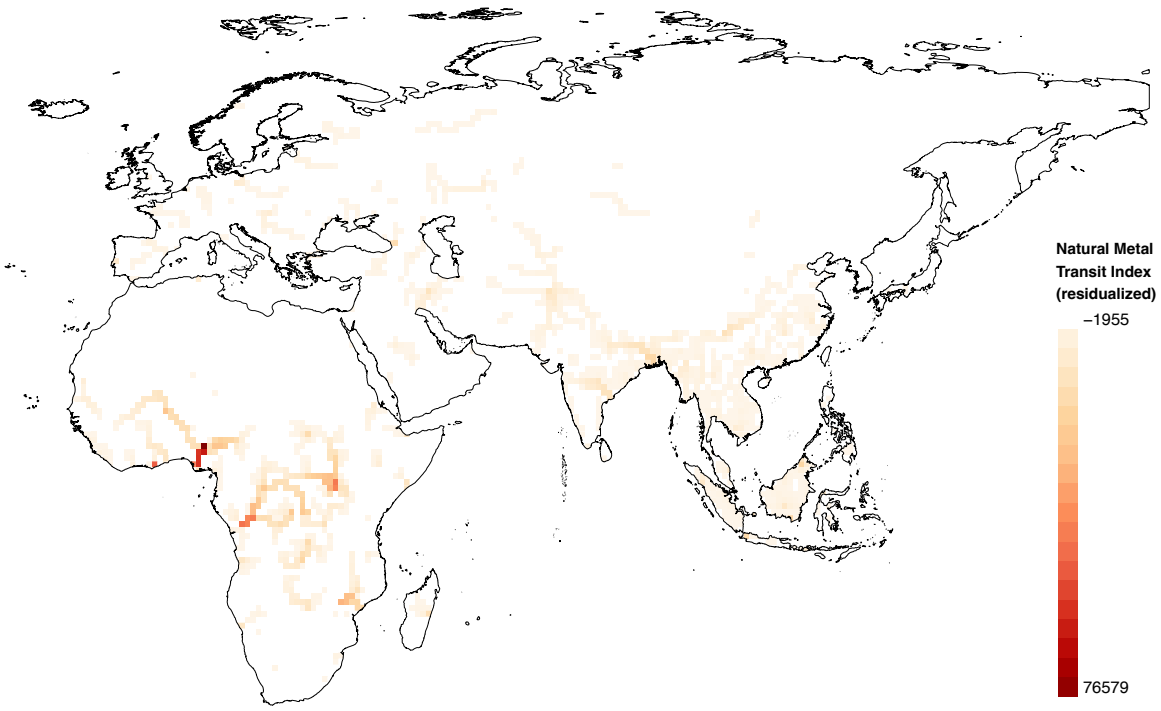


Figure B.2: Natural metal transit index
Figure visualises the instrumental variable (where continent dummies are partialled out).

Appendix C: Descriptive analysis

This appendix presents summary statistics for the key variables used in the main analysis, along with descriptive visualizations that illustrate relationships between selected variables. Specifically, we examine the interplay between metal transit trade and city presence.

C.1 Summary statistics

Table C.1: Summary statistics of key variables

Variable	Mean	Std. Dev.	Min.	Max.	Obs.
	A. Cross-sectional dataset (Section 4.1)				
Any city or citadel[a]	0.005	0.069	0	1	10970
# Cities or citadels[a]	0.006	0.096	0	4	10970
Any City by 1300 BC[b]	0.004	0.065	0	1	10970
# Cities by 1300 BC[b]	0.006	0.113	0	7	10970
Metal transit index	170.348	1009.305	0	30914.167	10970
Natural metal transit index	800.279	2934.963	0	78533.632	10970
Blockage cost	5.865	83.485	0	5603.685	10970
Proximity mines	26.098	32.779	0.007	1515.855	10970
Proximity croplands	203.179	116.551	0.172	854.335	10970
Sea	0.262	0.440	0	1	10970
River	0.162	0.368	0	1	10970
Mountains	0.021	0.143	0	1	10970
Centrality	6465.834	308265.612	0	21797914.336	10970
	B. Panel dataset archaeological sites (Section 4.2)				
Any Site[c]	0.049	0.216	0	1	21940
Any Settlement[c]	0.007	0.084	0	1	21940
Any Major Settlement[c]	0.003	0.053	0	1	21940
Any Elite Burial[c]	0.004	0.061	0	1	21940
Any Burial[c]	0.009	0.097	0	1	21940
Any Site[d]	0.018	0.131	0	1	21940
Any Settlement[d]	0.015	0.123	0	1	21940
Any Elite Burial[d]	0.001	0.032	0	1	21940
Any Burial[d]	0.004	0.063	0	1	21940
	C. China (Section 4.3)				
Any Criterion	0.179	0.384	0	1	2138
Principal component	0	1	-0.395	3.991	2138
Any Settlement	0.058	0.235	0	1	2138
Any Monumental Buildings	0.071	0.257	0	1	2138
Any Ruling Class	0.074	0.262	0	1	2138
Any Systems of Recording	0.093	0.291	0	1	2138
Any Writing	0.128	0.334	0	1	2138
Any Art	0.133	0.340	0	1	2138

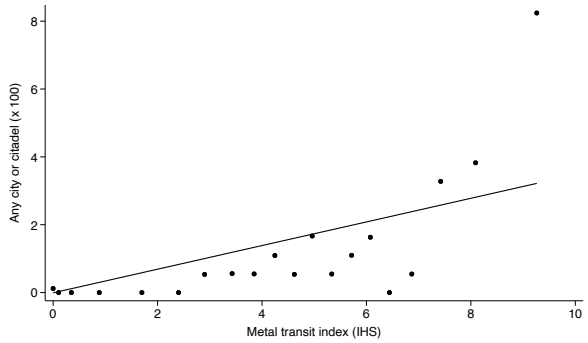
Notes: [a]data from Green et al. (2024); [b]data from Reba, Reitsma and Seto (2016); [c]data from Bahn (2000); [d]data from Pleiades.

C.2 Metal transit trade and cities

The binned scatterplots in Figure C.1 provide an alternative visualization of the positive relationship between metal transit trade volumes and city locations. The first row shows that higher values of the transit trade index are associated with a greater prevalence of cities. Panel (a) uses data from Green et al. (2024), while Panel (b) uses data from Reba, Reitsma and Seto (2016).

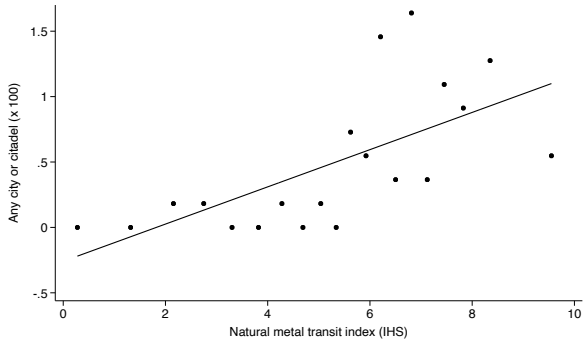
The second row illustrates the association between the natural metal transit index—i.e., our instrumental variable—and city occurrence. Again, we observe a clear positive relationship, irrespective of the city data used.

Metal transit index and cities



Panel (a)

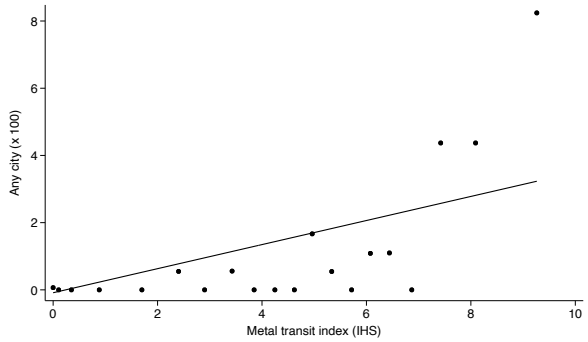
(a) The figure shows a binned scatterplot of the IHS-transformed metal transit index versus the occurrence of cities. City data are from Green et al. (2024).



Panel (b)

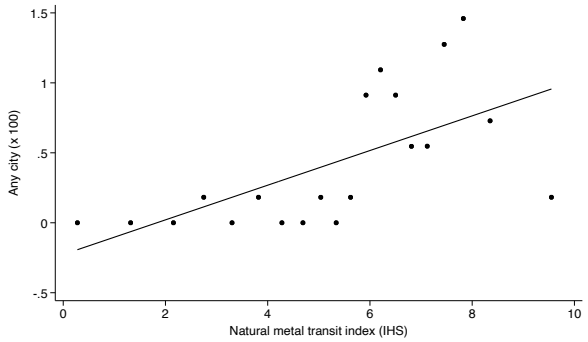
(b) The figure shows a binned scatterplot of the IHS-transformed metal transit index versus the occurrence of cities. City data are from Reba, Reitsma and Seto (2016).

Natural metal transit index and cities



Panel (c)

(c) The figure shows a binned scatterplot of the IHS-transformed natural metal transit index versus the occurrence of cities. City data are from Green et al. (2024).



Panel (d)

(d) The figure shows a binned scatterplot of the IHS-transformed natural metal transit index versus the occurrence of cities. City data are from Reba, Reitsma and Seto (2016).

Figure C.1: Scatterplots of metal transit trade versus city occurrence

Appendix D: Additional analysis and robustness checks

This appendix presents additional analyses conducted in support of our main findings. It also reports a wide range of robustness checks.

D.1 Additional analysis and robustness checks urban settlements

This section of the appendix presents robustness checks for the cross-sectional analysis of urban settlements reported in Table 1, along with supplementary analyses. For completeness, we first report the point estimates of the control variables and the reduced-form estimates (Sections D.1.1–D.1.2). Then we move on to discussing the additional analysis and robustness checks briefly outlined in the main paper. Specifically, we

1. analyze the effects of the metal transit index over time and how this relates to the transition from arsenic bronze to tin bronze (Section D.1.3).
2. address worries related to the possibility of the endogeneity of the relative transportation cost (Section D.1.4).
3. exploit data on megasites to illustrate that our effects are unlikely to capture persistence or path dependence, i.e., the possibility that Bronze Age urbanization patterns simply follow the trajectory of pre-existing Neolithic settlement patterns (Section D.1.5). In the separate appendix—Appendix D.4—we further show that our estimates do not conflate the effects of other widely traded goods.
4. dig deeper into the metal transit index and investigate how it compares to alternative measures of connectedness (Section D.1.6).
5. assess the effects of land productivity and agriculture on urbanization (Section D.1.7).
6. investigate heterogeneities of the effect of the metal transit index with respect to proximity to croplands and mines (Section D.1.8).
7. use alternative standard error clustering approaches to illustrate that our results are not dependent on one particular choice (Section D.1.9).
8. conduct further robustness checks (Section D.1.10). These include: (a) varying the geographical scope of our analysis, (b) adding additional control variables, (c) using smaller grid cells as units of observation, (d) reproducing our 2SLS IV results using the IV probit approach, and (e) using alternative urban population data.

D.1.1 Point estimates control variables

In Tables D.1 and D.2, we re-run the same regression models and specifications as in Table 1 Panel A and B. The only difference is that we not only show the coefficients of the main regressors of interest, but also report the point estimates of the control variables. Table D.1 uses the Green et al. (2024) data as outcome, while Table D.2 uses the Reba, Reitsma and Seto (2016) data. It is noteworthy that—as in any multivariate regression—the estimates of the controls reflect conditional effects, that is, their partial associations with Bronze Age urbanization, holding all other covariates constant.

As expected, proximity to cropland is positively and statistically significantly associated with the presence of urban settlements, underscoring the role of access to fertile lands in early urban development. Sea access and centrality in the transport network also exhibit positive and occasionally significant effects. In contrast, proximity to mines enters with a negative sign in some specifications, potentially because mines are typically situated in mountainous or agriculturally marginal regions.[50]

[50] Unconditionally, there is a positive association between the presence of cities and proximity to mines.

Table D.1: Metal transit trade and Bronze Age cities. Regressions of Table 1, Panel A, with coefficients of controls reported.

	OLS		Probit		2SLS IV			
	(1)	(2)	(3)	(4)	(5)	(6)	(7)	(8)
	Panel A: Second stage Green et al. (2024): Any city or citadel (×100)							
Metal transit index (IHS)	0.344	0.353	0.156	0.086	0.407	0.483		
	(0.074)	(0.076)	(0.025)	(0.028)	(0.089)	(0.126)		
	[0.094]	[0.097]	[0.009]	[0.012]	[0.123]	[0.164]		
Proximity mines		-0.420		0.063		-0.650		-1.346
		(0.333)		(0.120)		(0.353)		(0.572)
		[0.419]		[0.057]		[0.443]		[0.826]
Proximity croplands		0.639		1.030		0.841		1.627
		(0.389)		(0.223)		(0.403)		(0.656)
		[0.486]		[0.106]		[0.502]		[0.942]
River		0.120		0.058		-0.073		-0.900
		(0.265)		(0.141)		(0.346)		(0.501)
		[0.327]		[0.078]		[0.371]		[0.628]
Mountains		0.304				0.277		0.309
		(0.339)				(0.331)		(0.338)
		[0.365]				[0.349]		[0.357]
Sea		0.554		0.114		0.607		0.407
		(0.245)		(0.144)		(0.259)		(0.268)
		[0.253]		[0.062]		[0.275]		[0.274]
Centrality		0.020				0.002		-0.015
		(0.019)				(0.023)		(0.025)
		[0.021]				[0.026]		[0.030]
Metal transit index							0.002	0.003
							(0.001)	(0.001)
							[0.001]	[0.001]
					Panel B: First stage			
Natural metal transit index (IHS)					0.490	0.308	86.183	43.091
					(0.031)	(0.030)	(13.032)	(8.275)
					[0.051]	[0.048]	[18.407]	[11.294]
Geography controls	No	Yes	No	Yes	No	Yes	No	Yes
Continent dummies	Yes	Yes	Yes	Yes	Yes	Yes	Yes	Yes
Observations	10,970	10,970	10,970	10,970	10,970	10,970	10,970	10,970
Mean dependent variable	0.483	0.483	0.483	0.483	0.483	0.483	0.483	0.483
R-squared	0.016	0.018	0.177	0.259				
First-stage F-stat (5×5 grids)					251.000	102.261	43.734	27.115
First-stage F-stat (Conley 1000km)					92.374	40.999	21.690	14.389

Notes: Panel A reports cross-sectional OLS, probit, and 2SLS IV estimates of equation (4). Panel B reports the corresponding first-stage estimates (equation (5)). The unit of observation is a 1×1-degree grid cell k. 'Any city or citadel' equals 100 if a city or citadel was present in grid cell k during the Bronze Age (and 0 otherwise). 'Metal transit index' is defined by equation (2), while 'Natural metal transit index' is defined by equation (3). Footnotes 18 and 21 describe the construction of the controls: Geography controls include proximity to mines, proximity to croplands, sea dummy, river dummy, mountains dummy, and centrality in the transport network. Standard errors clustered at the level of 5×5 degree grid cells are reported in parentheses. Standard errors computed using the approach of Conley (1999) (cut-off 1000km) are reported in square brackets.

Table D.2: Metal transit trade and Bronze Age cities. Regressions of Table 1, Panel B, with coefficients of controls reported.

	OLS		Probit		2SLS IV			
	(1)	(2)	(3)	(4)	(5)	(6)	(7)	(8)
	Panel B: Second stage Reba, Reitsma and Seto (2016): Any city (×100)							
Metal transit index (IHS)	0.383	0.424	0.201	0.092	0.342	0.312		
	(0.087)	(0.093)	(0.029)	(0.033)	(0.083)	(0.095)		
	[0.134]	[0.141]	[0.011]	[0.012]	[0.124]	[0.127]		
Proximity mines		-1.238		-0.141		-1.041		-1.490
		(0.392)		(0.175)		(0.374)		(0.513)
		[0.594]		[0.066]		[0.543]		[0.766]
Proximity croplands		1.568		1.843		1.395		1.903
		(0.482)		(0.224)		(0.461)		(0.608)
		[0.738]		[0.123]		[0.686]		[0.919]
River		0.383		0.161		0.549		0.015
		(0.253)		(0.132)		(0.338)		(0.366)
		[0.356]		[0.069]		[0.483]		[0.545]
Mountains		-0.059				-0.036		-0.015
		(0.242)				(0.252)		(0.221)
		[0.291]				[0.312]		[0.259]
Sea		0.538		-0.119		0.492		0.363
		(0.198)		(0.180)		(0.197)		(0.183)
		[0.236]		[0.062]		[0.224]		[0.196]
Centrality		0.004				0.019		0.008
		(0.014)				(0.021)		(0.020)
		[0.023]				[0.033]		[0.031]
Metal transit index							0.002	0.002
							(0.000)	(0.001)
							[0.001]	[0.001]
					Panel B: First stage			
Natural metal transit index (IHS)					0.490	0.308	86.183	43.091
					(0.031)	(0.030)	(13.032)	(8.275)
					[0.051]	[0.048]	[18.407]	[11.294]
Geography controls	No	Yes	No	Yes	No	Yes	No	Yes
Continent dummies	Yes	Yes	Yes	Yes	Yes	Yes	Yes	Yes
Observations	10,970	10,970	10,970	10,970	10,970	10,970	10,970	10,970
Mean dependent variable	0.419	0.419	0.419	0.419	0.419	0.419	0.419	0.419
R-squared	0.022	0.028	0.254	0.422				
First-stage F-stat (5×5 grids)					251.000	102.261	43.734	27.115
First-stage F-stat (Conley 1000km)					92.374	40.999	21.690	14.389

Notes: Panel A reports cross-sectional OLS, probit, and 2SLS IV estimates of equation (4). Panel B reports the corresponding first-stage estimates (equation (5)). The unit of observation is a 1×1-degree grid cell k. 'Any city by 1300 BC' equals 100 if a city was present in grid cell k by 1300 BC (and 0 otherwise). 'Metal transit index' is defined by equation (2), while 'Natural metal transit index' is defined by equation (3). Footnotes 18 and 21 describe the construction of the controls: Geography controls include proximity to mines, proximity to croplands, sea dummy, river dummy, mountains dummy, and centrality in the transport network. Standard errors clustered at the level of 5×5 degree grid cells are reported in parentheses. Standard errors computed using the approach of Conley (1999) (cut-off 1000km) are reported in square brackets.

D.1.2 Reduced-form estimates

The reduced-form results reported in Table D.3 show a strong and robust association between the natural metal transit index and Bronze Age urbanization outcomes. Throughout, the reduced-form coefficients are positive and statistically significant at the 99% confidence level, regardless of whether control variables are included. These findings support the hypothesis that regions with greater exogenous potential for metal transit trade were more likely to develop urban settlements during the Bronze Age. This highlights both the relevance of the instrument and the economic justification behind our IV strategy.

Table D.3: Reduced-form estimates corresponding to Table 1: Natural metal transit index and Bronze Age cities

	(5)	(6)	(7)	(8)
	Panel A: Reduced-form Green et al. (2024): Any city or citadel (×100)			
Natural metal transit index (IHS)	0.199	0.149	0.199	0.149
	(0.046)	(0.042)	(0.046)	(0.042)
	[0.065]	[0.056]	[0.065]	[0.056]
	Panel B: Reduced-form Reba, Reitsma and Seto (2016): Any city (×100)			
Natural metal transit index (IHS)	0.168	0.096	0.168	0.096
	(0.043)	(0.032)	(0.043)	(0.032)
	[0.065]	[0.044]	[0.065]	[0.044]
Geography controls	No	Yes	No	Yes
Continent dummies	Yes	Yes	Yes	Yes
Observations	10,970	10,970	10,970	10,970
Mean dependent variable Panel A	0.483	0.483	0.483	0.483
Mean dependent variable Panel B	0.419	0.419	0.419	0.419
R-squared Panel A	0.006	0.008	0.006	0.008
R-squared Panel B	0.004	0.010	0.004	0.010

Notes: Panels A and B report cross-sectional reduced-form estimates of equation (4) corresponding to Table 1. The unit of observation is a 1×1-degree grid cell k. 'Any city or citadel' equals 100 if a city or citadel was present in grid cell k during the Bronze Age (and 0 otherwise). 'Any city by 1300 BC' equals 100 if a city was present in grid cell k by 1300 BC (and 0 otherwise). 'Natural metal transit index' is defined by equation (3). Footnotes 18 and 21 describe the construction of the controls: Geography controls include proximity to mines, proximity to croplands, sea dummy, river dummy, mountains dummy, and centrality in the transport network. Standard errors clustered at the level of 5×5 degree grid cells are reported in parentheses. Standard errors computed using the approach of Conley (1999) (cut-off 1000km) are reported in square brackets.

D.1.3 The transition from arsenic bronze to tin bronze

Using the city data from Reba, Reitsma and Seto (2016), Appendix Figure D.1 showcases the effects of the metal transit index over time. For every 500-year interval between 3300 BC and 1300 BC, we estimate our preferred cross-sectional 2SLS IV model (4), including the full set of geographic controls. The outcome variable is a binary indicator capturing whether a city had emerged in a given grid cell by the respective time period. The figure shows that while the estimated coefficient for the transit index is consistently positive, it rises between 3300 BC and 2300 BC and remains stable thereafter. Notably, it only becomes statistically significant from 2800 BC onwards. In Appendix Figures D.2 and D.3, the analysis differentiates between transit routes leading to copper and tin mines. As can be seen, the copper transit index becomes relevant from 2800 BC, while the tin transit index only five centuries later. As discussed in the main text, this timing aligns with the transition from arsenic bronze to tin bronze during the latter part of the third millennium BC.

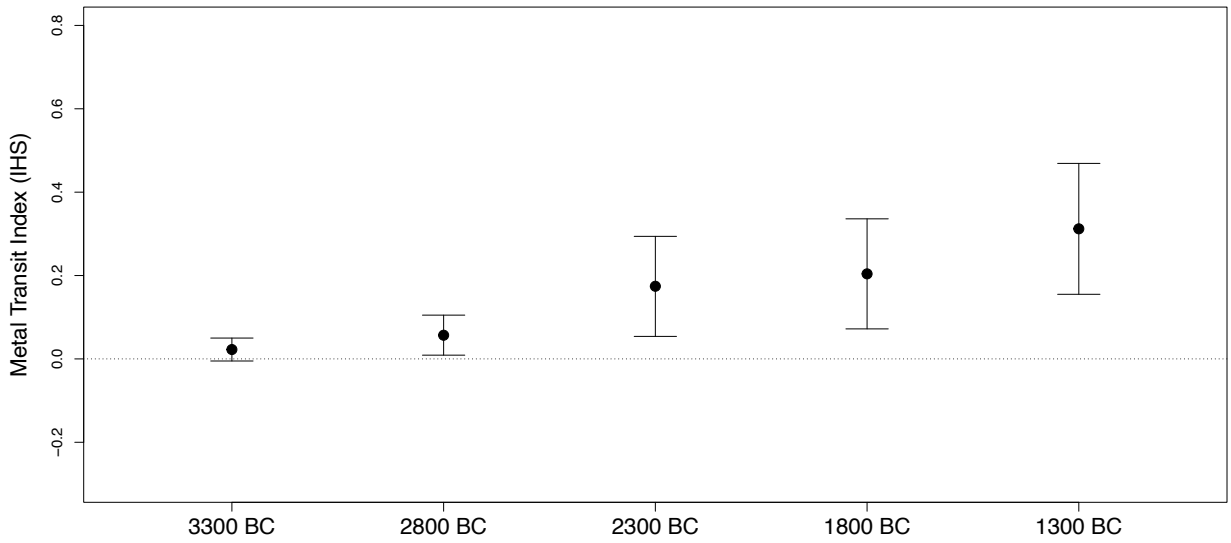


Figure D.1: Cities and metal transit index over time

Figure depicts cross-sectional 2SLS-IV point estimates and 90% confidence intervals of θ in equation (4). Standard errors are clustered at the level of 5×5 degree grid cells. Dependent variable is a dummy equal to 100 if a city site was present in a given 1×1 degree grid and period, and zero otherwise.

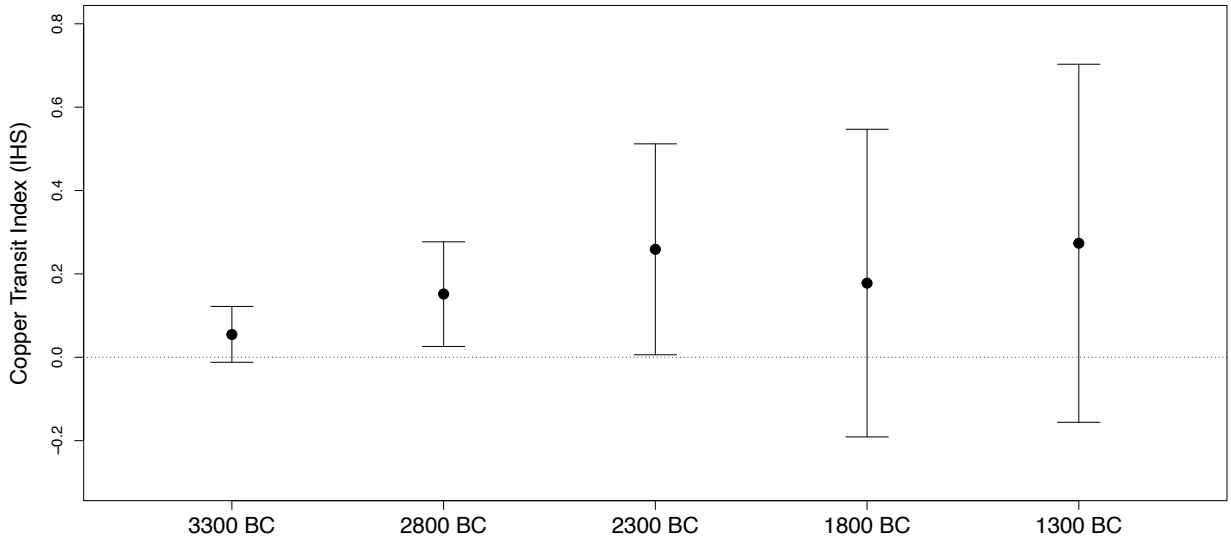


Figure D.2: Cities and copper transit index over time
Figure depicts cross-sectional 2SLS-IV point estimates and 90% confidence intervals of θ in equation (4). Standard errors are clustered at the level of 5×5 degree grid cells. Dependent variable is a dummy equal to 100 if a city site was present in a given 1×1 degree grid and period, and zero otherwise.

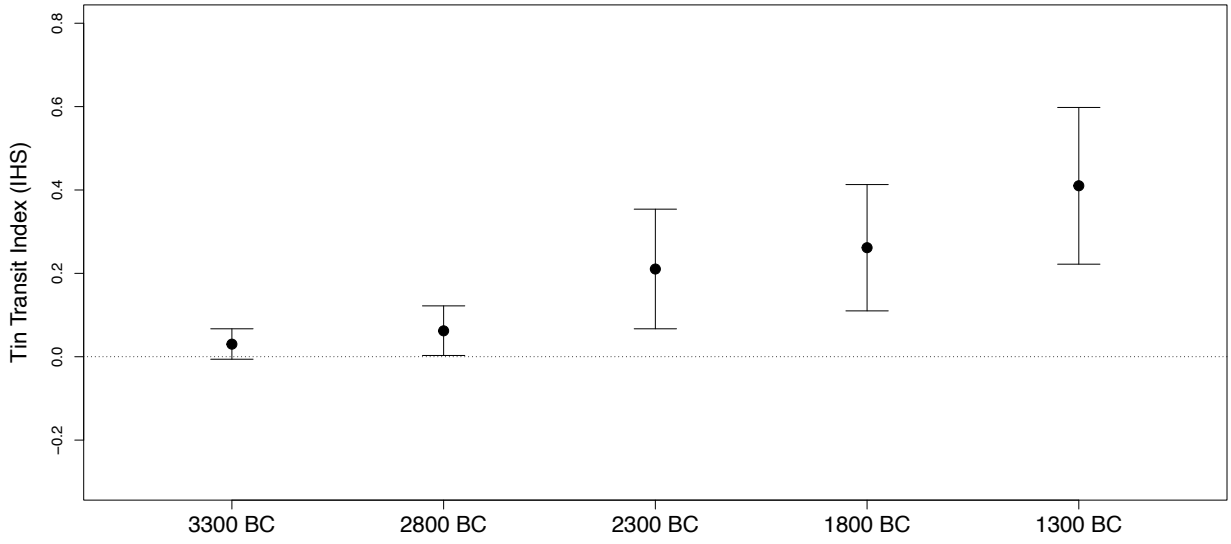


Figure D.3: Cities and tin transit index over time
Figure depicts cross-sectional 2SLS-IV point estimates and 90% confidence intervals of θ in equation (4). Standard errors are clustered at the level of 5×5 degree grid cells. Dependent variable is a dummy equal to 100 if a city site was present in a given 1×1 degree grid and period, and zero otherwise.

D.1.4 Endogeneity of relative transport costs

A potential concern regarding the exogeneity of our excluded instrument arises from the fact that part of its variation is driven by the estimates of mode-specific relative transport costs. As outlined in Section 3.1, these costs are estimated from Bronze Age trade relationships in Europe and the Middle East. This might pose a threat to our identification strategy since Bronze Age transportation technologies might have been specifically tailored to the needs of civilizations in Europe and the Middle East: cities might be central in the metal trade network not because they initially emerged in natural passage regions between mines and croplands but because they acquired this centrality by developing specific transportation technologies to gain easy access to cropland and mines. To address this concern, we conduct two robustness checks, which are reported in the first two columns of Appendix Table D.4. First, we document that our estimates remain stable if we restrict the spatial extent of our analysis to areas that are not used in the estimation of the relative transportation costs (columns (1)–(2)). Second, we employ relative transportation costs estimated for the Stone Age, rather than the Bronze Age, in constructing our instrument (columns (3)-(4)). In both cases, the results are virtually unchanged.

Table D.4: Robustness endogeneity $\boldsymbol{\alpha_{BA}}$: Metal transit trade and Bronze Age cities

	(1)	(2)	(3)	(4)
	Panel A: Second stage Green et al. (2024): Any city or citadel (×100)			
Metal transit index (IHS)	0.373	0.451	0.421	0.516
	(0.095)	(0.128)	(0.095)	(0.152)
	[0.131]	[0.162]	[0.134]	[0.199]
	Panel B: Second stage Reba, Reitsma and Seto (2016): Any city (×100)			
Metal transit index (IHS)	0.302	0.313	0.339	0.298
	(0.080)	(0.095)	(0.087)	(0.107)
	[0.116]	[0.124]	[0.121]	[0.129]
	Panel C: First stage			
Natural metal transit index (IHS)	0.444	0.287	0.450	0.271
	(0.031)	(0.030)	(0.029)	(0.027)
	[0.052]	[0.047]	[0.048]	[0.043]
Geography controls	No	Yes	No	Yes
Continent dummies	Yes	Yes	Yes	Yes
Observations	10,058	10,058	10,970	10,970
Mean dependent variable Panel A	0.328	0.328	0.483	0.483
Mean dependent variable Panel B	0.288	0.288	0.419	0.419
First-stage F-statistic (5×5 grids)	199.770	92.294	238.801	102.018
First-stage F-statistic (Conley 1000km)	73.275	36.829	87.467	39.124
Robustness check	Drop extent $\boldsymbol{\alpha_{BA}}$		Natural metal transit index using $\boldsymbol{\alpha_{SA}}$	

Notes: Panels A and B of this table report second-stage estimates of the cross-sectional 2SLS IV model (4). Panel C reports the corresponding first-stage estimates (equation (5)). The unit of observation is a 1×1 grid-cell k. 'Any city or citadel' equals 100 if a city or citadel was present in grid cell k during the Bronze Age (and 0 otherwise). 'Any city by 1300 BC' equals 100 if a city was present in grid cell k by 1300 BC (and 0 otherwise). 'Metal transit index' is defined by equation (2), while 'Natural metal transit index' is defined by equation (3). Columns (1)–(2) restrict the spatial extent of the analysis to grid cells not used in the estimation of the relative transport costs across different transportation modes during the Bronze Age. In columns (3)–(4), the instrumental variable is constructed using the relative transport costs estimated for the Stone Age rather than the Bronze Age. Geography controls include proximity to mines, proximity to croplands, sea dummy, river dummy, mountains dummy, and centrality in the transport network. Standard errors clustered at the level of 5×5 degree grid cells are reported in parentheses. Standard errors computed using the approach of Conley (1999) (cut-off 1000km) are reported in square brackets.

D.1.5 Exploiting Data on Megasites

In this appendix, we use information on the location of large Neolithic settlements—"megasites"—to test for pre-trends. In the first part, we incorporate additional data from Green et al. (2024); in the second part, we use landscape data from Lawrence, Hinojosa-Balino and Chelazzi (2025).

Megasites Green et al. (2024)

The Green et al. (2024) data include both large Neolithic settlements and Bronze Age urban settlements. This allows us to assess whether our main results reflect persistence or path dependence—i.e., the possibility that Bronze Age urbanization patterns simply follow the trajectory of pre-existing Neolithic settlement patterns. To this end, we apply our cross-sectional 2SLS IV approach (equation (4)) using our preferred specification (Table 1, column (6)). The only difference is that we use the presence of large Neolithic settlements, rather than Bronze Age urban areas, as the outcome variable.

Table D.5 presents the results. Reassuringly, we find no evidence that natural metal transit potential is associated with the presence of large Neolithic settlements. Coefficients are close to zero and statistically insignificant across all specifications and variations in the definition of the outcome variable. These findings suggest that Bronze Age urbanization does not merely reflect pre-existing Neolithic settlement dynamics, but instead represents a new urban geography which is influenced by long-distance metal trade during the Bronze Age. We further support this claim by

Table D.5: Neolithic: Transit trade, cities and citadels (Green et al., 2024)

	Any City or Citadel (×100)		Any Citadel (×100)		Any City (×100)	
	(1)	(2)	(3)	(4)	(5)	(6)
	Panel A: Second stage					
Metal transit index (IHS)	0.025		0.011		-0.001	
	(0.060)		(0.043)		(0.040)	
	[0.069]		[0.043]		[0.050]	
Metal transit index		0.000		0.000		-0.000
		(0.000)		(0.000)		(0.000)
		[0.000]		[0.000]		[0.000]
	Panel B: First stage					
Natural metal transit index (IHS)	0.308	43.091	0.308	43.091	0.308	43.091
	(0.030)	(8.274)	(0.030)	(8.274)	(0.030)	(8.274)
	[0.048]	[11.294]	[0.048]	[11.294]	[0.048]	[11.294]
Geography controls	Yes	Yes	Yes	Yes	Yes	Yes
Continent dummies	Yes	Yes	Yes	Yes	Yes	Yes
Observations	10,970	10,970	10,970	10,970	10,970	10,970
Mean dependent variable	0.164	0.164	0.055	0.055	0.100	0.100
First-stage F-stat (5×5 grids)	102.261	27.115	102.261	27.115	102.261	27.115
First-stage F-stat (Conley 1000km)	40.999	14.389	40.999	14.389	40.999	14.389

Notes: Panel A reports 2SLS estimates of equation (4). Panel B reports the corresponding first-stage estimates (equation (5)). The unit of observation is a 1×1 grid-cell k. 'Any city or citadel' ('Any Citadel', 'Any City') equals 100 rather than 0 for a grid cell k if there is at least one city or citadel (citadel, city) located in grid cell k. 'Metal transit index' is defined by equation (2), while 'Natural metal transit index' is defined by equation (3). Geography controls include proximity to mines, proximity to croplands, sea dummy, river dummy, mountains dummy, and centrality in the transport network. Panel B reports first-stage estimates (equation (7)). Standard errors clustered at the level of 5×5 degree grid cells are reported in parentheses. Standard errors computed using the approach of Conley (1999) (cut-off 1000km) are reported in square brackets.

jointly exploiting information on the locations of both Neolithic and Bronze Age settlements and implementing our standard 2SLS IV difference-in-differences approach (cf. equation (6)). Table D.6 shows that the metal transit index exerts a strong differential effect in the Bronze Age relative to the preceding Neolithic period. The interaction between the metal transit index and the Bronze Age indicator enters positively and significantly across all specifications—whether the outcome is defined as any city or citadel, only citadels, or only cities. The results are robust to using both the IHS-transformed and the raw values of the metal transit index. The corresponding first-stage estimates in Panel B confirm a strong and statistically significant relationship between the instrument (the natural metal transit index) and the endogenous regressor in this panel setting. Taken together, the

Table D.6: Difference-in-differences: Transit trade, cities and citadels (Green et al., 2024)

	Any City or Citadel (×100)		Any Citadel (×100)		Any City (×100)	
	(1)	(2)	(3)	(4)	(5)	(6)
	Panel A: Second stage					
Metal transit index (IHS) × Bronze Age	0.458		0.168		0.243	
	(0.124)		(0.083)		(0.071)	
	[0.115]		[0.075]		[0.064]	
Metal transit index × Bronze Age		0.003		0.001		0.002
		(0.001)		(0.001)		(0.000)
		[0.001]		[0.001]		[0.000]
	Panel B: First stage					
Natural metal transit index (IHS) × Bronze Age	0.308	43.091	0.308	43.091	0.308	43.091
	(0.030)	(8.274)	(0.030)	(8.274)	(0.030)	(8.274)
	[0.034]	[7.986]	[0.034]	[7.986]	[0.034]	[7.986]
Geography controls×Bronze Age	Yes	Yes	Yes	Yes	Yes	Yes
Grid cell fixed effects	Yes	Yes	Yes	Yes	Yes	Yes
Continent×Bronze Age	Yes	Yes	Yes	Yes	Yes	Yes
Observations	21,940	21,940	21,940	21,940	21,940	21,940
Mean dependent variable	0.324	0.324	0.132	0.132	0.164	0.164
First-stage F-stat (5×5 grids)	102.289	27.122	102.289	27.122	102.289	27.122
First-stage F-stat (Conley 1000km)	82.079	28.807	82.079	28.807	82.079	28.807

Notes: Panel A reports difference-in-differences 2SLS IV estimates of equation (6). Panel B reports the corresponding first-stage estimates (equation (7)). The unit of observation is a 1×1 grid-cell k in period p (Stone Age or Neolithic). 'Any city or citadel' ('Any Citadel', 'Any City') equals 100 rather than 0 for a grid cell k in period p if there is at least one city or citadel (citadel, city) dating from period p and located in grid cell k. 'Metal transit index' is defined by equation (2), while 'Natural metal transit index' is defined by equation (3). Geography controls include proximity to mines, proximity to croplands, sea dummy, river dummy, mountains dummy, and centrality in the transport network. Standard errors clustered at the level of 5×5 degree grid cells are reported in parentheses. Standard errors computed using the approach of Conley (1999) (cut-off 1000km) are reported in square brackets.

results presented in Tables D.5–D.6 suggest that our findings are not biased by path dependence or persistence in settlement patterns. However, an important caveat pertains to the relatively small number of large Neolithic settlements in the Green et al. (2024) dataset—only 18 observations in the pre-Bronze Age period—which may raise concerns about attenuation bias. To address this concern, we replicate the above exercises using a structurally different type of data.

Megasites Lawrence, Hinojosa-Balino and Chelazzi (2025)

To provide additional evidence that our results do not reflect effects of persistence, we draw on recent findings from the field of Landscape Archaeology. Specifically, we use data from Lawrence,

Hinojosa-Balino and Chelazzi (2025), who systematically map the dynamics of urbanization in Southwest Asia and Egypt.[51] Their database contains information on settlement sizes and locations across the study region over time. It includes all settlements that exceeded 10 hectares in size between 10,000 BP and 1,000 BP—the threshold used in this study to define an urban area. The main advantage of the Lawrence, Hinojosa-Balino and Chelazzi (2025) data is its consistent application of a size threshold and the availability of continuous measures of settlement area. The main drawback is its relatively limited geographical scope.

For our empirical analysis, we construct a panel dataset by aggregating the information at the 1×1-degree grid cell level, separately for the Neolithic and the Bronze Age.[52] The dependent variable is the total urban area within each grid cell. The spatial distribution of the 387 urban areas is shown as dots in panels (a) and (b) of Figure D.4. Across the study area, the number of urban areas increased substantially during the Bronze Age, most notably in Egypt and Lower Mesopotamia.

In analogy to the analysis above, we begin by focusing exclusively on the Neolithic period. Specifically, we apply our cross-sectional 2SLS IV model using the size of Neolithic settlements as the outcome, restricting the sample to grid cells that intersect with the Lawrence, Hinojosa-Balino and Chelazzi (2025) study area. These 40 grid cells are shaded in gray in Figure D.4.

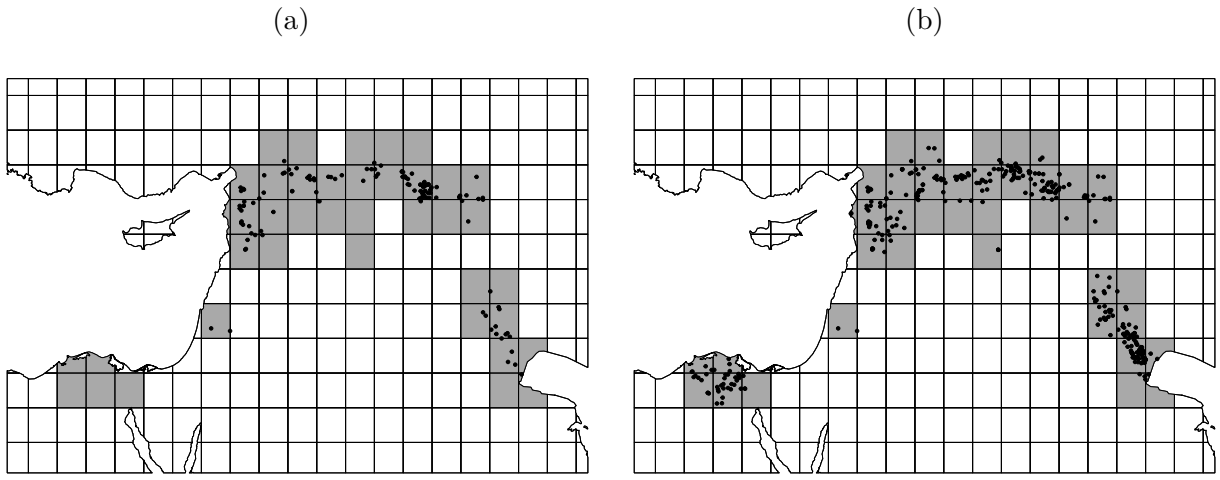


Figure D.4: Urban areas Lawrence, Hinojosa-Balino and Chelazzi (2025)
Figure depicts the location of urban areas—defined as settlements occupying more than 10 hectares–from Lawrence, Hinojosa-Balino and Chelazzi (2025). Panel (a) shows sites present in the Neolithic, panel (b) sites present in the Bronze Age. Grid cells shaded gray are included in our regression analysis.

Table D.7 illustrates that we continue to find no evidence of a relationship between the metal transit index and Neolithic settlement patterns. None of the regression specifications produce statistically significant results. This reinforces our earlier conclusion that the observed influence of metal transit trade on Bronze Age urbanization is unlikely to be driven by persistence in pre-existing settlement structures.[53]

In Table D.8, we exploit the full temporal dimension of the Lawrence, Hinojosa-Balino and Chelazzi (2025) data and implement our 2SLS IV difference-in-differences regression framework (see equa-

[51] We thank Daniel Lawrence for providing the data.

[52] We define the Bronze Age as spanning from 3300 BC to 1300 BC. Our results are robust to alternative cut-off values.

[53] A potential concern is the relatively low value of the first-stage F-statistic. However, the reduced-form regressions yield the same pattern of results: there is no statistically significant relationship between the natural metal transit index and the size of Neolithic settlement areas.

Table D.7: Neolithic: Urban areas and metal transit trade (Lawrence, Hinojosa-Balino and Chelazzi, 2025)

	Total Urban Area (IHS)		Total Urban Area	
	(1)	(2)	(3)	(4)
	Panel A: Second stage			
Metal transit index (IHS)	-0.361		-32.211	
	(0.342)		(39.521)	
	[0.370]		[33.860]	
Metal transit index		-0.000		-0.025
		(0.000)		(0.034)
		[0.000]		[0.026]
	Panel B: First stage			
Natural metal transit index (IHS)	1.293	1690.961	1.293	1690.961
	(0.542)	(702.151)	(0.542)	(702.151)
	[0.556]	[665.509]	[0.556]	[665.509]
Geography controls	Yes	Yes	Yes	Yes
Continent dummies	Yes	Yes	Yes	Yes
Observations	40	40	40	40
Mean dependent variable	3.199	3.199	138.690	138.690
First-stage F-stat (1×1 grids)	5.693	5.800	5.693	5.800
First-stage F-stat (Conley 1000km)	3.166	3.769	3.166	3.769

Panel A reports 2SLS estimates of equation (4), while panel B reports the first-stage estimates (equation (7)). The unit of observation is a 1×1 grid-cell k. 'Total Urban Area' is the total number of hectares occupied by settlements that occupy more than 10 hectares in grid cell k. 'Metal transit index' is defined by equation (2), while 'Natural metal transit index' is defined by equation (3). Geography controls include proximity to mines, proximity to croplands, sea dummy, river dummy, mountains dummy, and centrality in the transport network. Standard errors clustered at the level of 1×1 degree grid cells are reported in parentheses. Standard errors computed using the approach of Conley (1999) (cut-off 1000km) are reported in square brackets.

tion (6)), again restricting the analysis to the geographical scope of their study. Even within this limited region, we find evidence consistent with our argument that Bronze Age transit trade shaped the spatio-temporal pattern of urbanization. For example, the estimate reported in Panel A, column (4), implies that an additional metal transit path leading to a cropland area of 1,000 km increases urban area by 96 hectares. Evaluated at the sample mean, this corresponds to a doubling of urban area.

Table D.8: Difference-in-differences: Urban areas and metal transit trade (Lawrence, Hinojosa-Balino and Chelazzi, 2025)

	Total Urban Area (IHS)		Total Urban Area	
	(1)	(2)	(3)	(4)
	Panel A: Second stage			
Metal transit index (IHS)	0.805		125.071	
× Bronze Age	(0.472)		(73.369)	
	[0.353]		[33.010]	
Metal transit index		0.001		0.096
× Bronze Age		(0.000)		(0.067)
		[0.000]		[0.024]
	Panel B: First stage			
Natural metal transit index (IHS)	1.293	1690.961	1.293	1690.961
× Bronze Age	(0.390)	(660.368)	(0.390)	(660.368)
	[0.393]	[470.586]	[0.393]	[470.586]
Geography controls×Bronze Age	Yes	Yes	Yes	Yes
Grid cell fixed effects	Yes	Yes	Yes	Yes
Continent×Bronze Age	Yes	Yes	Yes	Yes
Observations	80	80	80	80
Mean dependent variable	4.528	4.528	271.697	271.697
First-stage F-stat (1×1 grids)	11.019	6.557	11.019	6.557
First-stage F-stat (Conley 1000km)	8.833	10.517	8.833	10.517

Panel A reports 2SLS estimates of equation (6), while panel B reports the first-stage estimates (equation (7)). The unit of observation is a 1×1 grid-cell k in period p (Stone Age or Bronze Age). 'Total Urban Area' is the total number of hectares occupied by settlements that occupy more than 10 hectares in grid cell k and period p. 'Metal transit index' is defined by equation (2), while 'Natural metal transit index' is defined by equation (3). Geography controls include proximity to mines, proximity to croplands, sea dummy, river dummy, mountains dummy, and centrality in the transport network. Standard errors clustered at the level of 1×1 degree grid cells are reported in parentheses. Standard errors computed using the approach of Conley (1999) (cut-off 1000km) are reported in square brackets.

D.1.6 Digging deeper into the metal transit index measure

Table D.9 (Panel A) delves deeper into identifying the specific components of the centrality measure that underpin the Urban Revolution, using the data from Green et al. (2024). Column (1) mirrors our standard OLS regression, identifying road-knots in the trade network via our benchmark metal transit index, which captures the least-cost paths linking square kilometers of farmland to the least-cost tin and copper mines. Subsequently, we explore three alternative transit indices. First, we consider a transit index that counts the least-cost paths passing through a cell, connecting every grid cell in the Old World to the nearest farmland (column 2). Second, we consider a transit index that counts the least-cost paths passing through a cell, connecting every grid cell in the Old World to the nearest tin and copper mine (column 3). Third, we consider a transit index similar to our benchmark, but based on the shortest paths—assuming equal transportation cost across sea, river, and land—between farmland and mines (column 4). The estimates reveal that while these alternative transit indices are somewhat linked to urban presence, including them as control variables (alone or jointly) does not notably change the association between our primary transit index and the existence of Bronze Age cities (see columns 5–8). Panel B of Table D.9 corroborates this insight using reduced-form estimates, where variation in the explanatory variables is driven by exogenous components (i.e., metal deposits and net primary productivity).

The takeaway from Table D.9 is that during the Bronze Age, the key factor for urban development was not simply being in a well-connected area with easy access to farmlands, mines, or other territories. Rather, it was crucial to be a transit hub that linked agricultural areas with tin and copper mines using Bronze Age transport technologies.

Table D.10 repeats the same exercise using the city data from Reba, Reitsma and Seto (2016). The qualitative pattern of results is equivalent.

Table D.9: Metal transit trade and Bronze Age cities (Green et al., 2024). Disentangling the transit index.

	Green et al. (2024): Any city or citadel (×100)							
	(1)	(2)	(3)	(4)	(5)	(6)	(7)	(8)
	Panel A: OLS							
Metal transit index (transport costs)	0.353 (0.076) [0.097]				0.353 (0.075) [0.094]	0.360 (0.073) [0.092]	0.236 (0.080) [0.096]	0.240 (0.073) [0.087]
Transit paths to cropland		-0.210 (0.065) [0.086]			0.001 (0.040) [0.044]			0.045 (0.040) [0.046]
Transit paths to mines			0.217 (0.088) [0.100]			-0.023 (0.066) [0.060]		0.003 (0.065) [0.060]
Metal transit index (distance)				0.299 (0.059) [0.071]			0.159 (0.054) [0.053]	0.165 (0.054) [0.053]
	Panel B: Reduced Form							
Natural metal transit index (transport costs)	0.149 (0.042) [0.056]				0.149 (0.043) [0.056]	0.152 (0.045) [0.059]	0.232 (0.105) [0.106]	0.262 (0.108) [0.105]
Transit paths to NPP		-0.355 (0.180) [0.144]			0.239 (0.345) [0.293]			0.544 (0.409) [0.342]
Transit paths to deposits			0.072 (0.072) [0.085]			-0.019 (0.075) [0.089]		-0.065 (0.067) [0.078]
Natural metal transit index (distance)				0.100 (0.048) [0.058]			-0.095 (0.113) [0.110]	-0.117 (0.113) [0.106]
Geography controls	Yes	Yes	Yes	Yes	Yes	Yes	Yes	Yes
Observations	10,970	10,970	10,970	10,970	10,970	10,970	10,970	10,970
Mean dependent variable	0.483	0.483	0.483	0.483	0.483	0.483	0.483	0.483

Notes: This table reports cross-sectional OLS estimates of equation (4) and cross-sectional reduced-form estimates. The unit of observation is a 1×1 grid-cell k. 'Any city or citadel' equals 100 if a city or citadel was present in grid cell k during the Bronze Age (and 0 otherwise). 'Metal transit index' is defined by equation (2), while 'Natural metal transit index' is defined by equation (3). 'Transit paths to cropland' counts the least-cost paths intersecting the cell while connecting every grid cell in the Old World to the nearest farmland. 'Transit paths to mines' counts the least-cost paths intersecting the cell while connecting every grid cell in the Old World to the nearest copper and tin mine. 'Transit paths to NPP' counts the least-cost paths intersecting the cell while connecting every grid cell in the Old World to the nearest cell with positive estimated net primary production. 'Transit paths to deposits' counts the least-cost paths intersecting the cell while connecting every grid cell in the Old World to the nearest copper and tin deposits. Geography controls include proximity to mines, proximity to croplands, sea dummy, river dummy, mountains dummy, and centrality in the transport network. Standard errors clustered at the level of 5×5 degree grid cells are reported in parentheses. Standard errors computed using the approach of Conley (1999) (cut-off 1000km) are reported in square brackets.

Table D.10: Metal transit trade and Bronze Age cities (Reba, Reitsma and Seto, 2016). Disentangling the transit index.

	Reba, Reitsma and Seto (2016): Any city by 1300 (×100)							
	(1)	(2)	(3)	(4)	(5)	(6)	(7)	(8)
	Panel A: OLS							
Metal transit index (transport costs)	0.424				0.418	0.433	0.322	0.325
	(0.093)				(0.089)	(0.099)	(0.075)	(0.080)
	[0.141]				[0.135]	[0.152]	[0.111]	[0.120]
Transit paths to cropland		-0.279			-0.030			0.009
		(0.085)			(0.043)			(0.041)
		[0.127]			[0.052]			[0.051]
Transit paths to mines			0.258			-0.031		-0.006
			(0.070)			(0.059)		(0.058)
			[0.101]			[0.087]		[0.084]
Metal transit index (distance)				0.330			0.140	0.140
				(0.077)			(0.049)	(0.048)
				[0.115]			[0.061]	[0.058]
	Panel B: Reduced Form							
Natural metal transit index (transport costs)	0.096				0.096	0.108	0.212	0.279
	(0.032)				(0.032)	(0.037)	(0.074)	(0.082)
	[0.044]				[0.044]	[0.057]	[0.089]	[0.108]
Transit paths to NPP		-0.430			-0.047			0.537
		(0.231)			(0.347)			(0.481)
		[0.234]			[0.322]			[0.468]
Transit paths to deposits			-0.014			-0.079		-0.149
			(0.077)			(0.086)		(0.088)
			[0.089]			[0.112]		[0.115]
Natural metal transit index (distance)				0.046			-0.132	-0.182
				(0.034)			(0.077)	(0.076)
				[0.048]			[0.097]	[0.096]
Geography controls	Yes	Yes	Yes	Yes	Yes	Yes	Yes	Yes
Observations	10,970	10,970	10,970	10,970	10,970	10,970	10,970	10,970
Mean dependent variable	0.419	0.419	0.419	0.419	0.419	0.419	0.419	0.419

Notes: This table reports cross-sectional OLS estimates of equation (4) and cross-sectional reduced-form estimates. The unit of observation is a 1×1 grid-cell k. 'Any city by 1300 BC' equals 100 if a city was present in grid cell k by 1300 BC (and 0 otherwise). 'Metal transit index' is defined by equation (2), while 'Natural metal transit index' is defined by equation (3). 'Transit paths to cropland' counts the least-cost paths intersecting the cell while connecting every grid cell in the Old World to the nearest farmland. 'Transit paths to mines' counts the least-cost paths intersecting the cell while connecting every grid cell in the Old World to the nearest copper and tin mine. 'Transit paths to NPP' counts the least-cost paths intersecting the cell while connecting every grid cell in the Old World to the nearest cell with positive estimated net primary production. 'Transit paths to deposits' counts the least-cost paths intersecting the cell while connecting every grid cell in the Old World to the nearest copper and tin deposits. Geography controls include proximity to mines, proximity to croplands, sea dummy, river dummy, mountains dummy, and centrality in the transport network. Standard errors clustered at the level of 5×5 degree grid cells are reported in parentheses. Standard errors computed using the approach of Conley (1999) (cut-off 1000km) are reported in square brackets.

D.1.7 Land productivity and agriculture

In Appendix Table D.11, we re-run our baseline 2SLS IV model (cf. Table 1, column (5)) while controlling for various measures of land productivity that have been employed in the comparative development literature. As discussed in Section 1, land productivity is commonly cited as a determinant of early urbanization and social hierarchy. However, conditional on the metal transit trade index, the measures of land productivity are generally not associated with the presence of cities. Furthermore, including land productivity as a control does not markedly affect the point estimate for the metal transit index.

Table D.11: Robustness check controlling for differences in land fertility: Metal transit trade and Bronze Age cities.

	(1)	(2)	(3)	(4)
	Panel A: Second stage Green et al. (2024): Any city or citadel (×100)			
Metal transit index (IHS)	0.376	0.518	0.570	0.665
	(0.086)	(0.257)	(0.161)	(0.179)
	[0.123]	[0.261]	[0.212]	[0.245]
Farming	0.260	-0.076	-0.049	-2.061
	(0.190)	(0.151)	(0.028)	(0.909)
	[0.189]	[0.131]	[0.032]	[1.171]
	Panel B: Second stage Reba, Reitsma and Seto (2016): Any city (×100)			
Metal transit index (IHS)	0.222	0.543	0.486	0.615
	(0.069)	(0.194)	(0.122)	(0.156)
	[0.087]	[0.272]	[0.166]	[0.224]
Farming	1.001	-0.136	-0.043	-2.175
	(0.473)	(0.116)	(0.020)	(0.758)
	[0.538]	[0.165]	[0.027]	[1.016]
	Panel C: First stage			
Natural metal transit index (IHS)	0.465	0.450	0.386	0.337
	(0.030)	(0.049)	(0.033)	(0.033)
	[0.048]	[0.076]	[0.050]	[0.053]
Farming land	Share cropland area	NPP	CSI Galor and Özak (2016)	Ramankutty et al (2011)
Geography controls	No	No	No	No
Continent fixed effects	Yes	Yes	Yes	Yes
Observations	10,970	10,970	10,970	10,970
Mean dependent variable Panel A	0.483	0.483	0.483	0.483
Mean dependent variable Panel B	0.419	0.419	0.419	0.419
First-stage F-stat (5×5 grids)	246.139	83.274	140.081	102.267
First-stage F-stat (Conley 1000km)	92.071	34.541	58.859	40.335

Notes: Panel A and B report cross-sectional 2SLS estimates of equation (4). Panel C reports the corresponding first-stage estimates (equation (5)). The unit of observation is a 1×1 grid-cell k. 'Any city or citadel' equals 100 if a city or citadel was present in grid cell k during the Bronze Age (and 0 otherwise). 'Any city by 1300 BC' equals 100 if a city was present in grid cell k by 1300 BC (and 0 otherwise). 'Metal transit index' is defined by equation (2), while 'Natural metal transit index' is defined by equation (3). 'Farming land' is 1) the share of cropland area in the grid cell in 3000 BC (column 1); 2) the Net Primary Production using reconstructed climatic conditions in 3000 BC (column 2); 3) the Caloric Suitability index (Galor and Özak, 2015) (column 3); 4) the fraction of land suitable for agriculture (Ramankutty et al., 2002) (column 4). Standard errors clustered at the level of 5×5 degree grid cells are reported in parentheses. Standard errors computed using the approach of Conley (1999) (cut-off 1000km) are reported in square brackets.

D.1.8 Heterogeneities

Table D.12 investigates whether the relationship between metal transit trade and Bronze Age urbanization varies depending on local access to key complementary resources—namely, fertile croplands and metal ore deposits. While our main analysis shows that metal transit trade might have played an important role in fostering the Urban Revolution, this effect might be amplified in places where local conditions also provide easy access to fertile land or metal resources. To explore the degree of heterogeneity along the first dimension, we split the grid cells into two groups according to whether the grid-cell-specific value of proximity to croplands lies above or below the sample median. For both groups, we then estimate separate slope coefficients for the metal transit effect. In columns (1)–(3), we report the corresponding results from OLS, reduced-form, and 2SLS IV regressions. Throughout, we use the city data from Green et al. (2024) as outcomes. Columns (1) and (2)—the OLS and reduced-form estimates—reveal that the estimated effect of metal transit potential is substantially larger and statistically significant in areas located relatively close to croplands, while it is small and not statistically different from zero in areas farther from fertile zones. This pattern is consistent with the idea that urbanization benefits from the interaction between metal trade centrality and easy access to fertile grounds, which—given the Malthusian setting—can also be interpreted as easy access to markets. In the 2SLS IV estimates in column (3), the point estimate of the transit index for areas far from cropland remains statistically insignificant but becomes large in magnitude. However, the magnitude of the coefficients should be interpreted cautiously, as the corresponding first-stage F-statistic lies well below the conventional threshold value of 10.

In columns (4)–(6), we investigate heterogeneities with respect to proximity to mines. Again, we group the grid cells into two categories according to whether they are located closer to or farther from metal mines than the sample median, and estimate separate coefficients. This produces a pattern of results similar to that observed for proximity to croplands: the effects of metal transit trade on urbanization are strongly concentrated in locations near metal resources.[54]

Taken together, the results suggest that the influence of metal transit corridors on urbanization was not uniform across space but was complementary to environments with favorable local conditions. The effects of metal transit trade are stronger and more precisely estimated in areas close to cropland and near metal resources, pointing to such a complementary relationship: transit hubs were more likely to evolve into urban centers when embedded in geography that supported food production or metallurgy.

[54] Again, the 2SLS IV results (column (6)) should be interpreted with caution given the relatively low first-stage F-statistic.

Table D.12: Heterogeneities: Metal transit trade, proximity to croplands, and proximity to mines.

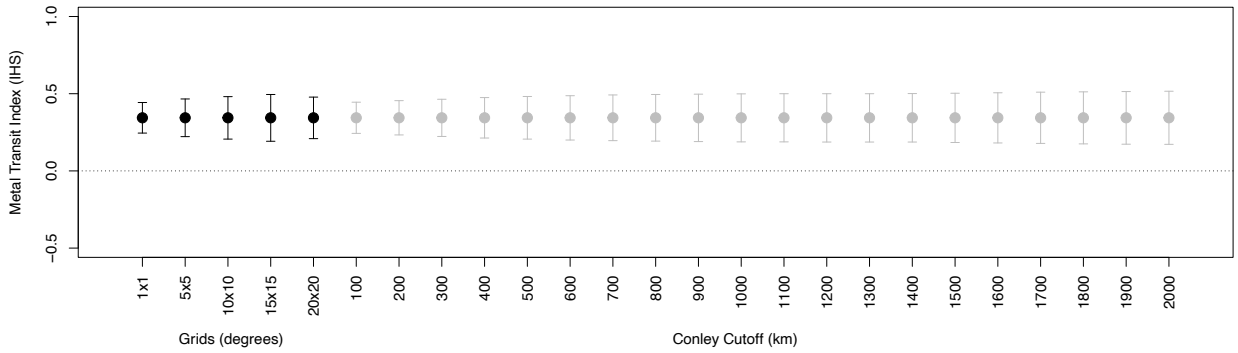
	Green et al. (2024): Any city or citadel (×100)					
	Heterogeneity: Proximity to croplands			Heterogeneity: Proximity to mines		
	OLS	Reduced form	2SLS IV	OLS	Reduced form	2SLS IV
	(1)	(2)	(3)	(4)	(5)	(6)
Far from croplands × Metal transit index (IHS)	0.042 (0.049) [0.061]		0.719 (1.240) [1.208]			
Close to croplands × Metal transit index (IHS)	0.373 (0.079) [0.098]		0.511 (0.130) [0.175]			
Far from croplands × Natural metal transit index (IHS)		0.010 (0.039) [0.039]				
Close to croplands × Natural metal transit index (IHS)		0.300 (0.078) [0.104]				
Far from mines × Metal transit index (IHS)				-0.011 (0.032) [0.034]		0.778 (1.038) [1.062]
Close to mines × Metal transit index (IHS)				0.365 (0.078) [0.097]		0.524 (0.159) [0.202]
Far from mines× Natural metal transit index (IHS)					0.050 (0.045) [0.047]	
Close to mines × Natural metal transit index (IHS)					0.196 (0.048) [0.064]	
Geography controls	Yes	Yes	Yes	Yes	Yes	Yes
Continent dummies	Yes	Yes	Yes	Yes	Yes	Yes
Observations	10,970	10,970	10,970	10,970	10,970	10,970
Mean dependent variable	0.483	0.483	0.483	0.483	0.483	0.483
First-stage F-stat (5×5 grids)			5.434			11.319
First-stage F-stat (Conley 1000km)			2.116			5.844

Notes: The table reports cross-sectional OLS, reduced-form and 2SLS IV estimates of equation (4). The unit of observation is a 1×1-degree grid cell k. 'Any city or citadel' equals 100 if a city or citadel was present in grid cell k during the Bronze Age (and 0 otherwise). 'Metal transit index' is defined by equation (2), while 'Natural metal transit index' is defined by equation (3). Footnotes 18 and 21 describe the construction of the controls: Geography controls include proximity to mines, proximity to croplands, sea dummy, river dummy, mountains dummy, and centrality in the transport network. The table reports separate slope coefficients for grid cells with proximity to croplands above (below) the median (rows 1–4), and for grid cells that are closer to (farther from) tin and copper mines than the median (rows 5–8). Standard errors clustered at the level of 5×5 degree grid cells are reported in parentheses. Standard errors computed using the approach of Conley (1999) (cut-off 1000km) are reported in square brackets.

D.1.9 Standard error clustering

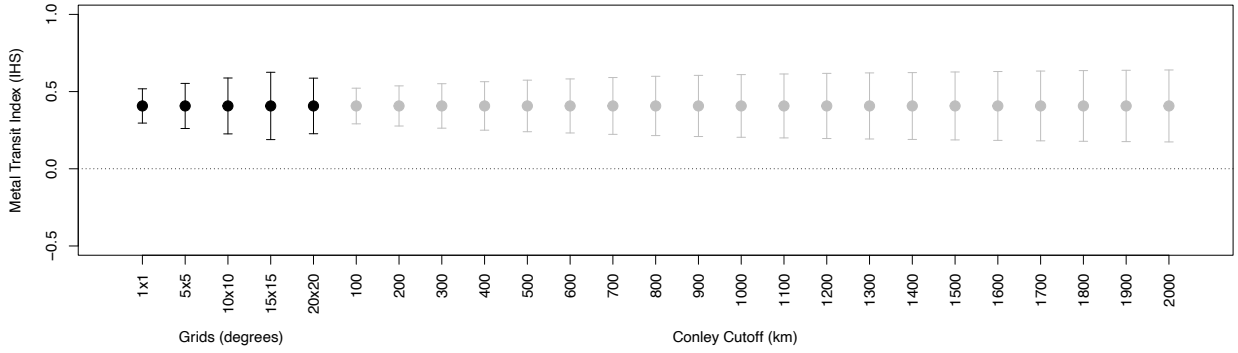
We use two approaches to correct for spatial autocorrelation of the error term: clustering at the 5×5 grid cell level, and Conley (1999) standard errors with distance cutoffs of 1,000 km. Here, we show how the cross-sectional results are affected by varying the size of the clustering grid (from 1×1 to 20×20) and the Conley cutoff (from 100 km to 2,000 km). The takeaway is that the size of the standard errors are only slightly affected by these changes.

Panel (a)



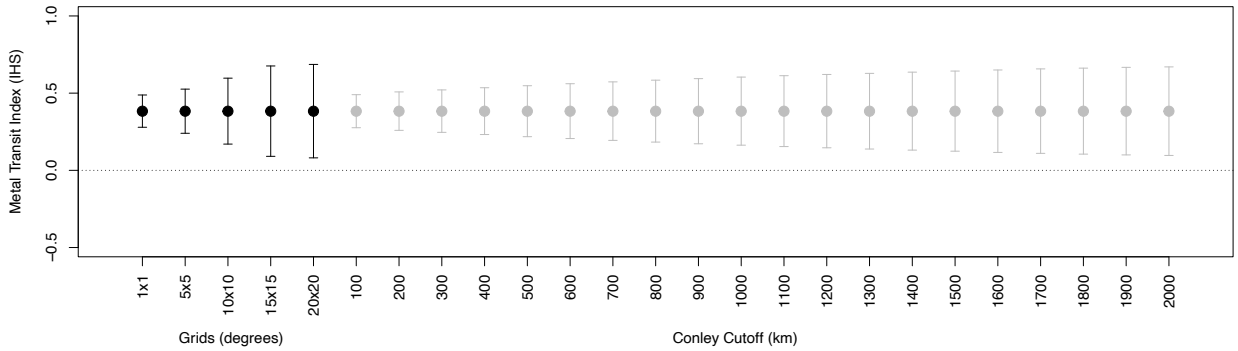
(a) Figure shows the OLS point estimate of Table 1 (Panel A column (1)) along with alternative standard error clustering approaches. Standard errors depicted in black are clustered at grid cells of various sizes, while Conley (1999) standard errors are shown in gray using different cutoff levels.

Panel (b)



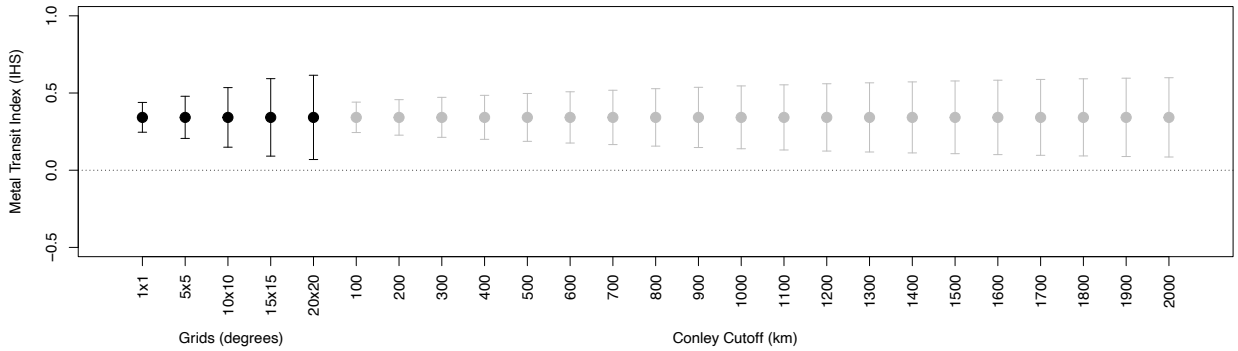
(b) Figure shows the 2SLS IV point estimate of Table 1 (Panel A column (5)) along with alternative standard error clustering approaches. Standard errors depicted in black are clustered at grid cells of various sizes, while Conley (1999) standard errors are shown in gray using different cutoff levels.

Panel (c)



(c) Figure shows the OLS point estimate of Table 1 (Panel B column (1)) along with alternative standard error clustering approaches. Standard errors depicted in black are clustered at grid cells of various sizes, while Conley (1999) standard errors are shown in gray using different cutoff levels.

Panel (d)



(d) Figure shows the 2SLS IVpoint estimate of Table 1 (Panel B column (5)) along with alternative standard error clustering approaches. Standard errors depicted in black are clustered at grid cells of various sizes, while Conley (1999) standard errors are shown in gray using different cutoff levels.

Figure D.5: Alternative standard error clustering approaches cross-sectional data

D.1.10 Other robustness checks

Restricting geographical scope and adding controls

Table D.13 reports robustness checks addressing concerns related to geographic scope and omitted environmental factors. Columns (1)–(5) restrict the analysis to areas with some Bronze Age urban activity by excluding Russia and Sub-Saharan Africa (column 1), focusing on UN-defined subregions (column 2) or countries (column 3) with at least one city or citadel, or by geographically limiting the sample to the bounding box (column 4) or the convex hull (column 5) surrounding all observed cities. These restrictions ensure that results are not driven by regions without any relevant settlement history. Throughout, the estimated effect of the metal transit index remains positive and statistically significant.

Column (6) uses the spatially unrestricted version of our dataset but adds the full set of environmental controls used by Henderson et al. (2018), capturing geographic and ecological variation.[55] The estimates remain robust. Panel C confirms strong first-stage relevance across all specifications, supporting the validity of the instrument.

[55]Specifically, we control for average temperature, precipitation, absolute latitude, distance to coastline, length of growing period, ruggedness, Kiszewski et al. (2004)'s malaria index, 14 biome indicators, and dummy variables indicating whether a natural harbour lies within the grid cell.

Table D.13: Robustness geographical extent and controls: Metal transit trade and Bronze Age cities

	(1)	(2)	(3)	(4)	(5)	(6)
	Panel A: Second stage Green et al. (2024): Any city or citadel (×100)					
Metal transit index (IHS)	0.579	0.478	0.575	0.737	1.207	0.881
	(0.191)	(0.127)	(0.149)	(0.250)	(0.362)	(0.261)
	[0.249]	[0.168]	[0.190]	[0.324]	[0.494]	[0.327]
	Panel B: Second stage Reba, Reitsma and Seto (2016): Any city (×100)					
Metal transit index (IHS)	0.131	0.356	0.520	0.250	0.494	0.494
	(0.132)	(0.096)	(0.119)	(0.177)	(0.239)	(0.184)
	[0.173]	[0.122]	[0.161]	[0.219]	[0.279]	[0.210]
	Panel C: First stage					
Natural metal transit index (IHS)	0.409	0.520	0.636	0.596	0.733	0.292
	(0.045)	(0.037)	(0.043)	(0.062)	(0.080)	(0.033)
	[0.065]	[0.054]	[0.062]	[0.080]	[0.106]	[0.046]
Areas included	No Russia or Sub-Saharan Africa	Subregions with cities	Countries with cities	Bounding box cities	Convex hull	All
Henderson et al. (2018) controls	No	No	No	No	No	Yes
Geography controls	Yes	Yes	Yes	Yes	Yes	Yes
Continent dummies	Yes	Yes	Yes	Yes	Yes	Yes
Observations	5,384	7,581	5,772	3,373	1,904	10,970
Mean dependent variable Panel A	0.966	0.699	0.918	1.571	2.784	0.483
Mean dependent variable Panel B	0.854	0.607	0.797	1.364	2.416	0.419
First-stage F-stat (5×5 grids)	82.180	197.683	223.653	93.766	83.789	78.468
First-stage F-stat (Conley 1000km)	39.533	92.193	105.265	54.860	46.576	40.451

Notes: Panels A and B of this table report second-stage estimates of the cross-sectional 2SLS IV model (4). Panel C reports the corresponding first-stage estimates (equation (5)). The unit of observation is a 1×1 grid-cell k. 'Any city or citadel' equals 100 if a city or citadel was present in grid cell k during the Bronze Age (and 0 otherwise). 'Any city by 1300 BC' equals 100 if a city was present in grid cell k by 1300 BC (and 0 otherwise). 'Metal transit index' is defined by equation (2), while 'Natural metal transit index' is defined by equation (3). The spatial extent of the analysis is restricted to the following areas: All countries except Russia and Sub-saharan African countries (column 1), geographical subregions (defined according to the United Nations geoscheme) with at least one city or citadel (column 2), countries with at least one city or citadel (column 3), bounding box of cities (column 4), and convex hull of cities (column 5). Column (6) extends the set of controls by the characteristics used in Henderson et al. (2018): average temperature, precipitation, (absolute) latitude, distance to the coastline, length of the growing season, ruggedness, Kiszewski et al. (2004)'s malaria index, 14 biome indicators, and natural harbors. Geography controls include proximity to mines, proximity to croplands, sea dummy, river dummy, mountains dummy, and centrality in the transport network. Standard errors clustered at the level of 5×5 degree grid cells are reported in parentheses. Standard errors computed using the approach of Conley (1999) (cut-off 1000km) are reported in square brackets.

Smaller units of observation

As an additional robustness check, we increase the spatial resolution of our analysis by using 0.5×0.5-degree grid cells instead of the 1×1-degree cells used in our main analysis. We first construct all variables following the same procedures described in Sections 2 and 3, as well as Appendix A.1. We then replicate the cross-sectional regressions reported in Table 1 using the more disaggregated grid structure.

As shown below, the qualitative pattern of results remains unchanged, illustrating that our findings are not sensitive to the choice of spatial resolution. Point estimates tend to be smaller, which is expected given the increase in the number of grid cells without observed urban settlements (i.e., the mean of the dependent variable declines).

Table D.14: Robustness 0.5×0.5 degree grid cells: Metal transit trade and Bronze Age cities

	OLS		Probit		2SLS IV			
	(1)	(2)	(3)	(4)	(5)	(6)	(7)	(8)
	Panel A: Second stage Green et al. (2024): Any city or citadel (×100)							
Metal transit index (IHS)	0.127	0.126	0.154	0.082	0.131	0.122		
	(0.029)	(0.029)	(0.023)	(0.028)	(0.032)	(0.041)		
	[0.035]	[0.035]	[0.007]	[0.010]	[0.042]	[0.049]		
Metal transit index							0.001	0.001
							(0.000)	(0.000)
							[0.000]	[0.001]
	Panel B: Second stage Reba, Reitsma and Seto (2016): Any city (×100)							
Metal transit index (IHS)	0.139	0.148	0.170	0.047	0.123	0.100		
	(0.038)	(0.040)	(0.021)	(0.031)	(0.032)	(0.033)		
	[0.051]	[0.052]	[0.007]	[0.012]	[0.045]	[0.042]		
Metal transit index							0.001	0.001
							(0.000)	(0.000)
							[0.000]	[0.000]
					Panel C: First stage			
Natural metal transit index (IHS)					0.413	0.263	52.551	23.602
					(0.027)	(0.025)	(7.793)	(4.346)
					[0.044]	[0.040]	[11.283]	[6.150]
Geography controls	No	Yes	No	Yes	No	Yes	No	Yes
Continent dummies	Yes	Yes	Yes	Yes	Yes	Yes	Yes	Yes
Observations	40,973	40,971	40,973	40,973	40,973	40,971	40,973	40,971
Mean dependent variable Panel A	0.142	0.142	0.142	0.142	0.142	0.142	0.142	0.142
Mean dependent variable Panel B	0.134	0.134	0.134	0.134	0.134	0.134	0.134	0.134
R-squared Panel A	0.006	0.006	0.158	0.221				
R-squared Panel B	0.007	0.010	0.193	0.378				
First-stage F-stat (5×5 grids)					238.997	113.417	45.471	29.500
First-stage F-stat (Conley 1000km)					85.908	43.621	21.472	14.573

Notes: Panels A and B report cross-sectional OLS, probit, and 2SLS IV estimates of equation (4). Panel C reports the corresponding first-stage estimates (equation (5)). The unit of observation is a 0.5×0.5-degree grid cell k. 'Any city or citadel' equals 100 if a city or citadel was present in grid cell k during the Bronze Age (and 0 otherwise). 'Any city by 1300 BC' equals 100 if a city was present in grid cell k by 1300 BC (and 0 otherwise). 'Metal transit index' is defined by equation (2), while 'Natural metal transit index' is defined by equation (3). Footnotes 18 and 21 describe the construction of the controls: Geography controls include proximity to mines, proximity to croplands, sea dummy, river dummy, mountains dummy, and centrality in the transport network. Standard errors clustered at the level of 5×5 degree grid cells are reported in parentheses. Standard errors computed using the approach of Conley (1999) (cut-off 1000km) are reported in square brackets.

IV-probit results

Appendix Table D.15 complements the linear 2SLS IV results from the main text (Table 1) by using an IV-probit approach. Panel A uses the city data from Green et al. (2024) as the outcome, while Panel B uses data from Reba, Reitsma and Seto (2016). In both panels, the transit index enters positively and is statistically significant across all specifications. The first-stage results in Panel C confirm that the instrument is strongly correlated with the transit index.

These IV-probit estimates reinforce the main findings: higher metal transit volumes are robustly associated with the presence of Bronze Age cities. As in the main analysis, standard errors are clustered at the level of 5×5-degree grid cells. However, Conley (1999) standard errors are not available for nonlinear IV estimators and are, consequently, not reported in the table.

Table D.15: Robustness IV probit: Metal transit trade and Bronze Age cities

	IV Probit			
	(1)	(2)	(3)	(4)
	Panel A: Second stage Green et al. (2024): Any city or citadel (×100)			
Metal transit index (IHS)	0.262	0.330		
	(0.046)	(0.060)		
Metal transit index			0.001	0.001
			(0.000)	(0.000)
	Panel B: Second stage Reba, Reitsma and Seto (2016): Any city (×100)			
Metal transit index (IHS)	0.183	0.169		
	(0.047)	(0.091)		
Metal transit index			0.001	0.001
			(0.000)	(0.000)
	Panel C: First stage			
Natural metal transit index (IHS)	0.490	0.305	86.183	42.228
	(0.031)	(0.031)	(13.032)	(8.273)
Geography controls	No	Yes	No	Yes
Continent dummies	Yes	Yes	Yes	Yes
Observations	10,970	10,726	10,970	10,726
Mean dependent variable Panel A	0.483	0.494	0.483	0.494
Mean dependent variable Panel B	0.419	0.429	0.419	0.429
First-stage F-stat (5×5 grids)	251.000	99.004	43.734	26.054

Notes: Panels A and B report IV probit estimates using regressions specifications analogous to the 2SLS-IV regressions reported in Table 1, columns (5)–(8). Panel C reports the corresponding first-stage estimates (equation (5)). The unit of observation is a 1×1-degree grid cell k. 'Any city or citadel' equals 100 if a city or citadel was present in grid cell k during the Bronze Age (and 0 otherwise). 'Any city by 1300 BC' equals 100 if a city was present in grid cell k by 1300 BC (and 0 otherwise). 'Metal transit index' is defined by equation (2), while 'Natural metal transit index' is defined by (3). Footnotes 18 and 21 describe the construction of the controls: Geography controls include proximity to mines, proximity to croplands, sea dummy, river dummy, mountains dummy, and centrality in the transport network. Standard errors clustered at the level of 5×5 degree grid cells are reported in parentheses.

HYDE 3.1 data

We repeat our main analysis using a second spatially explicit data source: HYDE 3.1 (Klein Goldewijk et al., 2011). Rather than identifying individual cities, this dataset provides rasterized estimates of urban population for every millennium BC since the Neolithic. The dependent variable is now an indicator for the presence of any urban population in 2000 BC—the latest data point available prior to the Bronze Age collapse. Once again, the pattern of results is consistent with metal transit trade having influenced the emergence of urban areas. Across all specifications, we find that a higher metal transit index statistically significantly increases the likelihood that urban dwellers reside in a given grid cell.

Table D.16: Robustness using HYDE 3.1 data on urban population: Metal transit trade and Bronze Age cities.

	OLS		Probit		2SLS IV			
	(1)	(2)	(3)	(4)	(5)	(6)	(7)	(8)
	Panel A: Second stage Klein Goldewijk et al. (2011): Any urban population (×100)							
Metal transit index (IHS)	3.204	2.200	0.122	0.081	8.579	12.254		
	(0.284)	(0.299)	(0.010)	(0.011)	(0.669)	(1.412)		
	[0.432]	[0.441]	[0.008]	[0.009]	[1.045]	[2.189]		
Metal transit index							0.049	0.087
							(0.007)	(0.017)
							[0.010]	[0.023]
					Panel B: First stage			
Natural metal transit index (IHS)					0.490	0.308	86.183	43.091
					(0.031)	(0.030)	(13.032)	(8.275)
					[0.051]	[0.048]	[18.407]	[11.294]
Geography controls	No	Yes	No	Yes	No	Yes	No	Yes
Continent dummies	Yes	Yes	Yes	Yes	Yes	Yes	Yes	Yes
Observations	10,970	10,970	10,970	10,970	10,970	10,970	10,970	10,970
Mean dependent variable	14.968	14.968	14.968	14.968	14.968	14.968	14.968	14.968
R-squared	0.072	0.131	0.077	0.153				
First-stage F-stat (5×5 grids)					251.000	102.261	43.734	27.115
First-stage F-stat (Conley 1000km)					92.374	40.999	21.690	14.389

Notes: Panel A reports cross-sectional OLS, probit, and 2SLS IV estimates of equation (4). Panel B reports the corresponding first-stage estimates (equation (5)). The unit of observation is a 1×1-degree grid cell k. 'Any urban population' equals 100 if any urban population was present in grid cell k during the Bronze Age (and 0 otherwise). 'Metal transit index' is defined by equation (2), while 'Natural metal transit index' is defined by equation (3). Footnotes 18 and 21 describe the construction of the controls: Geography controls include proximity to mines, proximity to croplands, sea dummy, river dummy, mountains dummy, and centrality in the transport network. Standard errors clustered at the level of 5×5 degree grid cells are reported in parentheses. Standard errors computed using the approach of Conley (1999) (cut-off 1000km) are reported in square brackets.

D.2 Additional analysis and robustness checks archaeological sites

In addition to reporting the reduced-form estimates corresponding to Table 2 and Figures 2–3, this appendix presents robustness checks for our difference-in-differences analysis using the Bahn (2000) and Bagnall (2022) data on archaeological sites. For completeness, we first report the reduced-form estimates (Section D.2.1). We then move on to discussing the additional analysis and robustness checks briefly outlined in the main paper. Specifically, we

1. address worries related to the possibility of the endogeneity of the relative transportation cost (Section D.2.2).
2. use alternative standard error clustering approaches to illustrate that our results are not dependent on one particular choice (Section D.2.3).
3. reproduce our results, including the statistical horse race between the metal transit index and the blockage cost, using smaller grid cells as units of observation (Section D.2.4).

In Appendix D.4 we further illustrate that controlling for non-metal transit trade leaves our estimates qualitatively unchanged.

D.2.1 Reduced-form estimates

The reduced-form results reported in Table D.17 document a positive and statistically significant differential effect of the natural metal transit index during the Bronze Age relative to the Stone Age. Using both outcome datasets—the historical atlas by Bahn (2000) and the Pleiades Gazetteer by Bagnall (2022)—the interaction term between the Bronze Age indicator and the natural metal transit index enters with a positive sign and remains statistically significant across specifications. These findings are robust to the inclusion of geographic controls and support the statistical relevance and economic rationale underlying our instrumental variable strategy. Figures D.6–D.7 report the reduced-form estimates corresponding to Figures 2–3 presented in the main text.

Table D.17: Reduced-form estimates corresponding to Table 2: Natural metal transit index and archaeological sites

	Any archaeological site (×100)			
	(5)	(6)	(7)	(8)
	Panel A: Second stage Bahn (2000)			
Natural metal transit index (IHS)	0.474	0.513	0.474	0.513
× Bronze Age	(0.211)	(0.228)	(0.211)	(0.228)
	[0.236]	[0.241]	[0.236]	[0.241]
	Panel B: Second stage Pleiades Gazetteer (Bagnall, 2022)			
Natural metal transit index (IHS)	0.268	0.146	0.268	0.146
× Bronze Age	(0.064)	(0.074)	(0.064)	(0.074)
	[0.068]	[0.073]	[0.068]	[0.073]
Geography controls×Bronze Age	No	Yes	No	Yes
Grid cell fixed effects	Yes	Yes	Yes	Yes
Continent×Bronze Age	Yes	Yes	Yes	Yes
Observations	21,940	21,940	21,940	21,940
Mean dependent variable Panel A	4.913	4.913	4.913	4.913
Mean dependent variable Panel B	1.759	1.759	1.759	1.759
R-squared Panel A	0.612	0.613	0.612	0.613
R-squared Panel B	0.821	0.823	0.821	0.823

Notes: Panels A and B report difference-in-differences reduced-form estimates of equation (6) corresponding to Table 2. The unit of observation is a 1×1 grid-cell k in period p (Stone Age or Bronze Age). 'Any Site' equals 100 rather than 0 for a grid cell k in period p if there is at least one archaeological site dating from period p and located in grid cell k. 'Natural metal transit index' is defined by equation (3). Geography controls include proximity to mines, proximity to croplands, sea dummy, river dummy, mountains dummy, and centrality in the transport network. Panel A uses archaeological data from Bahn (2000), while Panel B uses data from Bagnall (2022). Standard errors clustered at the level of 5×5 degree grid cells are reported in parentheses. Standard errors computed using the approach of Conley (1999) (cut-off 1000km) are reported in square brackets.

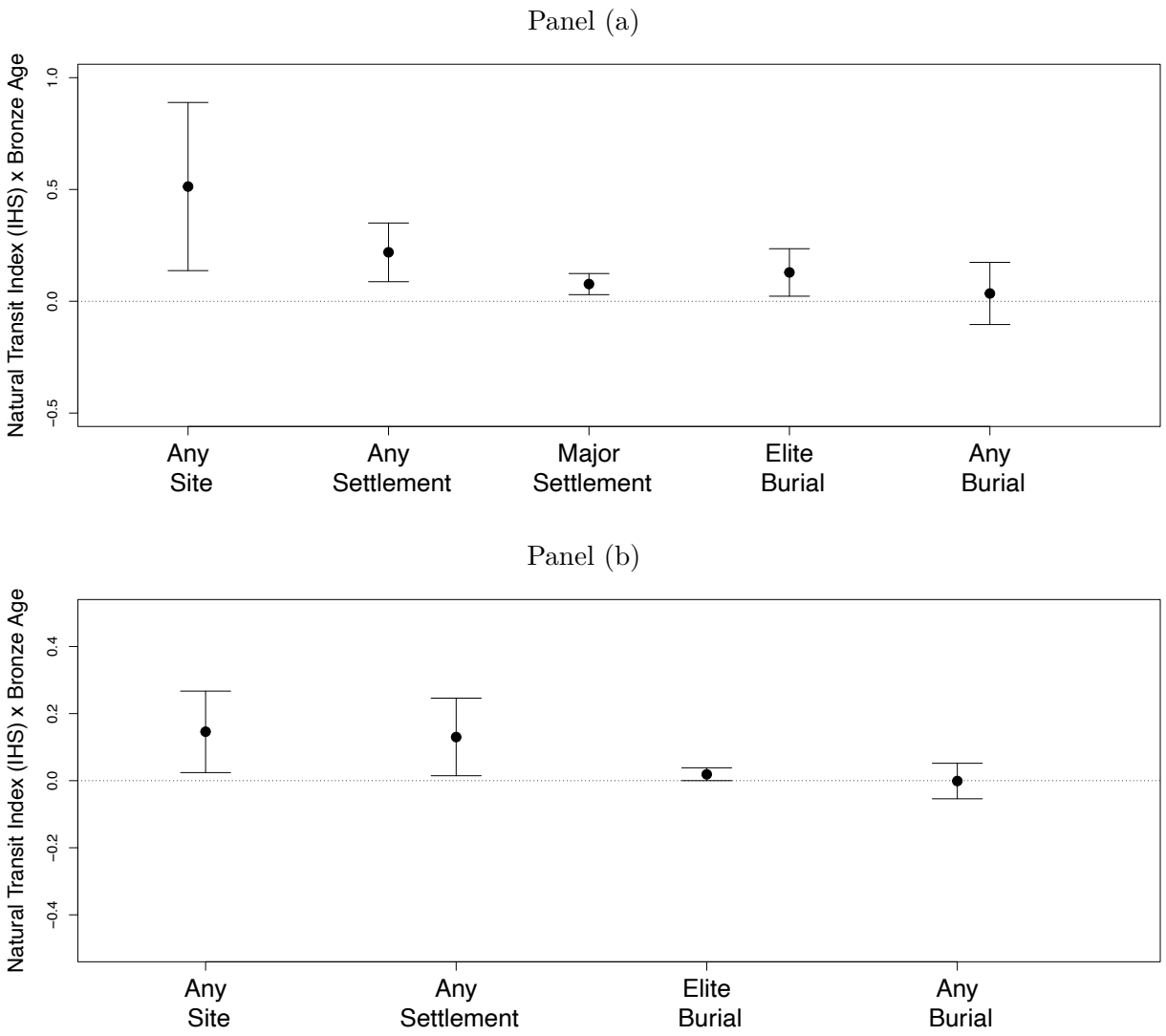


Figure D.6: Estimated impact of the natural transit index across different types of archaeological finds

Figure depicts reduced-form point estimates and 90% confidence intervals of equation (6). Standard errors are clustered at the level of 5×5 degree grid cells. Dependent variable equals 100 if an archaeological site is present in a given 1×1 grid cell k dating from period p and 0 otherwise. Panel (a) uses data on archaeological sites from Bahn (2000) and panel (b) uses data from Bagnall (2022)

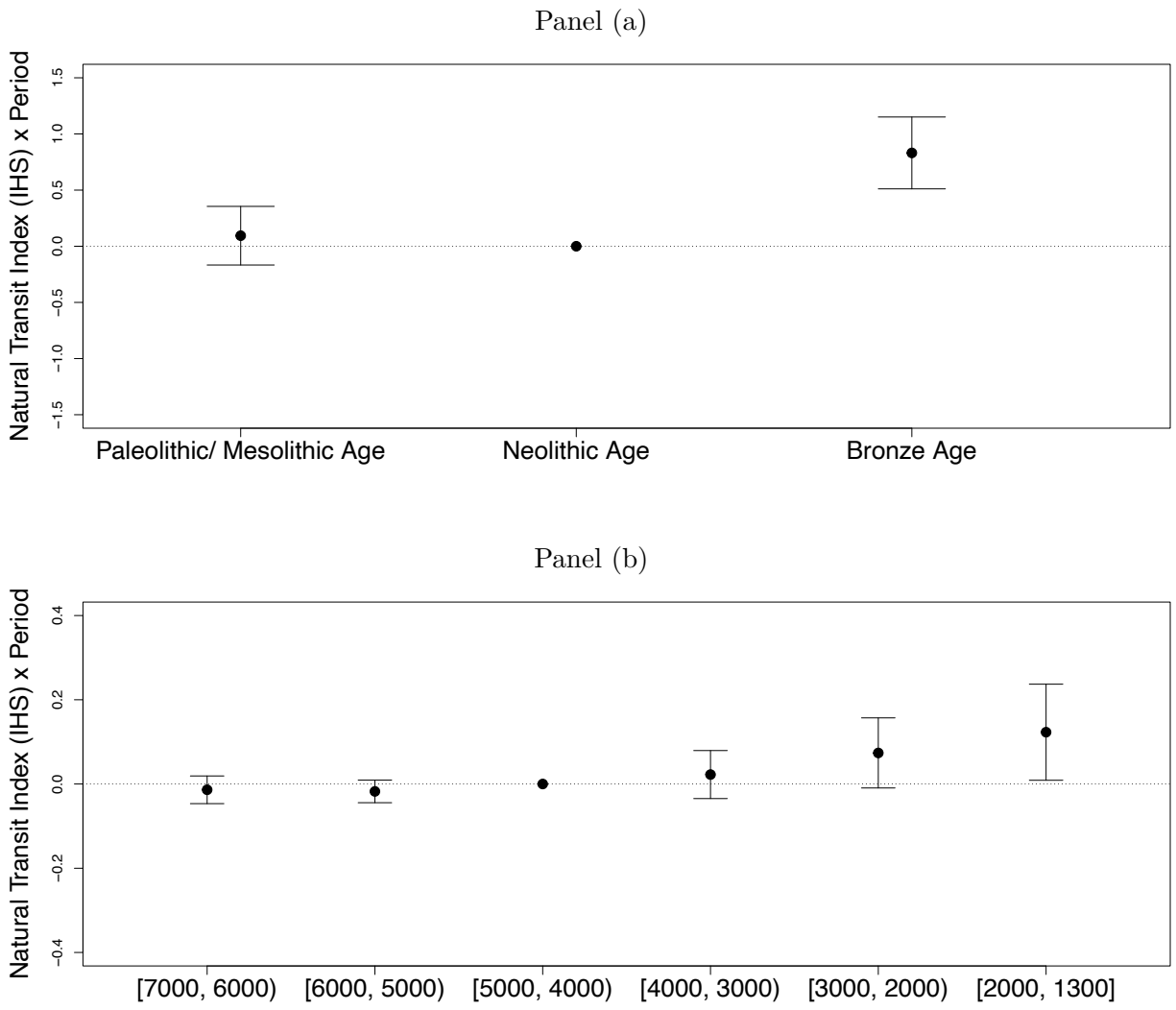


Figure D.7: Estimated impact of the natural transit index on the spatial location of archaeological sites over time

Figure depicts reduced-form point estimates and 90% confidence intervals of equation (8). Standard errors are clustered at the level of 5×5 degree grid cells. Dependent variable equals 100 if an archaeological site is present in a given 1×1 grid cell k dating from period p and 0 otherwise. Panel (a) uses data on archaeological sites from Bahn (2000); the reference period is the Neolithic Age. Panel (b) uses data from Bagnall (2022); the reference period is the time span $[5000, 4000)$ BC. See Section 2 for details on definition and construction of variables.

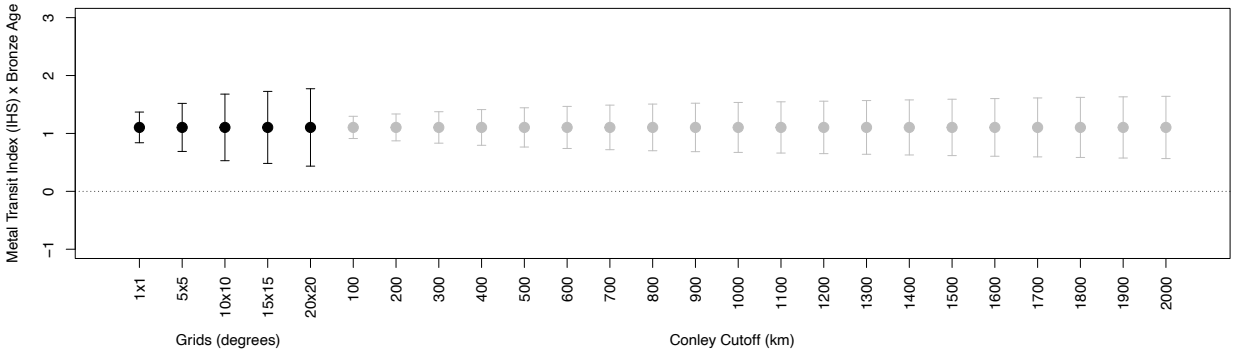
D.2.2 Endogeneity of relative transport costs

To address potential concerns regarding endogeneity related to the relative transport costs used in constructing the instrument, we replicate the two robustness checks from the previous analysis on urban settlements (Appendix D.1) in the difference-in-differences setting. First, we exclude regions used to estimate the relative transport costs. Second, we reconstruct the instrument using Stone Age transportation costs instead of Bronze Age values. As shown in Appendix Table D.18, the results remain positive and statistically significant, indicating that our difference-in-differences findings are not driven by the specific choice of transport cost parameters.

D.2.3 Standard error clustering

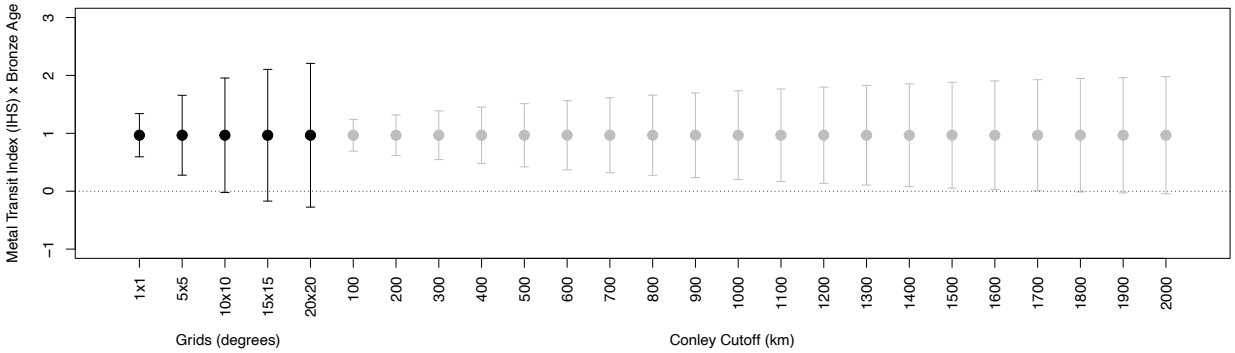
We use two approaches to correct for spatial autocorrelation of the error term: clustering at the 5×5 grid cell level, and Conley (1999) standard errors with distance cutoffs of 1,000 km. In Appendix Figure D.8, we show how the difference-in-differences results are affected by varying the size of the clustering grid (from 1×1 to 20×20) and the Conley cutoff (from 100 km to 2,000 km).

Panel (a)



(a) Figure shows the OLS point estimate of Table 2 (Panel A column (1)) along with alternative standard error clustering approaches. Standard errors depicted in black are clustered at grid cells of various sizes, while Conley (1999) standard errors are shown in gray using different cutoff levels.

Panel (b)



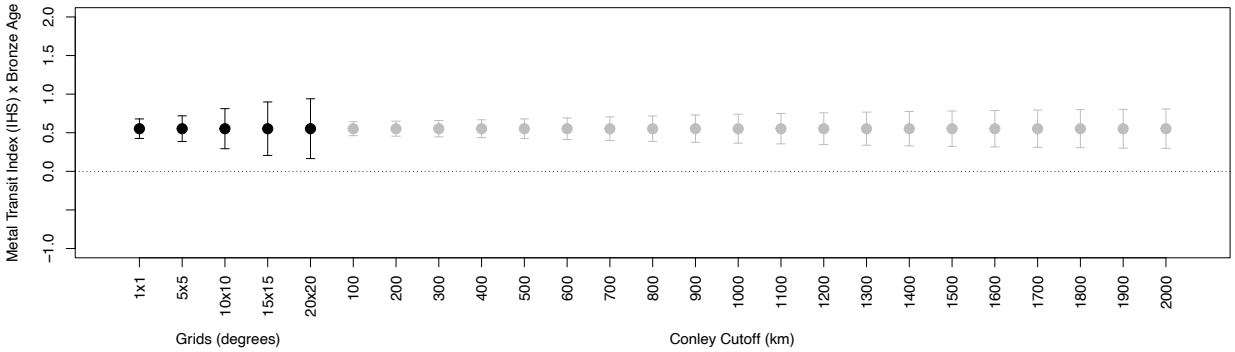
(b) Figure shows the 2SLS IV point estimate of Table 2 (Panel A column (3)) along with alternative standard error clustering approaches. Standard errors depicted in black are clustered at grid cells of various sizes, while Conley (1999) standard errors are shown in gray using different cutoff levels.

Table D.18: Robustness endogeneity $\boldsymbol{\alpha_{BA}}$: Metal transit trade and archaeological sites

	Any Site (×100)			
	(1)	(2)	(3)	(4)
	Panel A: Second stage Bahn (2000) archaeological sites			
Metal transit index (IHS)	1.782	2.287	1.058	1.911
× Bronze Age	(0.419)	(0.718)	(0.459)	(0.825)
	[0.446]	[0.746]	[0.507]	[0.839]
	Panel B: Second stage Pleiades Gazetteer (Bagnall, 2022)			
Metal transit index (IHS)	0.418	0.387	0.631	0.659
× Bronze Age	(0.106)	(0.175)	(0.123)	(0.226)
	[0.105]	[0.161]	[0.132]	[0.218]
	Panel C: First stage			
Natural metal transit index (IHS)	0.444	0.287	0.450	0.271
× Bronze Age	(0.031)	(0.030)	(0.029)	(0.027)
	[0.036]	[0.033]	[0.034]	[0.030]
Geography controls×Bronze Age	Yes	Yes	Yes	Yes
Grid cell fixed effects	Yes	Yes	Yes	Yes
Continent×Bronze Age	Yes	Yes	Yes	Yes
Observations	20,116	20,116	21,940	21,940
Mean dependent variable Panel A	3.042	3.042	4.913	4.913
Mean dependent variable Panel B	0.935	0.935	1.759	1.759
First-stage F-statistic (5×5 grids)	199.770	92.322	238.801	102.046
First-stage F-statistic (Conley 1000km)	146.623	73.739	175.014	78.326
Robustness check	Drop extent $\boldsymbol{\alpha_{BA}}$		Natural metal transit index using $\boldsymbol{\alpha_{SA}}$	

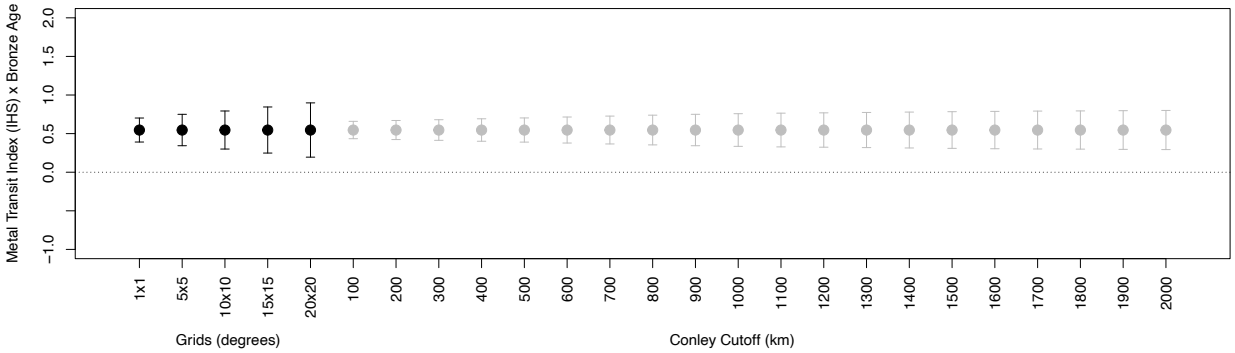
This table reports difference-in-difference 2SLS estimates of equation (6). The unit of observation is a 1×1 grid-cell k in period p (Stone Age or Bronze Age). 'Any Site' equals 100 (rather than 0) for a grid cell k in period p if there is at least one archaeological site in cell k dating from period p. 'Metal transit index' is defined by equation (2), while 'Natural metal transit index' is defined by equation (3). Geography controls include proximity to mines, proximity to croplands, sea dummy, river dummy, mountains dummy, and centrality. Panel A uses archaeological data from Bahn (2000), while Panel B uses data from Bagnall (2022). Panel C reports first-stage estimates (equation (7)). Columns (1)–(2) restrict the spatial extent of the analysis to grid cells not used in the estimation of the relative transport costs across different transportation modes during the Bronze Age. In columns (3)–(4), the instrumental variable is constructed using the relative transport costs estimated for the Stone Age rather than the Bronze Age. Geography controls include proximity to mines, proximity to croplands, sea dummy, river dummy, mountains dummy, and centrality in the transport network. Standard errors clustered at the level of 5×5 degree grid cells are reported in parentheses. Standard errors computed using the approach of Conley (1999) (cut-off 1000km) are reported in square brackets.

Panel (c)



(c) Figure shows the OLS point estimate of Table 2 (Panel B column (1)) along with alternative standard error clustering approaches. Standard errors depicted in black are clustered at grid cells of various sizes, while Conley (1999) standard errors are shown in gray using different cutoff levels.

Panel (d)



(d) Figure shows the 2SLS IV point estimate of Table 2 (Panel B column (3)) along with alternative standard error clustering approaches. Standard errors depicted in black are clustered at grid cells of various sizes, while Conley (1999) standard errors are shown in gray using different cutoff levels.

Figure D.8: Alternative standard error clustering approaches panel data

D.2.4 Other robustness checks

Smaller units of observation

Below, we demonstrate that the difference-in-differences results using the global dataset presented in the main paper are not dependent on the use of 1×1-degree raster cells. As shown in Table D.19 and Figures D.9–D.10, we obtain qualitatively equivalent estimates when using 0.5×0.5-degree grid cells as the unit of analysis. Table D.20 further shows that the horse race regressions produce the same pattern of results, regardless of whether we use 1×1 or 0.5×0.5-degree grid cells. Point estimates are smaller when we use smaller units of observation. As discussed above, this is entirely to be expected, given that disaggregation introduces many zero observations and thus lowers the mean of the dependent variables.

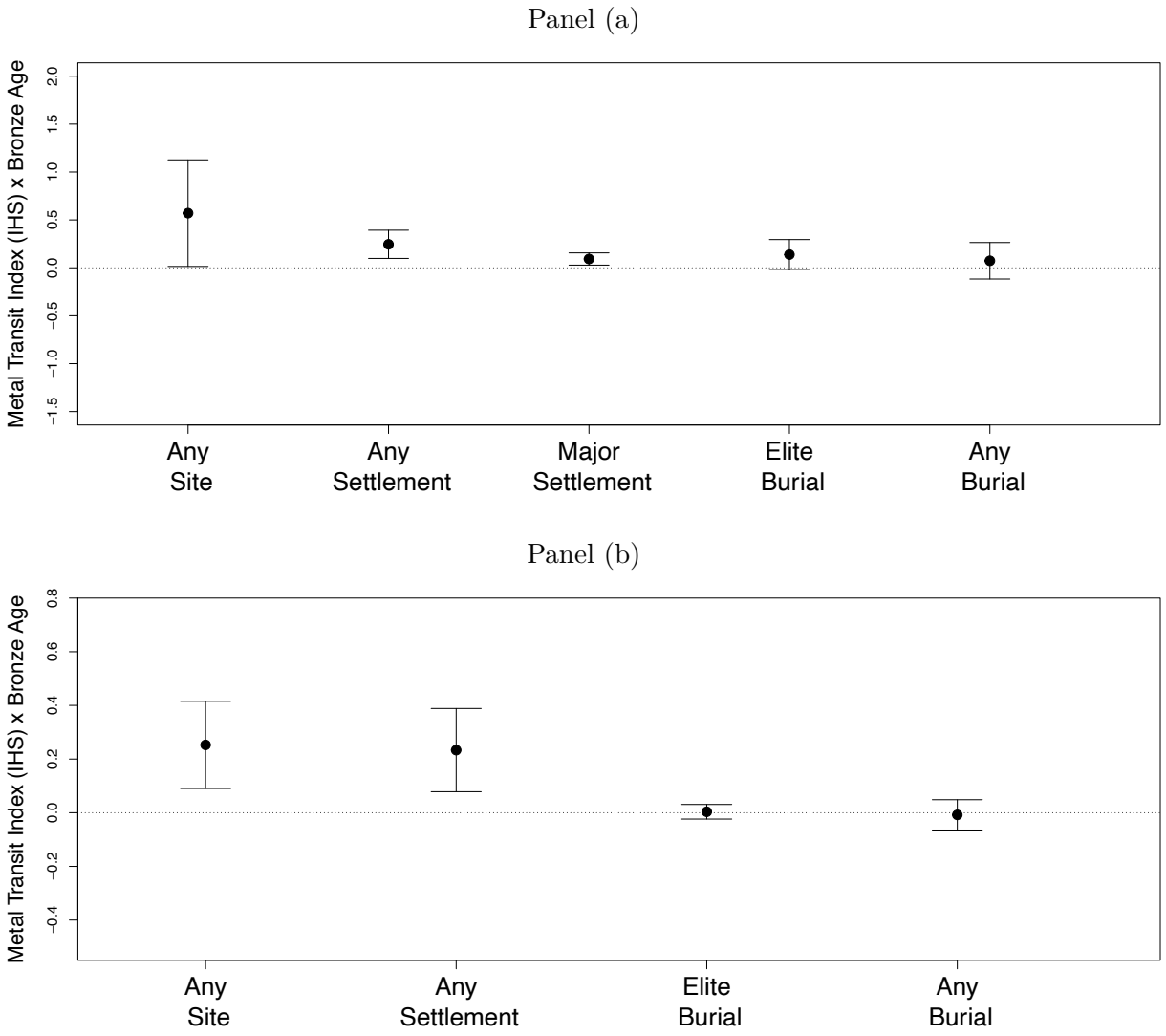


Figure D.9: Robustness 0.5×0.5 degree grid cells: Estimated impact of the metal transit index across different types of archaeological finds

Figure depicts 2SLS IV point estimates and 90% confidence intervals of β in equation (6). Standard errors are clustered at the level of 5×5 degree grid cells. Dependent variable equals 100 if an archaeological site is present in a given 0.5×0.5 grid cell k dating from period p and 0 otherwise. Panel (a) uses data on archaeological sites from Bahn (2000) and panel (b) uses data from Bagnall (2022)

Table D.19: Robustness 0.5×0.5 degree grid cells: Metal transit trade and archaeological sites. Difference-in-differences (Stone Age vs Bronze Age)

	Any archaeological site (×100)					
	OLS		2SLS IV			
	(1)	(2)	(3)	(4)	(5)	(6)
	Panel A: Second stage Bahn (2000)					
Metal transit index (IHS) × Bronze Age	0.582	0.711	0.484	0.570		
	(0.133)	(0.134)	(0.194)	(0.338)		
	[0.148]	[0.141]	[0.218]	[0.361]		
Metal transit index × Bronze Age					0.004	0.006
					(0.002)	(0.004)
					[0.002]	[0.004]
	Panel B: Second stage Pleiades Gazetteer (Bagnall, 2022)					
Metal transit index (IHS) × Bronze Age	0.325	0.307	0.290	0.253		
	(0.071)	(0.074)	(0.065)	(0.099)		
	[0.086]	[0.088]	[0.074]	[0.097]		
Metal transit index × Bronze Age					0.002	0.003
					(0.001)	(0.001)
					[0.001]	[0.001]
	Panel C: First stage					
Natural metal transit index (IHS) × Bronze Age			0.413	0.263	52.551	23.602
			(0.027)	(0.025)	(7.793)	(4.345)
			[0.031]	[0.028]	[7.979]	[4.349]
Geography controls×Bronze Age	No	Yes	No	Yes	No	Yes
Grid cell fixed effects	Yes	Yes	Yes	Yes	Yes	Yes
Continent×Bronze Age	Yes	Yes	Yes	Yes	Yes	Yes
Observations	81,946	81,942	81,946	81,942	81,946	81,942
Mean dependent variable Panel A	1.855	1.855	1.855	1.855	1.855	1.855
Mean dependent variable Panel B	0.631	0.631	0.631	0.631	0.631	0.631
R-squared Panel A	0.572	0.574				
R-squared Panel B	0.800	0.801				
First-stage F-stat (5×5 grids)			238.997	113.426	45.471	29.502
First-stage F-stat (Conley 1000km)			171.837	87.266	42.949	29.153

Notes: This table reports difference-in-differences OLS and 2SLS IV estimates of equation (6). The unit of observation is a 0.5×0.5 grid-cell k in period p (Stone Age or Bronze Age). 'Any Site' equals 100 rather than 0 for a grid cell k in period p if there is at least one archaeological site dating from period p and located in grid cell k. 'Metal transit index' is defined by equation (2), while 'Natural metal transit index' is defined by equation (3). Geography controls include proximity to mines, proximity to croplands, sea dummy, river dummy, mountains dummy, and centrality in the transport network. Panel A uses archaeological data from Bahn (2000), while Panel B uses data from Bagnall (2022). Panel C reports first-stage estimates (equation (7)). Standard errors clustered at the level of 5×5 degree grid cells are reported in parentheses. Standard errors computed using the approach of Conley (1999) (cut-off 1000km) are reported in square brackets.

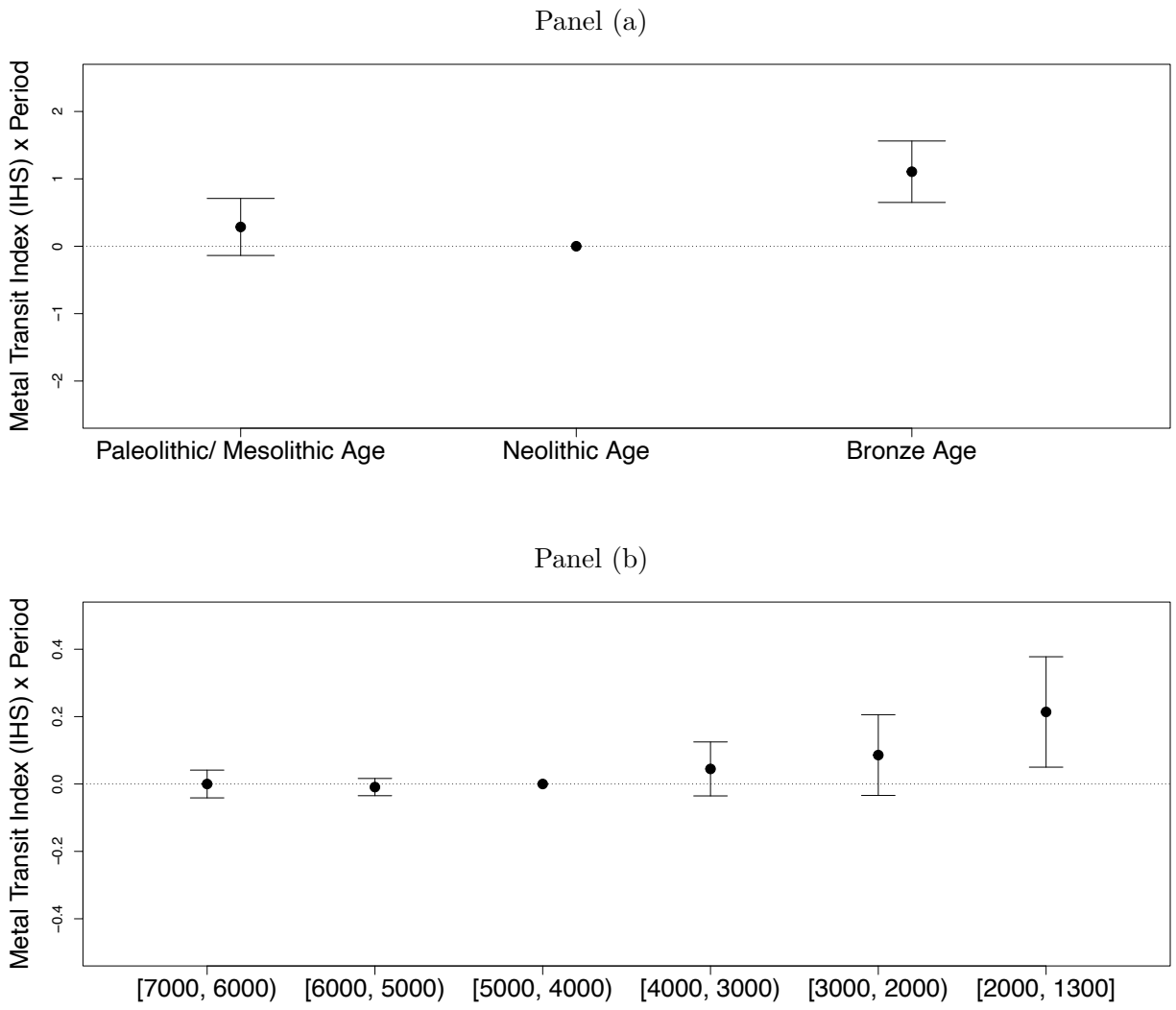


Figure D.10: Robustness 0.5×0.5 degree grid cells: Estimated impact of the metal transit index on the spatial location of archaeological sites over time

Figure depicts 2SLS IV point estimates and 90% confidence intervals of ψ_p in equation (8). Standard errors are clustered at the level of 5×5 degree grid cells. Dependent variable equals 100 if an archaeological site is present in a given 0.5×0.5 grid cell k dating from period p and 0 otherwise. Panel (a) uses data on archaeological sites from Bahn (2000); the reference period is the Neolithic Age. Panel (b) uses data from Bagnall (2022); the reference period is the time span $[5000, 4000)$ BC. See Section 2 for details on definition and construction of variables.

Table D.20: Robustness 0.5×0.5 degree grid cells: Horse race: Metal transit index vs blockage cost

	Any city or citadel (×100) Green et al. (2024)				Any Site (×100) Bahn (2000)		Any Criteria (×100) Atlas of Chinese Relics	
	OLS		Probit		OLS		OLS	
	(1)	(2)	(3)	(4)	(5)	(6)	(7)	(8)
Panel A: IHS-transformed explanatory variables								
Metal transit index (IHS)	0.126	0.042	0.082	0.059				
	(0.029)	(0.027)	(0.028)	(0.030)				
	[0.035]	[0.029]	[0.010]	[0.011]				
Blockage cost (IHS)		0.297		0.055				
		(0.106)		(0.035)				
		[0.102]		[0.011]				
Metal transit index (IHS)					0.711	0.531	2.793	2.300
× Bronze Age					(0.134)	(0.129)	(0.543)	(0.496)
					[0.141]	[0.129]	[0.453]	[0.456]
Blockage cost						0.639		1.743
× Bronze Age (IHS)						(0.299)		(1.033)
						[0.205]		[0.694]
Panel B: Standardized explanatory variables								
Metal transit index	0.247	0.119	0.025	0.001				
	(0.098)	(0.095)	(0.015)	(0.017)				
	[0.089]	[0.090]	[0.005]	[0.006]				
Blockage cost		0.241		0.068				
		(0.091)		(0.023)				
		[0.095]		[0.007]				
Metal transit index					0.737	0.523	2.488	1.554
× Bronze Age					(0.196)	(0.209)	(1.383)	(1.448)
					[0.168]	[0.169]	[0.795]	[0.827]
Blockage cost						0.404		1.565
× Bronze Age						(0.198)		(0.794)
						[0.154]		[0.597]
Geography controls	Yes	Yes	Yes	Yes	Yes	Yes	Yes	Yes
Grid cell fixed effects	No	No	No	No	Yes	Yes	Yes	Yes
Continent×period fixed effects	No	No	No	No	Yes	Yes	Yes	Yes
Observations	40,971	40,971	40,973	40,973	81,942	81,942	7,992	7,992
R-squared Panel A	0.006	0.009	0.221	0.224	0.574	0.574	0.688	0.689
R-squared Panel B	0.006	0.009	0.205	0.216	0.573	0.573	0.677	0.678
Mean dependent variable	0.142	0.142	0.142	0.142	1.855	1.855	7.345	7.345

Notes: This table reports probit and OLS estimates. 'Metal transit index' is defined by equation (2); Appendix B describes the construction of the variable 'Blockage cost'. The dependent variables and the 'Geography controls' are the same as in Tables 1 (for columns 1 and 2), Table 2 (for columns 3–6). Standard errors clustered at the level of 5×5 degree grid cells are reported in parentheses. Standard errors computed using the approach of Conley (1999) (cut-off 1000km) are reported in square brackets. In Panel A, the metal transit index and blockage cost are transformed using the hyperbolic sine transformation. In Panel B, the metal transit index and blockage cost are standardized to a mean of zero and a standard deviation of one. Blockage cost is winsorized at the 1% level.

D.3 Additional analysis and robustness checks China

This section of the appendix presents additional analyses and robustness checks for the case of China. For completeness, we first report the reduced-form estimates (Section D.3.1). We then show that we obtain qualitatively equivalent results when we redefine the units of observation as 0.5×0.5 grid cells (Section D.3.2).

D.3.1 Reduced-form estimates

Table D.21 reports the reduced-form estimates corresponding to Table 3 in the main text, while Figure D.11 presents the reduced-form estimates corresponding to Figure 4. The qualitative pattern of results closely mirrors that of the 2SLS IV specifications: the natural metal transit index exhibits a positive and statistically significant effect on the likelihood of observing sites with characteristics associated with the Urban Revolution.

Table D.21: Reduced-form estimates corresponding to Table 3: Natural metal transit index and archaeological sites in China. Difference-in-differences (Stone Age vs Bronze Age)

	Any Criteria (×100)	Principal Component (SD)	Any Criteria (×100)	Principal Component (SD)
	(3)	(4)	(5)	(6)
Natural metal transit index (IHS)	7.357	0.207	7.357	0.207
× Bronze Age	(1.025)	(0.040)	(1.025)	(0.040)
	[0.850]	[0.039]	[0.850]	[0.039]
Geography controls×Bronze Age	No	No	No	No
Grid cell fixed effects	Yes	Yes	Yes	Yes
Continent×Bronze Age	Yes	Yes	Yes	Yes
Observations	2,138	2,138	2,138	2,138
Mean dependent variable	17.914	0	17.914	17.914
R-squared	0.755	0.714	0.755	0.714

Notes: Table reports reduced-form estimates of equation (6). The unit of observation is a 1×1 grid-cell k in period p (Stone Age or Bronze Age). 'Any Criteria' equals 100 (rather than 0) if there is any archaeological site in grid cell k dating from period p that displays some evidence of at least one of the following features: large settlement, monumental building, a ruling class exempt from manual tasks, a system of recording, writing, art. 'Principal Component (SD)' is the standardized principal component. 'Natural metal transit index' is defined by equation (3). Geography controls include proximity to mines, proximity to croplands, sea dummy, river dummy, mountains dummy, and centrality in the transport network. Standard errors clustered at the level of 5×5 degree grid cells are reported in parentheses. Standard errors computed using the approach of Conley (1999) (cut-off 1000km) are reported in square brackets.

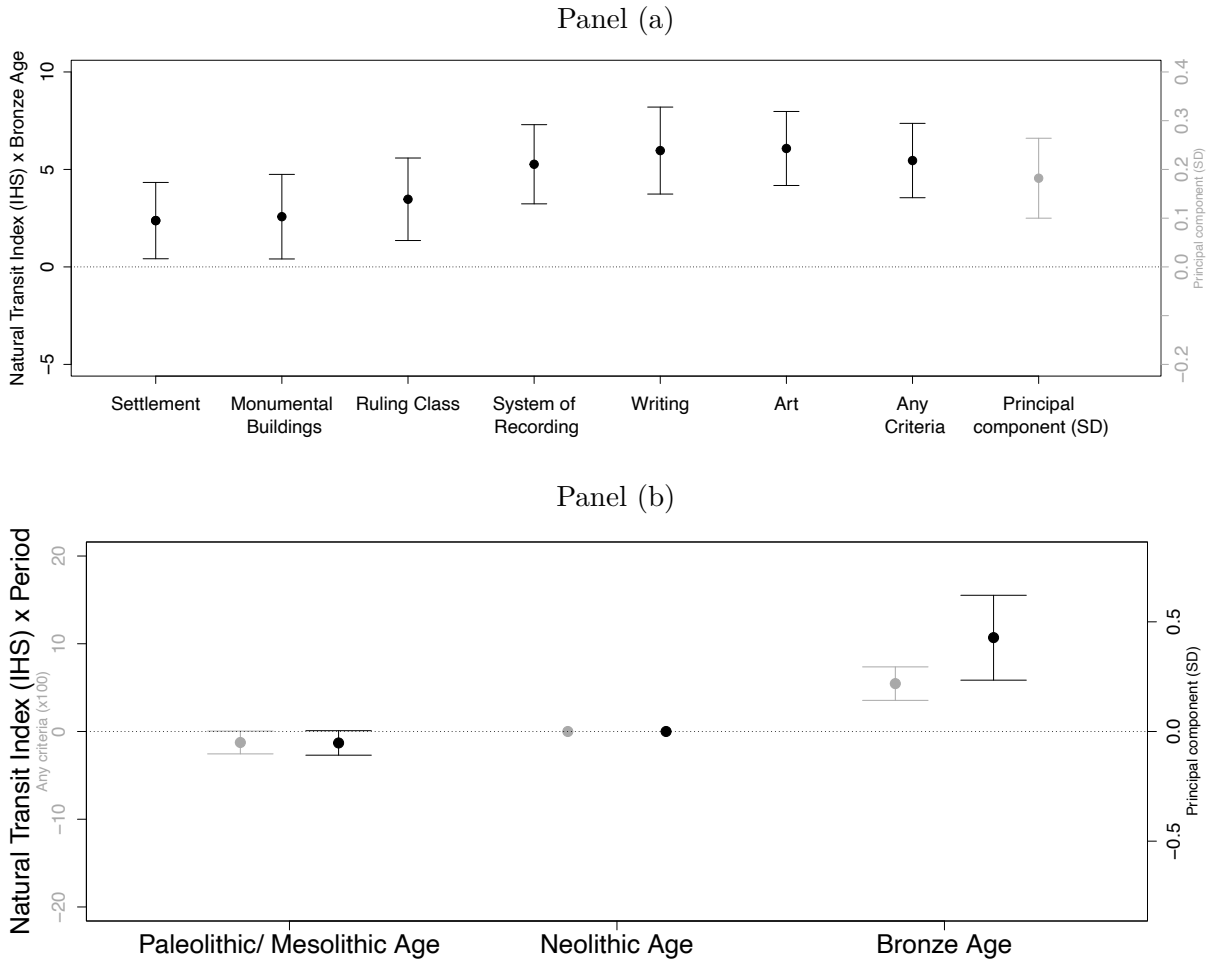


Figure D.11: Estimated impact of the natural transit index on the rise of the Urban Revolution in China

Panel (a) depicts reduced-form point estimates of equation (6) and 90% confidence intervals. Each data point corresponds to a regression with a different dependent variable. The dependent variable equals 100 (rather than 0) if there is any archaeological site in 1×1 degree grid cell k dating from period p (Stone Age or Bronze Age) that displays some evidence of: large settlements, monumental buildings, a ruling class exempt from manual tasks, a system of recording used in the production process, writing, figurative art. 'Any criteria' equals 100 (rather than 0) if there is any of the six features present in grid cell k dating from period p. Grey: Dependent variable is the (standardized) first principal component obtained from pooling these six features. Standard errors are clustered at the level of 5×5 degree grid cells. Panel (b) depicts reduced-form point estimates of equation (8) and 90% confidence intervals. Standard errors are clustered at the level of 5×5 degree grid cells. Grey: Dependent variable equals 100 (rather than 0) if at least one of the following features is present in sites in 1×1 degree grid cell k dating from period p: large settlements, monumental buildings, evidence of a ruling class exempt from manual tasks, a system of recording used in the production process, writing, figurative art. Black: Dependent variable is the (standardized) first principal component obtained from pooling these six features. The reference period is the Neolithic.

D.3.2 Other robustness checks

Smaller units of observation

Below, we show that the difference-in-differences results for China presented in the main paper are not dependent on the use of 1×1-degree raster cells. As shown in Table D.22 and Figure D.12, we obtain qualitatively equivalent estimates compared to our main results when using 0.5×0.5-degree grid cells as the unit of analysis.

Table D.22: Robustness 0.5×0.5 degree grid cells: Metal transit trade and archaeological sites in China. Difference-in-differences (Stone Age vs Bronze Age)

	OLS		2SLS IV			
	Any Criteria (×100)	Principal Component (SD)	Any Criteria (×100)	Principal Component (SD)	Any Criteria (×100)	Principal Component (SD)
	(1)	(2)	(3)	(4)	(5)	(6)
	Panel A: Second stage					
Metal transit index (IHS)	3.120	0.118	4.117	0.155		
× Bronze Age	(0.484)	(0.022)	(0.604)	(0.027)		
	[0.375]	[0.021]	[0.470]	[0.024]		
Metal transit index					0.024	0.001
× Bronze Age					(0.007)	(0.000)
					[0.005]	[0.000]
	Panel B: First stage					
Natural metal transit index (IHS)			0.836	0.836	145.003	145.003
× Bronze Age			(0.086)	(0.086)	(54.303)	(54.303)
			[0.086]	[0.086]	[48.651]	[48.651]
Geography controls×Bronze Age	No	No	No	No	No	No
Grid cell fixed effects	Yes	Yes	Yes	Yes	Yes	Yes
Continent×Bronze Age	Yes	Yes	Yes	Yes	Yes	Yes
Observations	7,992	7,992	7,992	7,992	7,992	7,992
Mean dependent variable	7.345	0	7.345	0	7.345	0
R-squared	0.685	0.653				
First-stage F-stat (5×5 grids)			94.005	94.005	7.130	7.130
First-stage F-stat (Conley 1000km)			93.493	93.493	8.792	8.792

Notes: Panel A reports difference-in-difference OLS (columns (1)–(2)) and 2SLS (columns (3)–(6)) estimates of equation (6), while panel B reports the first-stage estimates (equation (7)). The unit of observation is a 0.5×0.5 grid-cell k in period p (Stone Age or Bronze Age). 'Any Criteria' equals 100 (rather than 0) if there is any archaeological site in grid cell k dating from period p that displays some evidence of at least one of the following features: large settlement, monumental building, a ruling class exempt from manual tasks, a system of recording, writing, art. 'Principal Component (SD)' is the standardized principal component. 'Metal transit index' is defined by equation (2), while 'Natural metal transit index' is defined by equation (3). Geography controls include proximity to mines, proximity to croplands, sea dummy, river dummy, mountains dummy, and centrality in the transport network. Standard errors clustered at the level of 5×5 degree grid cells are reported in parentheses. Standard errors computed using the approach of Conley (1999) (cut-off 1000km) are reported in square brackets.

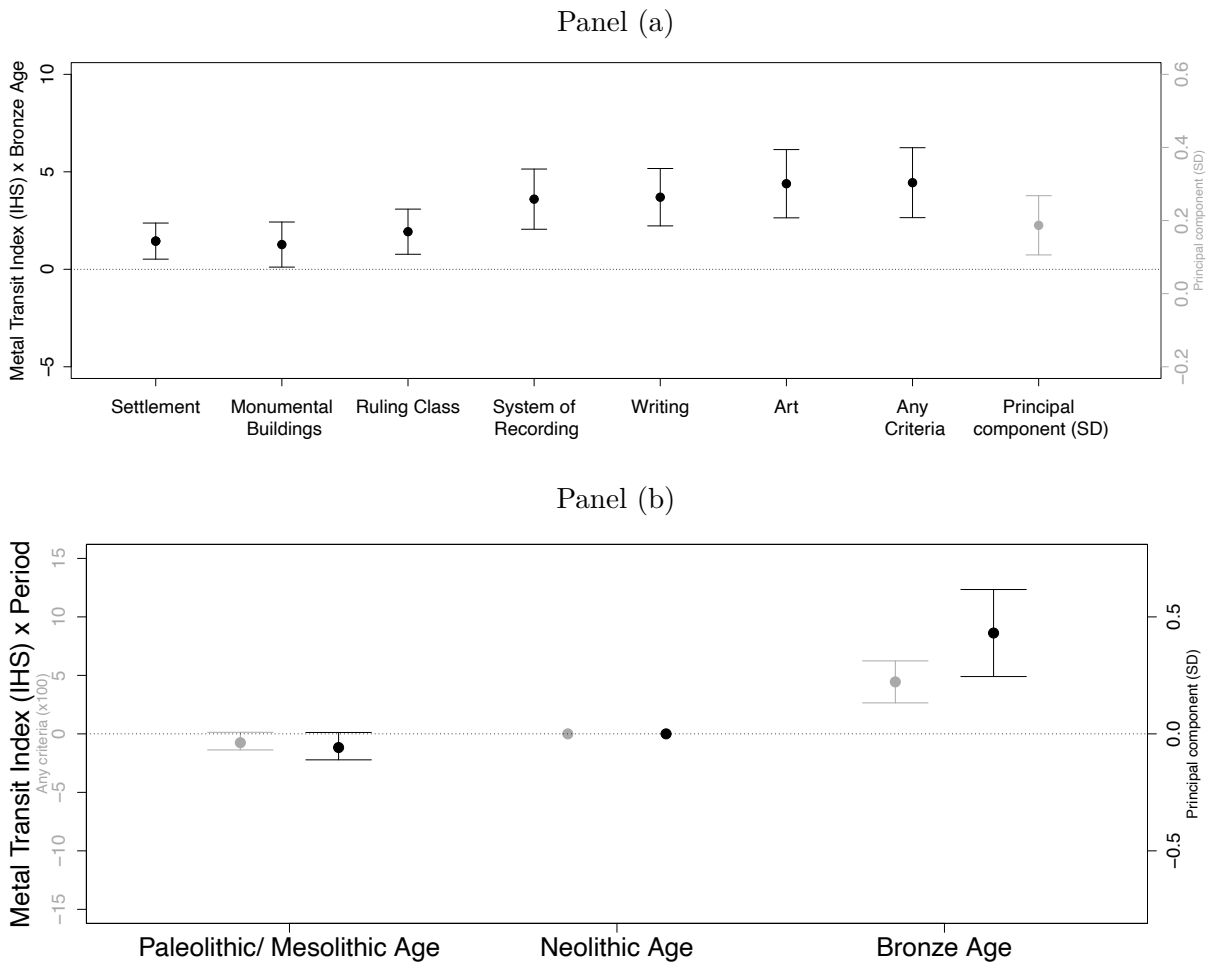


Figure D.12: Robustness 0.5×0.5 degree grid cells: Estimated impact of the metal transit index on the rise of the Urban Revolution in China

Panel (a) depicts 2SLS IV point estimates of β in equation (6) and 90% confidence intervals. Each data point corresponds to a regression with a different dependent variable. The dependent variable equals 100 (rather than 0) if there is any archaeological site in 0.5×0.5 degree grid cell k dating from period p (Stone Age or Bronze Age) that displays some evidence of: large settlements, monumental buildings, a ruling class exempt from manual tasks, a system of recording used in the production process, writing, figurative art. 'Any criteria' equals 100 (rather than 0) if there is any of the six features present in grid cell k dating from period p. Grey: Dependent variable is the (standardized) first principal component obtained from pooling these six features. Standard errors are clustered at the level of 5×5 degree grid cells. Panel (b) depicts 2SLS IV point estimates of ψ_p in equation (8) and 90% confidence intervals. Standard errors are clustered at the level of 5×5 degree grid cells. Grey: Dependent variable equals 100 (rather than 0) if at least one of the following features is present in sites in 0.5×0.5 degree grid cell k dating from period p: large settlements, monumental buildings, evidence of a ruling class exempt from manual tasks, a system of recording used in the production process, writing, figurative art. Black: Dependent variable is the (standardized) first principal component obtained from pooling these six features. The reference period is the Neolithic.

D.4 Metal-unrelated trade

The findings presented in the main part indicate that transit trade in metal played a significant role in determining where and when the first cities and civilizations emerged. A natural concern, however, is that our estimates may not capture the effects of metal trade specifically but rather transit trade more broadly, including non-metal goods. In this appendix, we provide two pieces of evidence suggesting that this is unlikely to be the case.

First, we show that our main estimates remain very stable when we control for a measure of a region's generic natural transit trade potential. Second, we demonstrate that our results hold even when accounting for the generic natural potential of obsidian transit trade—a good that was widely traded before, during, and after the Bronze Age (e.g., Renfrew, 1975).

D.4.1 Generic natural transit trade potential

Data and variables

In an effort to quantify general, metal-unrelated trade, we construct a measure of generic natural transit trade potential that incorporates the global distribution of primary land productivity. To this end, we first identify all bilateral least-cost paths between all 1×1 degree cell pairs within the Old World. In a second step, we calculate the natural transit trade potential of a given cell as the count of all least-cost paths that traverse this cell, weighted by the product of the NPP in the origin and destination cells. This weight serves as a proxy for the (potential) volume of bilateral trade between origin and destination, as higher values of NPP, ceteris paribus, indicate that the region can support larger populations. Formally, the generic natural transit trade potential of cell k, $GNTTP_k$, can be represented as:

$$GNTTP_k = \sum_{o \in o \setminus \{k\},\, d \in d \setminus \{k\}} \mathcal{I}_{P^{\star}_{od}}[k] \times NPP_o \times NPP_d, \tag{D.1}$$

where o and d are the sets of all origins and destinations; $P^{\star}_{od}$ denotes the least-cost path from a given origin to a given destination; $\mathcal{I}_{P^{\star}_{od}}[k]$ is an indicator function taking a value of one if the least-cost path connecting o and d intersects cell k, and zero otherwise; and NPP_o and NPP_d are the net primary productivity values in the origin and destination, respectively. Figure D.13 plots the distribution of the generic natural transit trade potential across space. The highest values are observed along rivers that lie in between (or within) productive areas.

Results

To test the possibility that our estimates conflate the effects of metal transit trade with those of generic trade, we re-run our main cross-sectional and difference-in-differences regressions, presented in Tables 1–2, while adding the generic natural transit trade potential to the set of control variables. The results are reported in Tables D.23 and D.24 below. Reassuringly, this exercise does not attenuate the estimated effect of the metal transit index. The OLS coefficients remain very similar to the baseline estimates, while some 2SLS coefficients become somewhat larger, although their signs, statistical significance, and broad magnitudes are preserved.

Table D.23: Robustness generic transit trade potential: Metal transit trade and Bronze Age cities

	OLS		Probit		2SLS IV			
	(1)	(2)	(3)	(4)	(5)	(6)	(7)	(8)
	Panel A: Second stage Green et al. (2024) data: Any city or citadel (×100)							
Metal transit index (IHS)	0.344	0.353	0.156	0.082	0.407	0.599		
	(0.074)	(0.077)	(0.025)	(0.032)	(0.088)	(0.157)		
	[0.094]	[0.096]	[0.009]	[0.012]	[0.123]	[0.199]		
Metal transit index							0.002	0.004
							(0.001)	(0.001)
							[0.001]	[0.002]
	Panel B: Second stage Reba, Reitsma and Seto (2016) data: Any city (×100)							
Metal transit index (IHS)	0.383	0.434	0.201	0.107	0.342	0.357		
	(0.087)	(0.094)	(0.029)	(0.034)	(0.083)	(0.133)		
	[0.134]	[0.143]	[0.011]	[0.014]	[0.124]	[0.166]		
Metal transit index							0.002	0.002
							(0.000)	(0.001)
							[0.001]	[0.001]
					Panel C: First stage			
Natural metal transit index (IHS)					0.490	0.224	86.183	32.132
					(0.031)	(0.032)	(13.032)	(8.204)
					[0.051]	[0.049]	[18.407]	[11.004]
Geography controls	No	Yes	No	Yes	No	Yes	No	Yes
Continent dummies	Yes	Yes	Yes	Yes	Yes	Yes	Yes	Yes
Observations	10,970	10,970	10,970	10,970	10,970	10,970	10,970	10,970
Mean dependent variable Panel A	0.483	0.483	0.483	0.483	0.483	0.483	0.483	0.483
Mean dependent variable Panel B	0.419	0.419	0.419	0.419	0.419	0.419	0.419	0.419
R-squared Panel A	0.016	0.018	0.177	0.259				
R-squared Panel B	0.022	0.028	0.254	0.423				
First-stage F-stat (5×5 grids)					251.000	50.389	43.734	15.340
First-stage F-stat (Conley 1000km)					92.374	21.022	21.690	8.427

Notes: Panels A and B report cross-sectional OLS, Probit, and 2SLS IV estimates of equation (4). Panel C reports the corresponding first-stage estimates (equation (5)). The unit of observation is a 1×1-degree grid cell k. 'Any city or citadel' equals 100 if a city or citadel was present in grid cell k during the Bronze Age (and 0 otherwise). 'Any city by 1300 BC' equals 100 if a city was present in grid cell k by 1300 BC (and 0 otherwise). 'Metal transit index' is defined by equation (2), while 'Natural metal transit index' is defined by equation (3). Footnotes 18 and 21 describe the construction of the controls: Geography controls include proximity to mines, proximity to croplands, sea dummy, river dummy, mountains dummy, eigenvector centrality in the transport network, and generic natural transit trade potential. Standard errors clustered at the level of 5×5 degree grid cells are reported in parentheses. Standard errors computed using the approach of Conley (1999) (cut-off 1000km) are reported in square brackets.

Table D.24: Robustness generic transit trade potential: Metal transit trade and archaeological sites. Difference-in-differences (Stone Age vs Bronze Age)

	Any archaeological site (× 100)					
	OLS		2SLS IV			
	(1)	(2)	(3)	(4)	(5)	(6)
	Panel A: Second stage Bahn (2000)					
Metal transit index (IHS) × Bronze Age	1.104	1.518	0.967	2.280		
	(0.252)	(0.266)	(0.419)	(1.080)		
	[0.262]	[0.256]	[0.466]	[1.094]		
Metal transit index × Bronze Age					0.005	0.016
					(0.002)	(0.008)
					[0.003]	[0.008]
	Panel B: Second stage Pleiades Gazetteer (Bagnall, 2022)					
Metal transit index (IHS) × Bronze Age	0.552	0.576	0.546	0.995		
	(0.101)	(0.112)	(0.124)	(0.396)		
	[0.114]	[0.124]	[0.129]	[0.372]		
Metal transit index × Bronze Age					0.003	0.007
					(0.001)	(0.003)
					[0.001]	[0.002]
	Panel C: First stage					
Natural metal transit index (IHS) × Bronze Age			0.490	0.224	86.183	32.132
			(0.031)	(0.032)	(13.032)	(8.203)
			[0.036]	[0.034]	[13.016]	[7.781]
Geography controls×Bronze Age	No	Yes	No	Yes	No	Yes
Grid cell fixed effects	Yes	Yes	Yes	Yes	Yes	Yes
Continent×Bronze Age	Yes	Yes	Yes	Yes	Yes	Yes
Observations	21,940	21,940	21,940	21,940	21,940	21,940
Mean dependent variable Panel A	4.913	4.913	4.913	4.913	4.913	4.913
Mean dependent variable Panel B	1.759	1.759	1.759	1.759	1.759	1.759
R-squared Panel A	0.615	0.618				
R-squared Panel B	0.823	0.825				
First-stage F-stat (5×5 grids)			251.000	50.405	43.734	15.344
First-stage F-stat (Conley 1000km)			184.831	42.090	43.400	16.872

Notes: This table reports difference-in-differences OLS and 2SLS IV estimates of equation (6). The unit of observation is a 1×1 grid-cell k in period p (Stone Age or Bronze Age). 'Any Site' equals 100 rather than 0 for a grid cell k in period p if there is at least one archaeological site dating from period p and located in grid cell k. 'Metal transit index' is defined by equation (2), while 'Natural metal transit index' is defined by equation (3). Geography controls include proximity to mines, proximity to croplands, sea dummy, river dummy, mountains dummy, eigenvector centrality in the transport network, and generic natural transit trade potential. Panel A uses archaeological data from Bahn (2000), while Panel B uses data from Bagnall (2022). Panel C reports first-stage estimates (equation (7)). Standard errors clustered at the level of 5×5 degree grid cells are reported in parentheses. Standard errors computed using the approach of Conley (1999) (cut-off 1000km) are reported in square brackets.

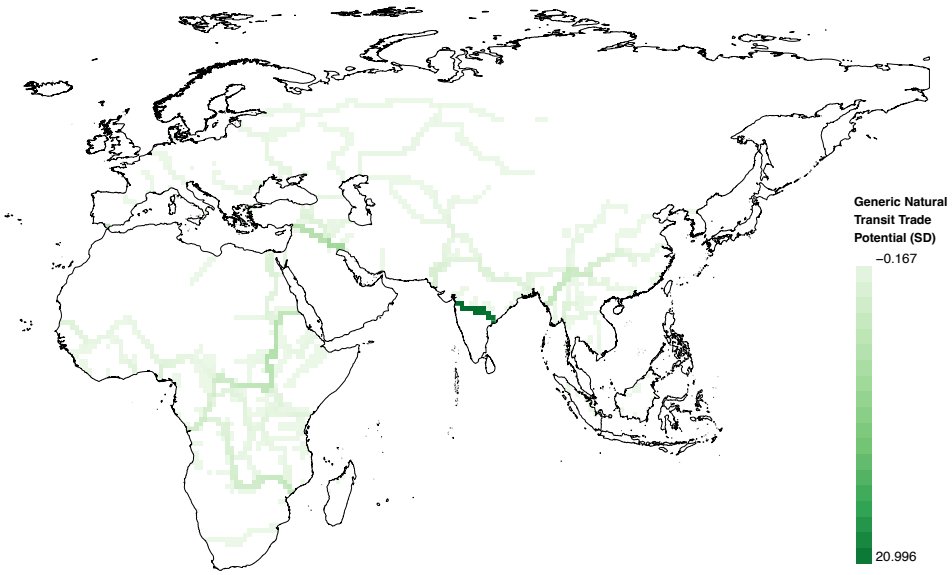


Figure D.13: Generic natural transit trade potential
Figure depicts the generic natural transit trade potential (as defined by equation (D.1)).

D.4.2 Natural obsidian transit trade potential

Obsidian is a volcanic glass that was traded widely before, during, and after the Bronze Age (e.g., Frahm, 2025; Renfrew, 1975; Tykot, 2002). A natural concern is that metal trade may have followed existing obsidian trade routes. If so, our estimates could be capturing the effects of obsidian transit trade rather than those of metal. To assess the relevance of this concern, we construct a measure of natural obsidian transit trade potential.

Data

Analogous to our main instrumental variable, we construct the measure of natural obsidian transit trade potential by identifying the least-cost paths between the closest potential obsidian deposits and productive land cells. To infer the location of potential obsidian deposits, we use the locations of volcanoes. This is motivated by the fact that obsidian forms naturally when lava from a volcanic eruption cools rapidly.[56] Formally, the natural obsidian transit trade potential, $OTTP$, is given by:

$$OTTP_k = \sum_{v \in \mathcal{V},\, p \in \mathcal{P}} \mathcal{I}_{P^\star_{vp}}[k] \times Prod_p, \tag{D.2}$$

where $\mathcal{V}$ and $\mathcal{P}$ denote the sets of all volcanoes and productive land cells, respectively; $P^\star_{vp}$ is the least-cost path from volcano v to productive land cell p; $\mathcal{I}_{P^\star_{vp}}[k]$ is an indicator function that equals one if $k \in P^\star_{vp}$ and zero otherwise; and $Prod_p$ is the net primary productivity of cell p in 3000 BC.

The data on volcanoes comes from the Global Volcanism Program database (Global Volcanism

[56]Note that not all eruptions are associated with the occurrence of obsidian. Obsidian glass typically forms from rhyolitic magma, which is characterized by a very high silica content. When this magma has low concentrations of gas and water and cools rapidly, it solidifies before crystals can form, resulting in a homogeneous, glassy material (Sheppard, 2008). The occurrence of obsidian-type glass has also been associated with eruptions that produce trachyte and dacite, and it has been found in volcanic settings characterized by andesite rock types (e.g., GeologyBase.com, 2025; D'Orazio, Gioncada and Bindi, 2018; Fink, 1983).

Program, 2025), which includes all volcanoes and their locations believed to have been active during the Pleistocene and Holocene periods (approximately the last 2.5 million years).[57,58] We exclude submarine volcanoes. The spatial distribution of the remaining volcanoes is displayed in Figure D.14.

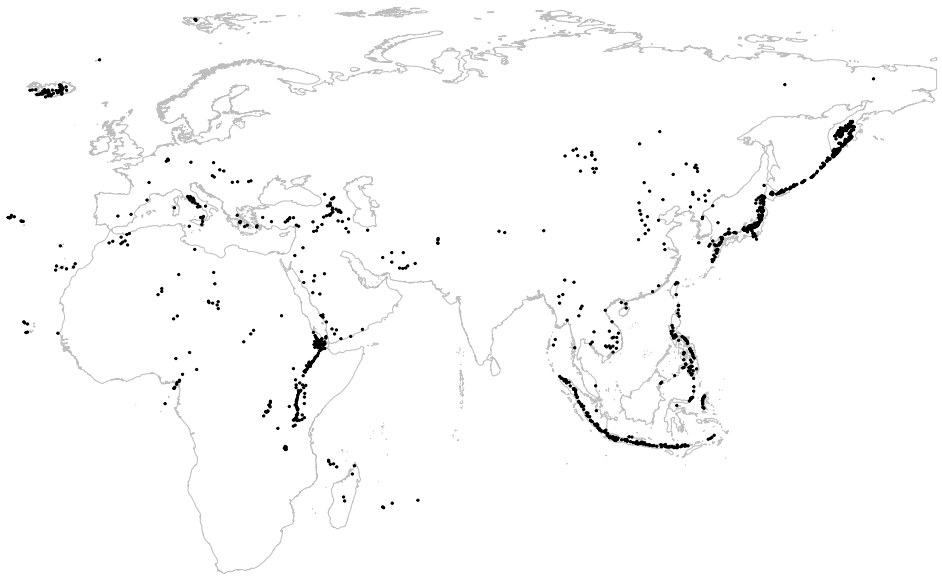


Figure D.14: Distribution of volcanoes
Figure shows the location of volcanoes with eruptions during the Pleistocene and Holocene.

Results

In Tables D.25 and D.26, we re-run our main cross-sectional and panel regressions, extending the set of control variables to include the natural obsidian transit trade potential. This constitutes a very demanding specification, as all the inputs used in constructing the natural obsidian transit potential index—except for the location of volcanoes—are identical to those used in our main instrumental variable. Nevertheless, the results reported below show that our main findings remain robust to the inclusion of the obsidian trade potential, particularly in the IHS specifications. The corresponding level-IV estimates are similar in magnitude, although the first stage becomes weak in the most saturated specifications and should therefore be interpreted with caution.

[57]We downloaded the data on 30 April 2025 from https://volcano.si.edu/volcanolist_holocene.cfm and https://volcano.si.edu/volcanolist_pleistocene.cfm, downloaded 30 April 2025.

[58]For 55% of the 2,662 volcanoes in the dataset, information on the dominant rock type is available. We obtain qualitatively equivalent results to those presented below when using the subset for which the dominant rock type is identified as rhyolite, dacite, trachyte, or andesite.

Table D.25: Robustness obsidian transit trade potential: Metal transit trade and Bronze Age cities

	OLS		Probit		2SLS IV			
	(1)	(2)	(3)	(4)	(5)	(6)	(7)	(8)
	Panel A: Second stage Green et al. (2024): Any city or citadel (×100)							
Metal transit index (IHS)	0.344	0.356	0.156	0.083	0.407	1.036		
	(0.074)	(0.080)	(0.025)	(0.030)	(0.088)	(0.458)		
	[0.094]	[0.096]	[0.009]	[0.012]	[0.123]	[0.435]		
Metal transit index							0.002	0.007
							(0.001)	(0.004)
							[0.001]	[0.005]
	Panel B: Second stage Reba, Reitsma and Seto (2016): Any city (×100)							
Metal transit index (IHS)	0.383	0.446	0.201	0.100	0.342	0.929		
	(0.087)	(0.096)	(0.029)	(0.034)	(0.083)	(0.339)		
	[0.134]	[0.148]	[0.011]	[0.013]	[0.124]	[0.442]		
Metal transit index							0.002	0.006
							(0.000)	(0.003)
							[0.001]	[0.004]
					Panel C: First stage			
Natural metal transit index (IHS)					0.490	0.209	86.183	32.925
					(0.031)	(0.039)	(13.032)	(15.920)
					[0.051]	[0.049]	[18.407]	[21.563]
Geography controls	No	Yes	No	Yes	No	Yes	No	Yes
Continent dummies	Yes	Yes	Yes	Yes	Yes	Yes	Yes	Yes
Observations	10,970	10,970	10,970	10,970	10,970	10,970	10,970	10,970
Mean dependent variable Panel A	0.483	0.483	0.483	0.483	0.483	0.483	0.483	0.483
Mean dependent variable Panel B	0.419	0.419	0.419	0.419	0.419	0.419	0.419	0.419
R-squared Panel A	0.016	0.018	0.177	0.259				
R-squared Panel B	0.022	0.029	0.254	0.423				
First-stage F-stat (5×5 grids)					251.000	28.277	43.734	4.277
First-stage F-stat (Conley 1000km)					92.374	17.800	21.690	2.304

Notes: Panels A and B report cross-sectional OLS, Probit, and 2SLS IV estimates of equation (4). Panel C reports the corresponding first-stage estimates (equation (5)). The unit of observation is a 1×1-degree grid cell k. 'Any city or citadel' equals 100 if a city or citadel was present in grid cell k during the Bronze Age (and 0 otherwise). 'Any city by 1300 BC' equals 100 if a city was present in grid cell k by 1300 BC (and 0 otherwise). 'Metal transit index' is defined by equation (2), while 'Natural metal transit index' is defined by equation (3). Footnotes 18 and 21 describe the construction of the controls: Geography controls include proximity to mines, proximity to croplands, sea dummy, river dummy, mountains dummy, eigenvector centrality in the transport network, and natural obsidian transit trade potential. Standard errors clustered at the level of 5×5 degree grid cells are reported in parentheses. Standard errors computed using the approach of Conley (1999) (cut-off 1000km) are reported in square brackets.

Table D.26: Robustness obsidian transit trade potential: Metal transit trade and archaeological sites. Difference-in-differences (Stone Age vs Bronze Age)

	Any archaeological site (×100)					
	OLS		2SLS IV			
	(1)	(2)	(3)	(4)	(5)	(6)
	Panel A: Second stage Bahn (2000)					
Metal transit index (IHS) ×Bronze Age	1.104	1.523	0.967	3.900		
	(0.252)	(0.274)	(0.419)	(1.492)		
	[0.262]	[0.257]	[0.466]	[1.292]		
Metal transit index ×Bronze Age					0.005	0.025
					(0.002)	(0.014)
					[0.003]	[0.013]
	Panel B: Second stage Pleiades Gazetteer (Bagnall, 2022)					
Metal transit index (IHS) ×Bronze Age	0.552	0.561	0.546	1.486		
	(0.101)	(0.115)	(0.124)	(0.558)		
	[0.114]	[0.124]	[0.129]	[0.446]		
Metal transit index ×Bronze Age					0.003	0.009
					(0.001)	(0.006)
					[0.001]	[0.005]
	Panel C: First stage					
Natural metal transit index (IHS) ×Bronze Age			0.490	0.209	86.183	32.925
			(0.031)	(0.039)	(13.032)	(15.917)
			[0.036]	[0.035]	[13.016]	[15.247]
Geography controls×Bronze Age	No	Yes	No	Yes	No	Yes
Grid cell fixed effects	Yes	Yes	Yes	Yes	Yes	Yes
Continent×Bronze Age	Yes	Yes	Yes	Yes	Yes	Yes
Observations	21,940	21,940	21,940	21,940	21,940	21,940
Mean dependent variable Panel A	4.913	4.913	4.913	4.913	4.913	4.913
Mean dependent variable Panel B	1.759	1.759	1.759	1.759	1.759	1.759
R-squared Panel A	0.615	0.618				
R-squared Panel B	0.823	0.825				
First-stage F-stat (5×5 grids)			251.000	28.286	43.734	4.279
First-stage F-stat (Conley 1000km)			184.831	35.639	43.400	4.613

Notes: This table reports difference-in-differences OLS and 2SLS IV estimates of equation (6). The unit of observation is a 1×1 grid-cell k in period p (Stone Age or Bronze Age). 'Any Site' equals 100 rather than 0 for a grid cell k in period p if there is at least one archaeological site dating from period p and located in grid cell k. 'Metal transit index' is defined by equation (2), while 'Natural metal transit index' is defined by equation (3). Geography controls include proximity to mines, proximity to croplands, sea dummy, river dummy, mountains dummy, eigenvector centrality in the transport network, and natural obsidian transit trade potential. Panel A uses archaeological data from Bahn (2000), while Panel B uses data from Bagnall (2022). Panel C reports first-stage estimates (equation (7)). Standard errors clustered at the level of 5×5 degree grid cells are reported in parentheses. Standard errors computed using the approach of Conley (1999) (cut-off 1000km) are reported in square brackets.

D.5 Warfare

In this appendix, we examine whether the spatial distribution of organized warfare during the Bronze Age can be partially explained by the economic and strategic value of locations within the long-distance metal trade network. A substantial body of archaeological and historical scholarship has emphasized that one of the key drivers of conflict and expansionist campaigns in the Bronze Age world was the need to control strategic nodes within regional and interregional trade systems. A classic example is the Trojan War, which several scholars have linked to Troy's control of the Dardanelles—the easiest crossing point between Europe and Asia (Rose, 1998; Cline, 2013, p. 47). Another classical example is the territorial expansion of the Hittite Empire. The Hittite military strategy was explicitly shaped by the need to secure control over trade corridors, particularly those providing access to metal-rich regions. Among these, the tin routes connecting Anatolia and Mesopotamia were especially important (Bryce, 2006, p. 81). In a regional analysis of weapon distribution in Central Europe, Kristiansen and Horn (2018) argue that the military elite emerged primarily to control high-value trade flows. He concludes: *"Thus, warriors played an essential role because they had many functions during the Bronze Age. The most important was to control trade and its valuables—from metal to amber and salt. Every community needed it."* He further notes that *"organized trade made warriors indispensable, and warfare could take on huge proportions when it came to the control of trade routes, or rather their most important hubs/bottlenecks, such as Bernstorf."*

These perspectives motivate the empirical analysis that follows. To our knowledge, no comprehensive dataset currently exists that systematically documents conflict events across a wide geographic scope for this period. As a first step, we compile a novel dataset capturing the spatial distribution of prehistoric weapons—used here as a proxy for organized military activity. In the second step, we test whether the advent of metallurgy is associated with a spatial shift in the distribution of such weapons toward metal trade corridors.

Data

To construct the dataset on prehistoric weapons, we systematically searched the online collections of five major museums: the Metropolitan Museum of Art (Met), the University of Pennsylvania Museum of Archaeology and Anthropology (Penn), the Phoebe A. Hearst Museum of Anthropology at UC Berkeley (Berkeley), the Smithsonian Institution, the Louvre Museum (Louvre), and the British Museum (British Museum). These institutions curate some of the most extensive collections of prehistoric Eurasian material culture. We focus specifically on objects identified as weapons, including daggers, swords, axes, knives, spears, and arrowheads. Our geographic scope is limited to Eurasia and Africa, and our temporal scope to the pre-Bronze Age and the Bronze Age. Search strategies were tailored to each institution's catalog system. In most cases, we relied on keyword searches for object types (e.g., "dagger", "spear", "sword", "bronze weapon"), while some platforms allowed for category-based filtering (e.g., weapons). Similarly, to identify the archaeological time period of the object, we used museum-specific archaeological classifications (e.g., "Naqada I–III", "Pleistocene–Holocene", or "Bronze Age"). To be included in our dataset, an artifact had to meet two criteria: (a) the find site must be precisely identifiable (we exclude entries with locations reported only at the province or broader regional level), and (b) the object must be reliably dated to either the pre-Bronze Age or the Bronze Age. In some cases, data could be downloaded in bulk;

however, in most instances, artifact-level information had to be collected manually. All artifact locations were subsequently georeferenced by hand, based on the reported find sites.

Figure D.15 maps the locations of all weapons in our dataset. Table D.27 reports the number of weapons contributed by each museum, disaggregated by period. Tables D.28–D.29 provide further details on the data collection process for the Neolithic and Bronze Age periods, respectively. For each institution, the tables specify the search queries, the download method, and provide direct links to the online collection databases.

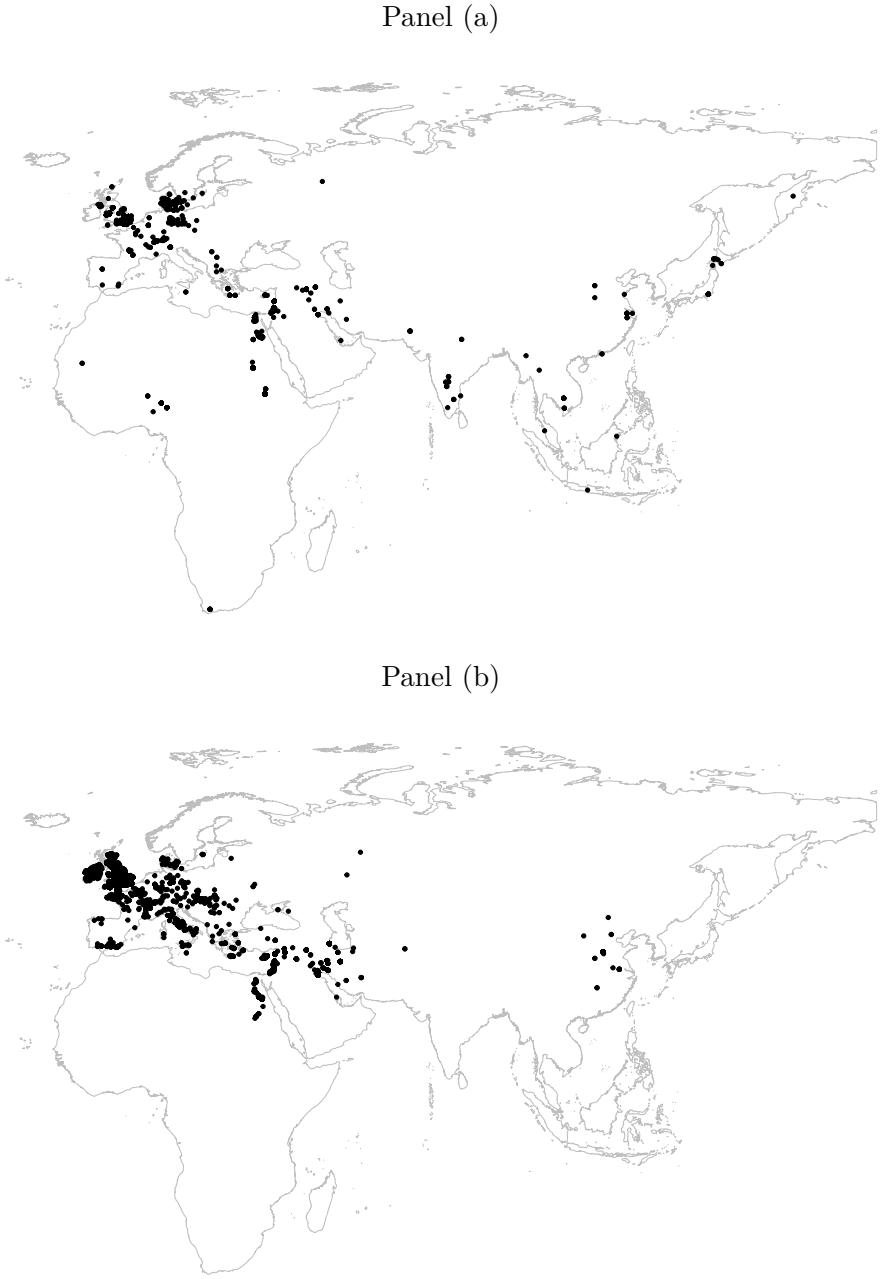


Figure D.15: Weapon finds

Figure depicts the location of weapon finds. Data come from the British Museum, the Louvre, the Met, the Penn Museum, the Phoebe A. Hearst Museum of Anthropology, and the Smithonian. Panel (a) shows sites present in the Stone Age, panel (b) sites present in the Bronze Age.

For our empirical analysis, we aggregate the artifact-level data to the 1×1 degree grid cell level, summing the number of weapon finds within each grid cell and period. We use an indicator variable for the presence of any weapon in a given grid cell and period as the outcome variable.

Table D.27: Weapons by museum and period

Weapons (Stone Age)	
British Museum	1441
Hearst Museum	14
Louvre	16
Metropolitan Museum of Art (New York)	132
Penn Museum	638
Smithsonian	9
Weapons (Bronze Age)	
British Museum	3583
Hearst Museum	7
Louvre	672
Metropolitan Museum of Art (New York)	89
Penn Museum	148
Smithsonian	13

Notes: This table lists the number of weapons extracted from each collection, separately for the pre-Bronze Age and the Bronze Age. More details on sources and the collection procedure are provided in Tables D.28–D.29.

Table D.28: Museum collection search approach: Stone Age

Download Date	Museum URL	Museum Name	Search Terms	Period	Download Method
25.04.–05.06.2025	https://www.penn.museum/collections/advanced.php	Penn Museum	arms, arrow, arrowheads, axe, blades, dagger, knife, spear, sword	all pre Bronze Age periods	manually, find site and period case by case
25.04.–05.06.2025	https://www.metmuseum.org/art/collection	Metropolitan Museum of Art	arms, arrow, arrowheads, axe, blades, dagger, knife, spear, sword	all pre Bronze Age periods	manually, find site and period case by case
25.04.–05.06.2025	https://portal.hearstmuseum.berkeley.edu/	Phoebe A. Hearst Museum	category: weapons	Naqada I–III, Solutrean, Stillbay, Pleistocene–Holocene	manually, find site case by case
25.04.–05.06.2025	https://www.si.edu/search/images	Smithsonian	arms, arrow, arrowheads, axe, blades, dagger, knife, spear, sword	all pre Bronze Age periods	manually, find site and period case by case
25.04.–05.06.2025	https://www.britishmuseum.org/collection/search	British Museum	object: weapon	period: prehistoric	bulk download
01.05.2025	https://collections.louvre.fr/en/recherche	Louvre	object: objects in Armes & équipements militaires	all pre Bronze Age periods	manually, find site and period case by case

Table D.29: Museum collection search approach: Bronze Age

Download Date	Museum URL	Museum Name	Search Terms	Period	Download Method
25.04.–05.06.2025	https://www.penn.museum/collections/advanced.php	Penn Museum	arms, arrow, arrowheads, axe, blades, dagger, knife, spear, sword	Bronze Age periods	manually, find site and period case by case
25.04.–05.06.2025	https://www.metmuseum.org/art/collection	Metropolitan Museum of Art	bronze artifacts: arms, arrow, axe, dagger, sword	Bronze Age periods	manually, find site and period case by case
25.04.–05.06.2025	https://portal.hearstmuseum.berkeley.edu/	Phoebe A. Hearst Museum	category: bronze weapons	Bronze Age periods	manually, find site case by case
25.04.–05.06.2025	https://www.si.edu/search/images	Smithsonian	arms, arrow, arrowheads, axe, blades, dagger, knife, spear, sword	Bronze Age periods	manually, find site and period case by case
30.04.2025	https://www.britishmuseum.org/collection/search	British Museum	object: weapon	period: Pre History	bulk download
01.05.2025	https://collections.louvre.fr/en/recherche	Louvre	object: bronze objects in Armes & équipements militaires	period: 5000 to 500 BC	manually, find site and period case by case

Empirical analysis

To test whether metal transit trade influenced the spatial distribution of conflict, we estimate the same 2SLS difference-in-differences model used in the main analysis (equation (6)). The only difference lies in the outcome variable, which is now defined as an indicator that takes the value 100 if a grid cell contains a weapon from a given period, and zero otherwise.

Table D.30 presents the results. Columns (1) and (2) report estimates using the inverse hyperbolic sine (IHS) transformation of the metal transit index, while columns (3) and (4) use the untransformed index. The coefficient on the interaction between the metal transit index and the Bronze Age indicator is estimated to be always positive and statistically significant at conventional confidence levels in three out of four cases.[59]

In columns (5) through (8), we repeat the same regressions as in the previous four columns, but restrict the analysis to grid cells in which at least one prehistoric weapon has been discovered. This helps mitigate concerns about sampling or excavation bias. Reassuringly, the main results remain robust to this restriction, with similar magnitudes and significance levels.

Together, these findings provide some empirical support for the hypothesis that the advent of metallurgy caused a spatial shift of military conflicts towards the road-knots of the metal trade network.

[59]The metal transit index coefficient in column (2) is bordering on statistical significance, with a p-value of 0.106.

Table D.30: Metal transit trade and warfare

	Any Weapon (×100)							
	Full Sample				Restricted Sample			
	(1)	(2)	(3)	(4)	(5)	(6)	(7)	(8)
	Panel A: Second stage							
Metal transit index (IHS)	0.759	0.491			8.152	17.718		
× Bronze Age	(0.213)	(0.310)			(3.316)	(5.665)		
	[0.207]	[0.304]			[2.152]	[4.156]		
Transit index			0.004	0.004			0.024	0.050
× Bronze Age			(0.001)	(0.002)			(0.011)	(0.021)
			[0.001]	[0.002]			[0.007]	[0.016]
	Panel B: First stage							
Natural metal transit index (IHS)	0.490	0.308	86.183	43.091	1.101	0.664	379.852	233.736
× Bronze Age	(0.031)	(0.030)	(13.032)	(8.274)	(0.137)	(0.147)	(93.728)	(74.819)
	[0.036]	[0.034]	[13.016]	[7.986]	[0.106]	[0.116]	[80.897]	[62.220]
Geography controls	No	Yes	No	Yes	No	Yes	No	Yes
Continent dummies	Yes	Yes	Yes	Yes	Yes	Yes	Yes	Yes
Observations	21,940	21,940	21,940	21,940	732	732	732	732
Mean dependent variable	2.051	2.051	2.051	2.051	61.475	61.475	61.475	61.475
First-stage F-stat (5×5 grids)	251.000	102.289	43.734	27.122	64.937	20.345	16.424	9.760
First-stage F-stat (Conley 1000km)	184.831	82.079	43.400	28.807	106.435	31.902	21.768	13.704

The full sample includes all grid cells, while the restricted sample includes only those grid cells with a strictly positive value of the dependent variable in at least one period (Stone Age or Bronze Age). Panel A reports 2SLS estimates of equation (6), while panel B reports the first-stage estimates (equation (7)). The unit of observation is a 1×1 grid-cell k in period p (Stone Age or Bronze Age). 'Any Weapon' is a dummy equal to 100 if a weapon dated to period p was excavated in grid cell k, and zero otherwise. 'Metal transit index' is defined by equation (2), while 'Natural metal transit index' is defined by equation (3). Footnotes 18 and 21 describe the construction of the controls: Geography controls include proximity to mines, proximity to croplands, sea dummy, river dummy, mountains dummy, and centrality in the transport network. Standard errors clustered at the level of 5×5 degree grid cells are reported in parentheses. Standard errors computed using the approach of Conley (1999) (cut-off 1000km) are reported in square brackets.

D.6 Europe

This appendix focuses on the European Bronze Age, the most extensively studied period in world archaeology (Radivojević et al., 2019). The rich archaeological record, combined with radiocarbon dating, makes it possible to trace changes in metal transit trade potential and socio-economic stratification *within* the Bronze Age. Specifically, we examine variation resulting from the discovery of new mines (and the depletion of old ones) that occurred between the Early/Middle and Late Bronze Age in Central Europe. We then study how these changes influenced the development of complex hierarchies.

As previously noted, Central and Western Europe did not witness the emergence of fully-fledged civilizations or cities during the Bronze Age. Nonetheless, the region experienced a transition from classless bands and tribes to hierarchically structured societies—i.e., chiefdoms—where local leaders exercised a degree of centralized decision-making authority. We capture this development using data on carbon-dated Bronze Age elite burials, focusing specifically on those containing bronze weapons. Such burials are a significant archaeological indicator of the presence of local chiefdoms (Earle et al., 2015, Renfrew and Bahn, 2016, pp. 175).

Below, we first describe the data gathering and construction process. We then present our main empirical approach, which exploits variation within the European Bronze Age, along with the corresponding regression results. In an auxiliary analysis, we reproduce the pattern of results using our main cross-sectional approach (cf. Section 4.1).

Data

To capture the diffusion of burials with metal weapons, we digitized the *Prähistorische Bronzefunde* (PBF). This project systematically compiles information on archaeological metal artifacts found across Europe. Since 1966, it has published 186 volumes documenting individual metal finds dating from 3000 to 500 BC. The PBF organizes these into book series, or *Abteilungen* (divisions), by artifact type. For instance, *Abteilung IX*, which covers axes and hatchets, comprises 29 volumes, each focusing on a specific region. An expert archaeologist from the respective region typically compiles this information from various sources, such as museum catalogs.[60]

We focus on weapons, specifically those classified as "axes and hatchets" and "swords" (*Abteilung IV* and *Abteilung IX*, for a total of 39 volumes). We augment this dataset with artifacts from the "Bronze und urnenfelderzeitliche Schwerter" database (Hahnekamp, 2011). Combined, the PBF volumes and Hahnekamp's data encompass Central and Western Europe. Table D.34 at the end of this appendix provides the full list of volumes included, while Figure D.16 below illustrates the find locations and the spatial scope of our Bronze Age analysis.

For each artifact in our database, we note three key details: (i) the coordinates of the excavation site, (ii) the site's nature (e.g., burial site), and (iii) the artifact's archaeological type or family (e.g., Pădureni axe type). Using (ii), we identify the elite burials, while (iii) allows us to link the burial to specific time periods (Early, Middle, and Late Bronze Age in Central Europe). For example, entry 13 from *Prähistorische Bronzefunde, Abteilung IV, Book 2*, is a "hilt plate short sword of the Sauerbrunn type", a sword associated with the Göggenhofen culture and thus dating back to the Central European Middle Bronze Age (Schauer, 1971, p. 22). Figure D.17, shown at the end of this

[60] For example, the volumes on bronze axes and hatchets excavated in Romania (*Abteilung IX: Äxte, Beile—Die Äxte und Beile in Rumänien I–II*) were written by Alexandru Vulpe, a Romanian archaeologist.

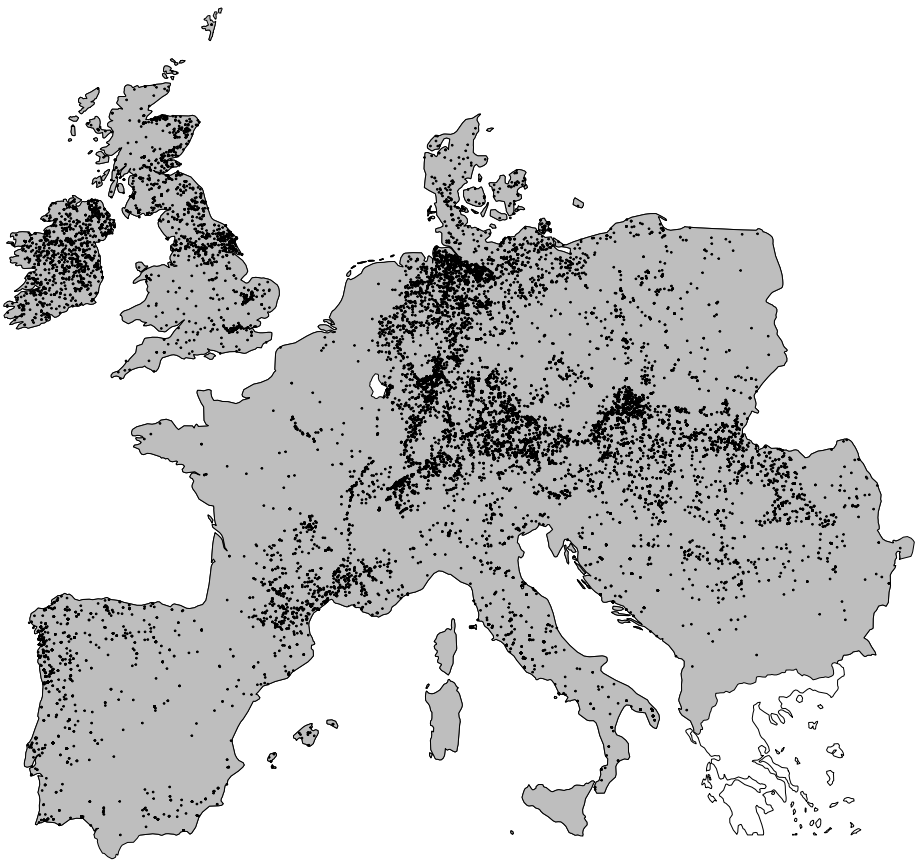


Figure D.16: Bronze weapons finds
Figure depicts the location of bronze weapon finds as recorded by Prähistorische Bronzefunde (*Abteilung IV* and *Abteilung IX*). Regions shaded in gray are included in our analysis.

appendix, presents a book excerpt to illustrate the entry structure.

For our main empirical analysis, we create a 1×1-degree grid-cell panel dataset comprising two time periods, corresponding to the Central European Early/Middle Bronze Age [3000 BC, 1300 BC) and the Late Bronze Age [1300 BC, 750 BC]. For each period, we identify the grid cells containing at least one elite burial. Additionally, we compute a time-varying version of the metal trade index (cf. equation (2)) by considering only the mines that can be identified as active during the respective time period.

Table D.31 reports the summary statistics of the dataset, including a decomposition of the variance between and within grid cells. A substantial share of the variance in metal transit trade is within grid cells. Our main empirical strategy, described below, relies on this within-grid-cell variation.

Table D.31: Summary statistics of key variables (Europe)

		Std. Dev.					
Variable	**Mean**	**Total**	**Between**	**Within**	**Min.**	**Max.**	**Obs.**
Any elite burial (×100)	22.948	42.068	38.000	18.081	0	100	1194
Metal transit index	977.827	3182.699	2694.866	1695.098	0	40877.495	1194

Main empirical analysis: within Bronze Age panel data

Because we focus on within–Bronze Age dynamics, we cannot employ our usual 2SLS IV strategy as the metal deposit data are time-invariant and thus offer no within-Bronze Age variation that can be exploited for identification. We therefore resort to the following simple OLS panel data regression model to analyze the effect of metal transit trade on the emergence of elites during the European Bronze Age:

$$y_{k,p} = \beta\, IHS(T_{k,p}) + X_{k,p}\,\chi + \mu_k + \tau_p + \psi_{k,p}. \tag{D.3}$$

The dependent variable, $y_{k,p}$, is an indicator for the presence of elite burials dating from period p in grid cell k. The main explanatory variable is the metal transit index for cell k in period p, $T_{k,p}$. The vector $X_{k,p}$ represents control variables. Grid cell fixed effects and period fixed effects are denoted by μ_k and τ_p, respectively.

Table D.32 presents the results of our within–Bronze Age panel data analysis on the relationship between the metal transit index and elite burials. Columns (1) and (2) report estimates where the metal transit index is transformed using the inverse hyperbolic sine (IHS) function. Column (1) includes only grid cell and period fixed effects, while column (2) additionally controls for proximity to mines—the only time-varying geographic characteristic. In columns (3) and (4), we use the untransformed metal transit index as the main explanatory variable.

Across all specifications, the estimated coefficients of the metal transit index are positive and statistically significant at the 90% confidence level or higher. The point estimate in column (4) implies that an increase of 2,225 square kilometers in cropland connected to a mine via a route traversing the grid cell—corresponding to a shift from the lowest to the highest percentile in the metal transit index distribution—increases the probability of an elite burial in a given grid cell and period by 2.2 percentage points. Evaluated at the sample mean, this corresponds to 10%. These results provide strong initial evidence supporting the argument that metal transit trade played a

Table D.32: Metal transit trade and elite burials in Europe

	Any Elite Burial (×100)			
	(1)	(2)	(3)	(4)
Metal transit index (IHS)	0.959	0.745		
	(0.481)	(0.430)		
	[0.351]	[0.324]		
Metal transit index			0.001	0.001
			(0.001)	(0.001)
			[0.000]	[0.000]
Geography controls	No	Yes	No	Yes
Grid cell fixed effects	Yes	Yes	Yes	Yes
Period fixed effects	Yes	Yes	Yes	Yes
Observations	1,194	1,194	1,194	1,194
Mean dependent variable	22.948	22.948	22.948	22.948
R-squared	0.633	0.634	0.636	0.637

Notes: This table reports OLS estimates of equation (D.3). The unit of observation is a 1×1 grid-cell k in period p. There are two periods: Central-Europe Early/Middle Bronze Age [3000-1300 BC) and Late Bronze Age [1300-750 BC]. 'Any Elite Burial' equals 100 if there is any elite burial (i.e., grave with metal weapon) dating from period p in grid cell k and 0 otherwise. 'Metal transit index' is defined by equation (2). 'Geography controls' include the time-varying proximity to mines. Standard errors clustered at 5×5 degree grid cells are reported in parentheses. Standard errors computed using the approach of Conley (1999) (cut-off 1000km) are reported in square brackets.

significant role in the development and intensification of hierarchical social and political institutions in prehistoric Europe.

Auxiliary analysis: cross-sectional data

A main benefit of the panel data analysis presented above is that it allows us to investigate the dynamic effects of the metal transit trade during the Bronze Age, whilst accounting for unobserved time-invariant local characteristics. However, the results do not directly imply that European regions with high metal transit volumes throughout the Bronze Age also had a higher probability of elites emerging.

Furthermore, a concern related to our panel data analysis is that changes in metal transit trade could be endogenous to elite formation. In our setting, this would be the case, for example, if (emerging) elites influenced the opening and closure of metal mines. To address these concerns, we employ our standard cross-sectional 2SLS IV approach, outlined in detail in Section 4.1. This allows us to exploit exogenous sources of variation.[61] The only two modifications are that (i) we now use an indicator that captures whether any Bronze Age elite burial—regardless of the sub-period of the Bronze Age—is present in a grid cell as the outcome variable, and (ii) we restrict the geographical scope of our analysis to the central and western areas of Europe shown in Figure D.16.

Before presenting the results, it is worthwhile noting that while the cross-sectional approach offers some benefits over the panel data approach, it also comes with drawbacks. Most importantly, we reduce the degrees of variation and increase the potential for excavation biases—i.e., non-classical measurement errors—to influence our estimates. Given that we are focusing on small geographical variations, we also substantially reduce the variation in our main explanatory variables, i.e., the metal transit index and the natural metal transit index. The subsequent cross-sectional results should therefore be interpreted with particular caution. Table D.33 presents the estimates. In

[61] We cannot implement an IV approach in the within-Bronze Age panel setting because none of the components used in the construction of our IV exhibit any variation over time.

Table D.33: Cross-sectional analysis: Metal transit trade and elite burials in Europe

	OLS		Probit		2SLS IV			
	(1)	(2)	(3)	(4)	(5)	(6)	(7)	(8)
	Panel A: Any elite burial (×100)							
Metal transit index (IHS)	2.782	1.485	0.091	0.051	5.365	4.236		
	(0.925)	(0.743)	(0.026)	(0.024)	(1.440)	(2.106)		
	[1.208]	[0.820]	[0.020]	[0.017]	[1.701]	[1.661]		
Metal transit index							0.021	0.022
							(0.008)	(0.013)
							[0.010]	[0.011]
					Panel B: First stage			
Natural metal transit index (IHS)					1.049	0.671	265.288	131.024
					(0.063)	(0.072)	(72.148)	(53.732)
					[0.087]	[0.083]	[104.266]	[62.964]
Geography controls	No	Yes	No	Yes	No	Yes	No	Yes
Continent dummies	Yes	Yes	Yes	Yes	Yes	Yes	Yes	Yes
Observations	597	597	597	597	597	597	597	597
Mean dependent variable	29.481	29.481	29.481	29.481	29.481	29.481	29.481	29.481
R-squared	0.052	0.110	0.039	0.098				
First-stage F-stat (5×5 grids)					279.734	87.434	13.520	5.946
First-stage F-stat (Conley 1000km)					142.332	63.259	6.344	4.158

Notes: Panels A reports cross-sectional OLS, probit, and 2SLS IV estimates of equation (4). Panel B reports the corresponding first-stage estimates (equation (5)). The unit of observation is a 1×1-degree grid cell k. 'Any Elite Burial' equals 100 if there is any elite burial (i.e., grave with metal weapon) dating from the Bronze Age in grid cell k and 0 otherwise. 'Metal transit index' is defined by equation (2), while 'Natural metal transit index' is defined by equation (3). Footnotes 18 and 21 describe the construction of the controls: Geography controls include proximity to mines, proximity to croplands, sea dummy, river dummy, mountains dummy, and centrality in the transport network. Standard errors clustered at the level of 5×5 degree grid cells are reported in parentheses. Standard errors computed using the approach of Conley (1999) (cut-off 1000km) are reported in square brackets.

analogy to our main analysis (cf. Table 1), we start with a parsimonious OLS specification, which uses the IHS-transformed metal transit index as the sole regressor in column (1). In column (2), we add the geographical control variables; columns (3)–(4) repeat the same exercise using probit. Throughout, we observe a positive and statistically significant relationship between the metal transit index and the occurrence of elite burials. In columns (5)–(6), we implement our 2SLS IV strategy. The first-stage F-statistics are—despite the reduced geographical extent—well above conventional threshold levels. The second-stage point estimates are positive and statistically significant at the 90% confidence level. This provides additional evidence for the importance of metal transit trade in shaping the geography of social stratification during the Bronze Age in Europe.

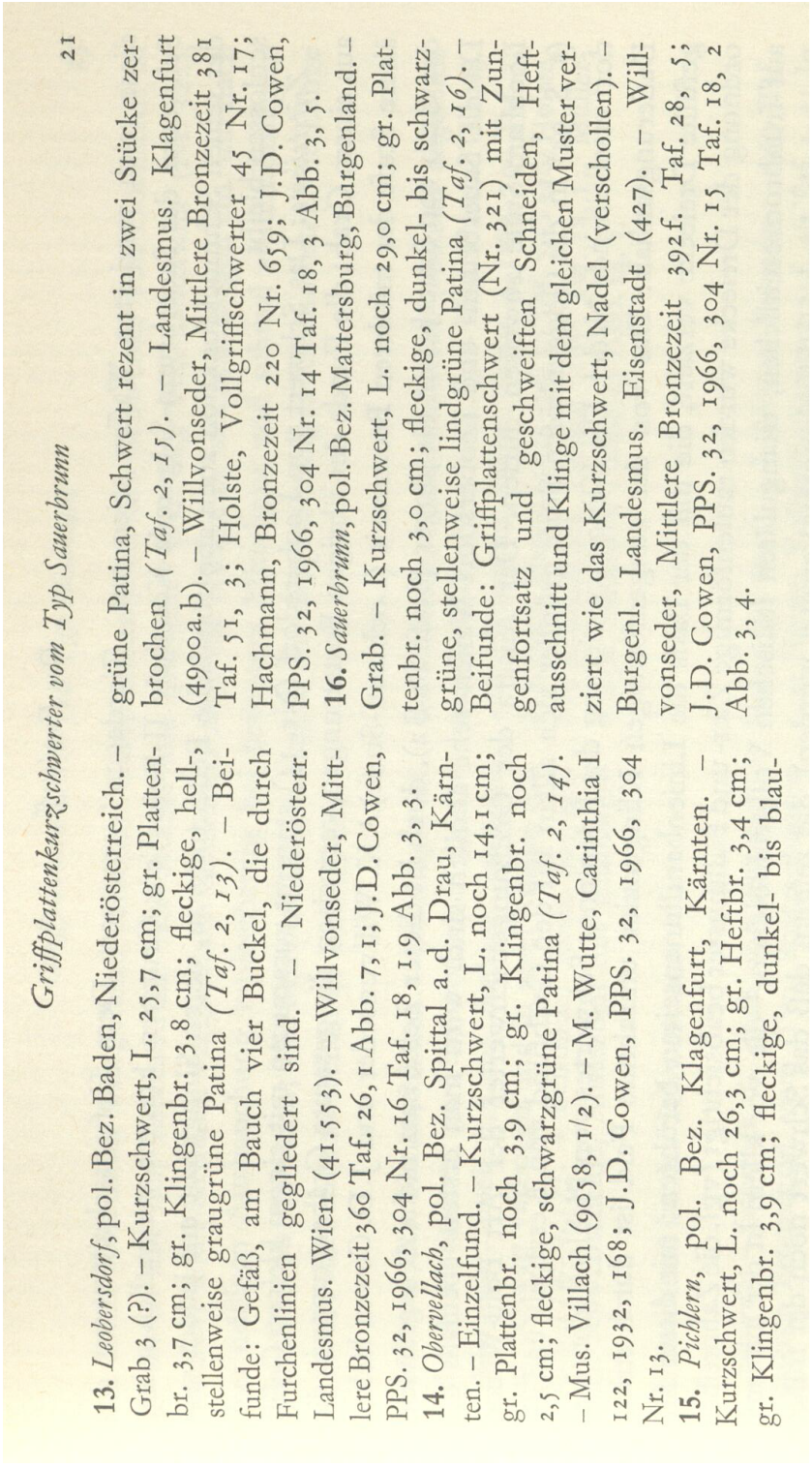
The qualitative pattern of results remains unchanged when we use the untransformed metal transit index in columns (7)–(8). The coefficients suggest that moving from the lowest to the highest percentile in the metal transit index distribution leads to a 29.5 percentage point increase in the probability of elite burials.[62] When evaluated at the sample mean, this corresponds to a doubling of the baseline probability. However, given the relatively low first-stage F-statistic, the size of the point estimates and their economic magnitude should be interpreted with caution.

Taken together, this appendix documents that metal trade influenced the spatial patterns and dynamics of socio-economic development during the European Bronze Age.

[62] Moving from the lowest to the highest percentile in the metal transit index distribution corresponds to a jump in the index of 1,407.

Additional Figures and Tables

Figure D.17 depicts an illustrative excerpt from the *Prähistorische Bronzefunde*. Table D.34 lists the references and the number of artifacts per book.



Griffplattenkurzschwerter vom Typ Sauerbrunn 21

13. *Leobersdorf*, pol. Bez. Baden, Niederösterreich. – Grab 3 (?). – Kurzschwert, L. 25,7 cm; gr. Plattenbr. 3,7 cm; gr. Klingenbr. 3,8 cm; fleckige, hellstellenweise graugrüne Patina (*Taf. 2, 13*). – Beifunde: Gefäß, am Bauch vier Buckel, die durch Furchenlinien gegliedert sind. – Niederösterr. Landesmus. Wien (41.553). – Willvonseder, Mittlere Bronzezeit 360 Taf. 26, 1 Abb. 7, 1; J.D. Cowen, PPS. 32, 1966, 304 Nr. 16 Taf. 18, 1.9 Abb. 3, 3.

14. *Obervellach*, pol. Bez. Spittal a.d. Drau, Kärnten. – Einzelfund. – Kurzschwert, L. noch 14,1 cm; gr. Plattenbr. noch 3,9 cm; gr. Klingenbr. noch 2,5 cm; fleckige, schwarzgrüne Patina (*Taf. 2, 14*). – Mus. Villach (9058, 1/2). – M. Wutte, Carinthia I 122, 1932, 168; J.D. Cowen, PPS. 32, 1966, 304 Nr. 13.

15. *Pichlern*, pol. Bez. Klagenfurt, Kärnten. – Kurzschwert, L. noch 26,3 cm; gr. Heftbr. 3,4 cm; gr. Klingenbr. 3,9 cm; fleckige, dunkel- bis blaugrüne Patina, Schwert rezent in zwei Stücke zerbrochen (*Taf. 2, 15*). – Landesmus. Klagenfurt (4900a.b). – Willvonseder, Mittlere Bronzezeit 381 Taf. 51, 3; Holste, Vollgriffschwerter 45 Nr. 17; Hachmann, Bronzezeit 220 Nr. 659; J.D. Cowen, PPS. 32, 1966, 304 Nr. 14 Taf. 18, 3 Abb. 3, 5.

16. *Sauerbrunn*, pol. Bez. Mattersburg, Burgenland. – Grab. – Kurzschwert, L. noch 29,0 cm; gr. Plattenbr. noch 3,0 cm; fleckige, dunkel- bis schwarzgrüne, stellenweise lindgrüne Patina (*Taf. 2, 16*). – Beifunde: Griffplattenschwert (Nr. 321) mit Zungenfortsatz und geschweiften Schneiden, Heftausschnitt und Klinge mit dem gleichen Muster verziert wie das Kurzschwert, Nadel (verschollen). – Burgenl. Landesmus. Eisenstadt (427). – Willvonseder, Mittlere Bronzezeit 392f. Taf. 28, 5; J.D. Cowen, PPS. 32, 1966, 304 Nr. 15 Taf. 18, 2 Abb. 3, 4.

Figure D.17: Example entry *Prähistorische Bronzefunde IV, Band 02*: page 21 of Schauer (1971).

Prähistorische Bronzefunde			
		Abt. IX: Äxte, Beile	
Book number	Author	Book title and publication year	# Artifacts
1.	P. Harbison	The Axes of the Early Bronze Age in Ireland (1969)	746
2.	A. Vulpe	Die Äxte und Beile in Rumänien I (1970)	276
3.	M. Novotná	Die Äxte und Beile in der Slowakei (1970)	540
4.	B.-U. Abels	Die Randleistenbeile in Baden-Württemberg, dem Elsaß, der Franche-Comté und der Schweiz (1972)	508
5.	A. Vulpe	Die Äxte und Beile in Rumänien II (1975)	119
6.	L. Monteagudo	Die Beile auf der Iberischen Halbinsel (1977)	1246
7.	P. K. Schmidt and C. B. Burgess	The Axes of Scotland and Northern England (1981)	1663
8.	H. Erkanal	Die Äxte und Beile des 2. Jahrtausends in Zentralanatolien (1977)	203
9.	E. F. Mayer	Die Äxte und Beile in Österreich (1977)	905
10.	K. Kibbert	Die Äxte und Beile im mittleren Westdeutschland I (1980)	626
11.	M.-B. Chardenoux and J.-C. Courtois	Les haches dans la France Méridionale (1979)	1015
12.	G. L. Carancini	Le asce nell'Italia continentale II (1984)	1846
13.	K. Kibbert	Die Äxte und Beile im mittleren Westdeutschland II (1984)	701
14.	H. Todorova	Die kupferzeitlichen Äxte und Beile in Bulgarien (1981)	not Bronze Age
15.	P. Patay	Die kupferzeitlichen Meißel, Beile und Äxte in Ungarn (1984)	not Bronze Age
16.	A. Szpunar	Die Beile in Polen I (Flachbeile, Randleistenbeile, Randleistenmeißel) (1987)	230
17.	J. Říhovský	Die Äxte, Beile, Meißel und Hämmer in Mähren (1992)	906
18.	Z. Žeravica	Äxte und Beile aus Dalmatien und anderen Teilen Kroatiens, Montenegro,Bosnien und Herzegowina (1993)	435
19.	E. Miron	Axes and Adzes from Canaan (1992)	not Europe
20.	K. Pászthory and E. F. Mayer	Die Äxte und Beile in Bayern (1998)	1114
21.	J. Kuśnierz	Die Beile in Polen III (Tüllenbeile) (1998)	273
22.	G. Eogan	The Socketed Axes in Ireland (2000)	883
23.	F. Laux	Die Äxte und Beile in Niedersachen I (Flach-, Randleisten- und Absatzbeile) (2000)	948
24.	M. Gedl	Die Beile in Polen IV (Metalläxte, Eisenbeile, Hämmer, Ambosse, Meißel, Pfrieme) (2004)	114
25.	F. Laux	Die Äxte und Beile in Niedersachsen II (2005)	337
26.	M. Michler	Les haches du Chalcolithique et de l'Âge du Bronze en Alsace (2013)	163
27.	D. Antonović	Kupferzeitliche Äxte und Beile in Serbien (2014)	122
		Total	15919

Table D.34: References and number of artifacts per book
Table lists the references for database of European bronze artifacts.

Prähistorische Bronzefunde			
		Abt. IV: Schwerter	
Book number	Author	Book title and publication year	# Artifacts
1.	V. Bianco Peroni	Die Schwerter in Italien. Le spade nell'Italia continentale (1970).	211
2.	P. Schauer	Die Schwerter in Süddeutschland, Österreich und der Schweiz I . (Griffplatten-, Griffangel- und Griffzungenschwerter) (1971).	435
3.	H. Reim	Die spätbronzezeitlichen Griffplatten-, Griffdorn- und Griffangelschwerter in Ostfrankreich (1974).	37
4.	P. Novák	Die Schwerter in der Tschechoslowakei I (1975).	110
5.	I. A. Colquhoun and C. B. Burgess	The Swords of Britain (1988).	659
6.	T. Kemenczei	Die Schwerter in Ungarn I (Griffplatten-, Griffangel- und Griffzungenschwerter) (1988).	311
7.	C. B. Burgess and S. Gerloff	The Dirks and Rapiers of Great Britain and Ireland (1981).	1000
8.	T. Bader	Die Schwerter in Rumänien (1991).	355
9.	T. Kemenczei	Die Schwerter in Ungarn II (Vollgriffschwerter) (1991).	354
10.	W. Krämer	Die Vollgriffschwerter in Österreich und der Schweiz (1985).	175
11.	I. v. Quillfeldt	Die Vollgriffschwerter in Süddeutschland (1995).	284
12.	I. Kilian-Dirlmeier	Die Schwerter in Griechenland (außerhalb der Peloponnes), Bulgarien und Albanien (1993).	471
13.	S. Shalev	Swords and Daggers in Late Bronze Age Canaan (2004).	not Europe
14.	A. F. Harding	Die Schwerter im ehemaligen Jugoslawien (1995).	431
15.	H. Wüstemann	Die Schwerter in Ostdeutschland (2004).	560
16.	D. Brandherm	Las Espadas del Bronce Final en la Península Ibérica y Baleares (2007).	166
17.	F. Laux	Die Schwerter in Niedersachsen (2009).	327
18.	M. Novotná	Die Vollgriffschwerter in der Slowakei (2014).	184
19.	J. Winiker	Die bronzezeitlichen Vollgriffschwerter in Böhmen (2015).	34
		Total	6104

D.7 Shapley decomposition

In this appendix, we more closely examine the relative importance of our proposed mechanism for triggering the Urban Revolution: the emergence of a trade-taxing elite. We compare its role in explaining Bronze Age urbanization with other, complementary, geography-driven mechanisms identified in previous studies. Specifically, the alternative mechanisms we focus on are: the emergence of farming surplus, the potential for irrigation, the rise of conflict in circumscribed environments, and the appropriability of cereal grains.

We start our analysis by estimating a cross-sectional probit model in which the presence of a city within a grid cell is regressed on our measure for the metal transit tax potential of a region, i.e., the blockage cost, along with four measures, each developed to capture one of the mechanisms mentioned above. We proxy farming surplus by a grid cell's share of cropland area around 3000 BC (Klein Goldewijk et al., 2011). To capture the local irrigation potential, we draw on the index developed in Bentzen, Kaarsen and Wingender (2017), which measures the irrigation potential based solely on exogenous geographical and climatic variables. The potential for appropriability of cereals is measured by the distance to cereal domestication regions (Mayshar, Moav and Pascali, 2022). Finally, circumscription is computed following the procedure developed in Schönholzer and François (2023). The resulting index captures the differential agricultural productivity of a cell relative to its surroundings.

Before discussing regression results, it is worth mentioning a caveat pertaining to the different natures of the measures introduced above. While variation in some of them is exclusively driven by exogenous factors (e.g., the irrigation potential), others have potentially endogenous components, importantly, our blockade cost measure. This should be kept in mind when interpreting the subsequent results.

The first row of Table D.35, Panel A, reports the pseudo R^2 as a measure of goodness of fit for regressions that account for the five mechanisms and continent dummies.[63] In column (1), we use the data from Green et al. (2024) as the outcome, and in column (2), the data from Reba, Reitsma and Seto (2016). In both cases, the R^2 is substantial, lying at 0.324 using the former data and even at 0.418 using the latter. This illustrates that, together, the five mechanisms are important contributors to Bronze Age urbanization.

In rows (2)–(6), we shed more light on the explanatory power of the individual mechanisms by running bivariate regressions using only one measure at a time as a regressor. When using the Green et al. (2024) data, the blockage cost has the highest R^2 value (0.160), followed by the measure for farming surplus (0.152) and environmental circumscription (0.112). The explanatory power of the irrigation potential and the cereal appropriability measures is also non-negligible (both around 0.06), whereas the continent dummies have a low R^2 (0.028).

In column (2) of Panel A, rows (2)–(6), we repeat the same exercise using the Reba, Reitsma and Seto (2016) city data. Again, the individual explanatory power of the five measures is substantial, with the bivariate regression using the proxy for surplus farming producing the highest R^2 (0.295), closely followed by the blockage cost (0.213). The continent dummies again have little explanatory power.

The results presented in Panel A show that—in isolation—metal transit tax potential, farming

[63] Specifically, we report the McFadden pseudo R^2: $R^2 = 1 - L_M/L_0$, where L_0 is the log-likelihood of the intercept-only model and L_M is the log-likelihood of the probit model with the full set of variables.

Table D.35: R-squared and Shapley values from regressions predicting the presence of Bronze Age cities

	Any city or citadel Green et al. (2024)	Any city Reba, Reitsma and Seto (2016)
	(1)	(2)
Panel A: R-squared		
(1) All variables (N = 9,562)	0.324	0.418
(2) Blockage Cost	0.160	0.213
(3) Agriculture	0.152	0.295
(4) Irrigation Potential	0.062	0.074
(5) Distance to cereal domestication	0.060	0.137
(6) Circumscription	0.112	0.093
(7) Continent dummies	0.028	0.023
Panel B: Shapley values		
(1) Blockage	0.085	0.103
(2) Agriculture	0.063	0.154
(3) Irrigation Potential	0.034	0.034
(5) Distance to cereal domestication	0.038	0.065
(6) Circumscription	0.070	0.041
(7) Continent dummies	0.035	0.021

Notes: Each cell in Panel A reports McFadden's pseudo R^2 from a separate probit regression, where the dependent variable is a dummy indicating the presence of any Bronze Age city, and the explanatory variables are those listed in the corresponding row. Each column in Panel B corresponds to a separate regression. The values shown are Shapley values.

surplus, irrigation potential, appropriability of cereals, and environmental circumscription are all relevant factors in explaining the spatial distribution of Bronze Age urbanization. However, because the different mechanisms are not mutually exclusive, the results of Panel A do not offer any definite insights regarding their relative importance. To shed light on this, we decompose the overall R^2, i.e., the pseudo R^2 of the regressions reported in row (1) of Panel A, using the Shapley decomposition (Shorrocks, 2013).[64]

In column (1) of Panel B, we report the results of this decomposition for the Green et al. (2024) data. Each row reports the average marginal contribution of the corresponding measure to the overall R^2. The Shapley value is highest for our measure of metal transit trade potential, i.e., the blockage cost. Evaluated at the overall R^2 of 0.324, its Shapley value of 0.085 amounts to 26%. The decomposition further reveals that the Shapley values are high for the measures of environmental circumscription (0.070) and agricultural surplus (0.063). The Shapley value is somewhat lower, but still substantial, for measures of cereal appropriability (0.038) and irrigation potential (0.034). Finally, the Shapley value for continent dummies is 0.035. This corresponds to 11% of the overall R^2.

Column (2) of Panel B shows the Shapley decomposition using the Reba, Reitsma and Seto (2016) city data. The pattern of results is very similar to that in column (1). We again find that the marginal contribution of the blockage cost is very high, with a Shapley value of 0.103. Measured as a proportion of the overall R^2, this represents around 25%. Consistent with the results in

[64]The Shapley value of a variable is its average marginal contribution to the model's overall fit (pseudo R^2), averaged across all possible permutations in which the groups of regressors can be entered into the model.

Panel A, we find that the Shapley value is even a bit higher for the proxy for farming surplus (0.154). The remaining three mechanisms also have a substantial marginal contribution, with Shapley values of 0.065 (cereal appropriability), 0.041 (environmental circumscription), and 0.034 (irrigation potential). The Shapley value is lowest for the continent dummies.

Taken together, the key takeaway from Table D.35 is that including the blockage cost in a regression of Bronze Age city location on commonly studied geographic determinants leads to a substantial increase in the model's R^2. This implies that the emergence of a trade-taxing elite is an important explanation for the urban geography that emerged during the Bronze Age.

D.8 Appropriability mechanism

In this appendix, we present our theoretical model, which focuses on the appropriability of the metal transit trade. We then describe how we operationalize the model's key parameter—local tax potential—by translating it into an empirically measurable quantity: the blockage cost. In a third step, we discuss the relationship between the blockage cost and metal transit trade.

D.8.1 Theoretical Model

Prelude

The model is inspired by Mayshar, Moav and Pascali (2022) but features a spatial dimension. Space, mirroring our empirical setup, is structured into grid cells. Transport costs to traverse cells and the distribution of mines and farmland are the key exogenous features. Grid cells can be organized as hierarchy, with a king that establishes the monopoly of violence and employs tax collectors, or as anarchy, with unorganized roving bandits. The model includes three key agent types: farmers, foragers, and traders. Farmers are located in grid cells and produce crops using metal and cropland. Foragers are also located in grid cells and can earn a fixed exogenous income from foraging: otherwise they can choose to become bandits (under anarchy) or tax collectors employed by the king (under hierarchy). Traders transport metal from mines to farmers using the route that minimizes trade costs resulting from traversing through grid cells. Trade costs depend on transportation costs and expropriation rates along the route. The expropriation technology gives the number of bandits in cells under anarchy and of the number of tax collectors in cells under hierarchy as a strictly increasing, convex function of the expropriation rates.

In the following sections, we will provide a detailed description of each agent type and state.

Farmers

Farmers in cell k utilize their cropland, denoted as L_k, and metals, represented as M_k, as perfect complements in the production of crops, Y_k:

$$Y_k = \min\{M_k, L_k\}. \tag{D.4}$$

Consequently, the demand for metals in cell k corresponds to the quantity L_k.

We assume that crops are sufficiently valuable, implying it is always optimal to produce them, regardless of the prevailing metal prices. Additionally, we assume that if cell k contains cropland, $L_k = 1$, and if it does not contain cropland, $L_k = 0$. Consequently, the demand for metals in cell k can be described as follows:

$$M_k = M = \begin{cases} 1 & \text{in cells with cropland,} \\ 0 & \text{in cells without cropland.} \end{cases} \tag{D.5}$$

This formulation delineates the metal demand in two distinct scenarios: one in regions with cropland and one in regions without cropland.

Traders

Traders play a crucial role in the metal trade process, transporting metals from mines to destination cells and selling them to farmers. We assume that the cost of mining metals is the same across

all mines and that traders operate under perfect competition on each transport route (i.e., metals shipped from any mine to any destination cell are traded under perfectly competitive conditions). Together, these assumptions imply that differences in trade costs fully determine differences in metal prices at the destination cells. Consequently, each destination cell sources its metals from a single mine—the one associated with the lowest trade costs.

Traders move along transport routes that connect mines to cells containing farmland. Since space is organized as a grid, the length of each route is measured by the number of grid cells it crosses. Trade costs along the route from mine m to farmers in cell f have two components. The first is a transportation cost, which depends on the topology of the route. The second is an expropriation cost incurred along the route. These expropriation costs take the form of tolls paid either to kings in cells organized under hierarchy or to bandits in cells characterized by anarchy.

Traders may choose among different routes when transporting metals from mines to farmers. We denote P_{mf} a generic path connecting mine m to farmers in cell f, and $\mathcal{P}_{mf}$ the set of all feasible paths from mine m to cell f.

Traders choose routes according to a least-cost criterion, taking into account both transportation costs and expropriation costs along each path. We assume that traders optimize each route independently, so that no economies of scale arise from serving multiple routes. We also assume that there are no capacity constraints on the number of routes that can be served. We denote $P^{\star}_{mf}$ the least-cost path connecting mine m to cell f, and LC_{mf} the associated trade cost.

Given the externally determined costs of metals at the mine ($c_m = c$), the profit function for traders engaged in the sale of metals from mines in cell m to farmers in cell f can be stated as follows:

$$\pi^{T}_{mf} = p_f M - cM - LC_{mf}, \tag{D.6}$$

where p_f denotes the price of metals M in cell f. We assume a specific functional form for the least-cost calculations:

$$LC_{mf} = \min_{P_{mf} \in \mathcal{P}_{mf}} \sum_{k \in K} \left(t_k + \tau^{T}_{mf,k} + \tau^{B}_{mf,k} \right) \mathcal{I}_{P_{mf}}[k]\, cM. \tag{D.7}$$

Here, $\mathcal{I}_{P_{mf}}[k]$ is the indicator function:

$$\mathcal{I}_{P_{mf}}[k] = \begin{cases} 1 & \text{if} \quad k \in P_{mf}, \\ 0 & \text{if} \quad k \notin P_{mf}, \end{cases} \tag{D.8}$$

that equals one if the path from m to f, P_{mf}, passes through cell k, and zero otherwise. Essentially, this indicator function captures all cells belonging to a specific path from m to f. The transport costs to traverse cell k, denoted as $t_k \geq 0$, are determined by the most cost-effective transport mode available in that cell.[65] Additionally, traders may be subject to taxes, $\tau^{T}_{mf,k} \geq 0$, imposed by the king governing cell k along the route from m to f. Alternatively, if cell k is not under the rule of a

[65] These cell-specific transport costs are defined by the cheapest available transport mode in cell k:

$$t_k = \begin{cases} \alpha_{sea} & \text{if} \quad k \in \text{sea grid}, \\ \alpha_{river} & \text{if} \quad k \in \text{river grid}, \\ \alpha_{land} & \text{if} \quad k \in \text{land grid}. \end{cases} \tag{D.9}$$

king, traders may pay tolls, $\tau^B_{mf,k} \geq 0$, to bandits for metals transported from m to f through that cell. The total costs of moving metals from cell m to cell f are calculated as the sum over all cells k from the set of cells K that the path P_{mf} passes through. In other words, this includes all cells where the indicator function $\mathcal{I}_{P_{mf}}[k]$ for the path P_{mf} is one.

As already explained, our assumptions of perfect competition and uniform production costs across all mines imply that metal prices at different mines are homogeneous, with trade costs fully determining the prices at the destination cell. Hence, only the mine from the set of mines $\mathcal{M}$ with the least trade costs will supply a certain destination cell: $LC_{m^\star(f),f} = \min_{m\in\mathcal{M}} LC_{mf}$, where $m^\star(f)$ is the mine that serves cell f at the lowest trade costs and $P^\star_{m^\star(f),f}$ is the associated path.

Metal prices (p_f) can be expressed as follows:

$$p_f = c\left(1 + \sum_{k\in K}\left(t_k + \tau^T_{mf,k} + \tau^B_{mf,k}\right)\mathcal{I}_{P^\star_{m^\star(f),f}}[k]\right). \tag{D.10}$$

Given the assumption of perfect competition, profits for each route $m^\star(f)$ to f in equilibrium are zero:

$$\begin{aligned}
\pi^T_{m^\star(f),f} &= p_f M - cM - LC_{m^\star(f),f} \\
&= p_f M - cM \\
&\quad - \sum_{k\in K}\left(t_k + \tau^T_{mf,k} + \tau^B_{mf,k}\right)\mathcal{I}_{P^\star_{m^\star(f),f}}[k]\, cM \\
&= \left(1 + \sum_{k\in K}\left(t_k + \tau^T_{mf,k} + \tau^B_{mf,k}\right)\mathcal{I}_{P^\star_{m^\star(f),f}}[k]\right) cM - cM \\
&\quad - \sum_{k\in K}\left(t_k + \tau^T_{mf,k} + \tau^B_{mf,k}\right)\mathcal{I}_{P^\star_{m^\star(f),f}}[k]\, cM \\
&= 0.
\end{aligned}$$

Foragers

Foragers are assumed to earn a constant income $s > 0$. Under anarchy, some foragers may turn into bandits. Under hierarchy, i.e., when a king emerges, he hires tax collectors among the foragers. Hence, foraging serves as an outside option for bandits and tax collectors.

Anarchy

In cells without a king, traders face the risk of bandit raids. Let $\tau^B_{mf,k}$ denote the toll that traders must pay to bandits in order to transport metals from location m to location f through cell k.

The income earned by a bandit in cell k from trade between mine $m^\star(f)$ and destination cell f is given by:

$$R^B_{m^\star(f),f,k} = \frac{\tau^B_{m^\star(f),f,k}\mathcal{I}_{P^\star_{m^\star(f),f}}[k]\, cM}{\lambda[\tau^B_{m^\star(f),f,k}]}, \tag{D.11}$$

where $\lambda[\tau^B_{m^\star(f),f,k}]$ denotes the number of bandits required to sustain the expropriation rate $\tau^B_{m^\star(f),f,k}$. More generally, $\lambda(\cdot)$ captures the expropriation technology and is assumed to be strictly increasing, strictly convex, and satisfies: $\lambda[0] = 0$, $\lim_{\tau\searrow 0}\lambda'(\tau) = 0$, $\lim_{\tau\nearrow\bar{\tau}}\lambda'(\tau) = \infty$, and $\lim_{\tau\nearrow\bar{\tau}}\lambda(\tau) = \infty$, with $\bar{\tau} \leq 1$. Convexity implies diminishing returns to predation: with increasing expropriation

rates, more and more bandits are necessary to sustain the expropriation rate. The boundary condition $\lambda[0] = 0$ implies that no bandits are needed to sustain a zero expropriation rate, while the limit conditions imply that as the expropriation rate approaches its upper bound $\bar{\tau}$, the number of bandits required to sustain it becomes infinitely large.

In equilibrium, bandits are indifferent between staying forager or becoming a bandit. Therefore, it must be the case that:

$$\frac{\tau^B_{m^\star(f),f,k}\mathcal{I}_{P^\star_{m^\star(f),f}}[k]\,cM}{\lambda[\tau^B_{m^\star(f),f,k}]} = s \Rightarrow$$
$$\tau^B_{m^\star(f),f,k}\mathcal{I}_{P^\star_{m^\star(f),f}}[k]\,cM = s\lambda[\tau^B_{m^\star(f),f,k}].$$

For all cells that are part of the least-cost route, $\mathcal{I}_{P^\star_{m^\star(f),f}}[k] = 1$. Hence,

$$\tau^B_{m^\star(f),f,k}cM = s\lambda[\tau^B_{m^\star(f),f,k}]. \tag{D.12}$$

As c, M, and s are identical across cells, we have $\tau^B_{m^\star(f),f,k} = \tau^B$.

Hierarchy: Kings and Tax Collectors

Kings hold a monopoly on the use of force (and taxation) in cells organized under hierarchy. Establishing this monopoly requires paying a fixed cost, denoted by $G > 0$.

The king employs a certain number of tax collectors from the pool of potential foragers and guarantees them a wage equal to their outside option, s. The king chooses tax rates to maximize net revenue, taking into account the responses of traders and farmers. More precisely, in cell k, the king chooses a path-specific tax rate, $\tau^T_{m^\star(f),f,k}$, for each path originating from mine $m^\star(f)$ and serving destination cell f along the least-cost path $P^\star_{m^\star(f),f}$. The king's problem is therefore:

$$\max_{\tau^T_{m^\star(f),f,k}\geq 0} R^T_{m^\star(f),f,k} = \tau^T_{m^\star(f),f,k}\mathcal{I}_{P^\star_{m^\star(f),f}}[k]\,cM - s\lambda[\tau^T_{m^\star(f),f,k}], \tag{D.13}$$

where $\lambda[\tau^T_{m^\star(f),f,k}]$ denotes the number of tax collectors required to enforce tax rate $\tau^T_{m^\star(f),f,k}$. Notice that $\lambda(\cdot)$ is the same expropriation technology that we have under anarchy.

Optimal Taxes and Tax Revenues

Assuming for a moment that $\mathcal{I}_{P^\star_{m^\star(f),f}}$ is taken as given by the king, the first-order condition for $\tau^T_{m^\star(f),f,k}$ is given by:

$$\mathcal{I}_{P^\star_{m^\star(f),f}}[k]\,cM = s\frac{\partial\lambda[\tau^T_{m^\star(f),f,k}]}{\partial\tau^T_{m^\star(f),f,k}}. \tag{D.14}$$

The left-hand side term captures the positive direct effect of higher taxes on tax revenues, while the right-hand side term accounts for the cost increase of tax collection caused by the higher tax rate.

Denoting the optimal, path-specific tax rate as $\tau^{T,\star}_{m^\star(f),f,k}$, the resulting total tax revenues of a king in cell k, $R^{T,\star}_k$, are given by the sum of $R^{T,\star}_{m^\star(f),f,k}$ for all f in the set of all cells with cropland/farmers

(excluding the destination cell k), $\mathcal{F}\backslash\{k\}$, i.e.:

$$R_k^{T,\star} = \sum_{f\in\mathcal{F}\backslash\{k\}} R_{m^\star(f),f,k}^{T,\star} = \sum_{f\in\mathcal{F}\backslash\{k\}} \left(\tau_{m^\star(f),f,k}^{T,\star} \mathcal{I}_{P^\star_{m^\star(f),f}}[k]\, cM - s\lambda[\tau_{m^\star(f),f,k}^{T,\star}]\right). \tag{D.15}$$

Several things are noteworthy from equations (D.14) and (D.15):

1. If the optimal least-cost path from $m^\star(f)$ to f does not go through cell k, i.e., $\mathcal{I}_{P^\star_{m^\star(f),f}}[k] = 0$, then there is also no tax to be collected.

2. The more central cell k is in the network, the more trade flows will go through cell k, i.e., $\mathcal{I}_{P^\star_{m^\star(f),f}}[k]$ will be equal to one for more trade routes $P^\star_{m^\star(f),f}$, $f \in \mathcal{F}$. This allows more taxes to be collected. With a unique least-cost path between each mine and destination, the betweenness centrality for cell k, T_k, is given by (see Newman, 2018, for example):

$$T_k = \sum_{f\in\mathcal{F}\backslash\{k\}} \mathcal{I}_{P^\star_{m^\star(f),f}}[k]\, cM,$$

   where cM serves as weights. A higher value of betweenness centrality for cell k indicates that kings in that cell have a broader tax base because a greater amount of metals will pass through their territory. We call T_k "transit index" in the main text and use as weights cropland area (measured in square kilometers) in grid cell f in 3000 BC.

In summary, the greater the centrality of a cell, meaning the higher the volume of trade passing through it, the more substantial the resulting net tax revenues. This explains why kings tend to establish their authority in central cells, where numerous least-cost paths pass through (i.e., when T_k is large), and where there is a significant amount of metal trade.

Comparing the Optimality Conditions under Anarchy and Hierarchy

In equilibrium, the optimal tax rate under anarchy is determined by the following condition:

$$\begin{aligned} \tau^B \mathcal{I}_{P^\star_{m^\star(f),f}}[k]\, cM &= s\lambda[\tau^B] \Rightarrow \\ \mathcal{I}_{P^\star_{m^\star(f),f}}[k]\, cM &= s\frac{\lambda[\tau^B]}{\tau^B}. \end{aligned} \tag{D.16}$$

Under hierarchy we have:

$$\mathcal{I}_{P^\star_{m^\star(f),f}}[k]\, cM = s\frac{\partial\lambda[\tau_{m^\star(f),f,k}^{T,\star}]}{\partial\tau_{m^\star(f),f,k}^{T,\star}}. \tag{D.17}$$

The left-hand sides of equations (D.16) and (D.17) are identical. $\lambda[\tau]$ is strictly increasing and strictly convex and for $\tau = 0$, $\lambda[\tau = 0] = 0$, i.e, it follows that $\partial\lambda[\tau]/\partial\tau > \lambda[\tau]/\tau$ and as a consequence, we have $\tau^B > \tau_{m^\star(f),f,k}^{T,\star}$. Lower optimal taxes under hierarchy have important welfare consequences for agents in the respective cell. Traders are under perfect competition, but have lower costs of transportation. Kings are covering all their costs, otherwise they would not come into power. And bandits always earn a constant income s. Hence, the ruling of a king in a cell k leads to the same welfare or welfare-improvements for all agents directly related to cell k.

Blockage Costs

Up to this point, we assumed that the king takes $\mathcal{I}_{P^{\star}_{m^{\star}(f),f}}[k] = 1$ as given. However, whether a specific grid cell, say $k = l$, is part of a specific least-cost path depends, of course, on the tax rate set in cell l.

Intuitively (assuming that l is a segment of the least-cost route $P^{\star}_{m^{\star}(f),f}$), taxes in cell l cannot continually increase without limit because traders have the ability to avoid high-tax grid cells by selecting alternative routes that bypass cell l. The adaptability of traders in choosing their optimal path places a constraint on the maximum tax rate that a king can impose.

For a more formal examination, let's focus on the scenario where, for a given tax rate $\tau^{T}_{mf,l}$, the least-cost path $P^{\star}_{m^{\star}(f),f}$, i.e., the path with the minimum costs for destination cell f to obtain metals, defining the optimal mine $m^{\star}(f)$, includes cell l, i.e., $\mathcal{I}_{P^{\star}_{m^{\star}(f),f}}[l] = 1$. The associated least-costs for cell f to obtain metals are then given by:

$$LC_{m^{\star}(f),f} = \min_{m \in \mathcal{M}} \min_{P_{mf} \in \mathcal{P}_{mf}} \sum_{k \in K} \left(t_k + \tau^{T}_{mf,k} + \tau^{B} \right) \mathcal{I}_{P_{mf}}[k]\, cM. \tag{D.18}$$

Next, we explore the potential for increasing taxes in cell l. To assess this, we will calculate the least-cost route to serve cell f when we eliminate cell l from the network, meaning that traders will use an alternative path to avoid cell l:

$$LC^{\setminus\{l\}}_{m^{\setminus\{l\}\star}(f),f} = \min_{m \in \mathcal{M}} \min_{P_{mf} \in \mathcal{P}^{\setminus\{l\}}_{mf}} \sum_{k \in K \setminus \{l\}} \left(t_k + \tau^{T}_{mf,k} + \tau^{B} \right) \mathcal{I}_{P_{mf}}[k]\, cM. \tag{D.19}$$

Thus, $LC^{\setminus\{l\}}_{m^{\setminus\{l\}\star}(f),f}$ represents the lowest costs associated with the least-cost path $P^{\star}_{m^{\setminus\{l\}\star}(f),f}$ for serving cell f when using cell l is not an option, where $\mathcal{P}^{\setminus\{l\}}_{mf}$ denotes the set of paths from m to f that do not path through cell l, and $m^{\setminus\{l\}\star}(f)$ is the mine that serves cell f at the lowest costs when cell l is blocked for transit trade.

The non-negative difference between $LC^{\setminus\{l\}}_{m^{\setminus\{l\}\star}(f),f}$ and $LC_{m^{\star}(f),f}$ indicates the maximum possible tax rate in cell l before traders become indifferent to switching to an alternative transportation route, bypassing cell l to avoid paying taxes there.

In a similar manner, we can compute the total maximum tax that a king can impose in cell l. To do this, we calculate the sum of the differences between all least-cost paths passing through cell l and their respective second-best routes (without cell l), which traders can use. In essence, we

"block" grid cell l for transit trade:

$$
\begin{aligned}
B_l &= \sum_{f\in\mathcal{F}\setminus\{l\}} B_{f,l} = \sum_{f\in\mathcal{F}\setminus\{l\}} \max\left\{LC^{\setminus\{l\}}_{m^{\setminus\{l\}\star}(f),f} - LC_{m^\star(f),f}, 0\right\} \\
&= \sum_{f\in\mathcal{F}\setminus\{l\}} \max\Bigg\{ \min_{m\in\mathcal{M}} \min_{P_{mf}\in\mathcal{P}^{\setminus\{l\}}_{mf}} \sum_{k\in K\setminus\{l\}} \left(t_k + \tau^T_{mf,k} + \tau^B\right)\mathcal{I}_{P_{mf}}[k]\, cM \\
&\quad - \min_{m\in\mathcal{M}} \min_{P_{mf}\in\mathcal{P}_{mf}} \sum_{k\in K} \left(t_k + \tau^T_{mf,k} + \tau^B\right)\mathcal{I}_{P_{mf}}[k]\, cM, 0\Bigg\} \\
&= \sum_{f\in\mathcal{F}\setminus\{l\}} \max\Bigg\{ \min_{m\in\mathcal{M}} \min_{P_{mf}\in\mathcal{P}^{\setminus\{l\}}_{mf}} \sum_{k\in K\setminus\{l\}} \left(t_k + \tau^T_{mf,k} + \tau^B\right)\mathcal{I}_{P_{mf}}[k] \\
&\quad - \min_{m\in\mathcal{M}} \min_{P_{mf}\in\mathcal{P}_{mf}} \sum_{k\in K} \left(t_k + \tau^T_{mf,k} + \tau^B\right)\mathcal{I}_{P_{mf}}[k], 0\Bigg\} cM.
\end{aligned}
\tag{D.20}
$$

The blockage costs B_l are similar in spirit to the efficiency centrality (see Wang, Du and Deng, 2017) and the modified efficiency centrality (see Wang, Wang and Deng, 2019). They represent the total trade cost increase the network will incur, if grid cell l is removed from the network.

From the king's perspective, B_l gives the maximum amount of taxes that the king in cell l can collect on each path P_{mf} while keeping traders indifferent between using this path or bypassing cell l by switching to another path. The maximum tax amount $\bar{\tau}^T_{m^\star(f),f,l}$ that the king can collect before traders opt to avoid passing through cell l, assuming $\tau^T_{mf,l} = 0$, is given by:

$$
\begin{aligned}
\bar{\tau}^T_{m^\star(f),f,l} = \max\Bigg\{ &\min_{m\in\mathcal{M}} \min_{P_{mf}\in\mathcal{P}^{\setminus\{l\}}_{mf}} \sum_{k\in K\setminus\{l\}} \left(t_k + \tau^T_{mf,k} + \tau^B\right)\mathcal{I}_{P_{mf}}[k] \\
&- \min_{m\in\mathcal{M}} \min_{P_{mf}\in\mathcal{P}_{mf}} \sum_{k\in K} \left(t_k + \tau^T_{mf,k} + \tau^B\right)\mathcal{I}_{P_{mf}}[k], 0\Bigg\}.
\end{aligned}
\tag{D.21}
$$

Whenever the optimal tax $\tau^{T,\star}_{m^\star(f),f,l}$ determined by equation (D.13) is above the maximum amount of the tax $\bar{\tau}^T_{m^\star(f),f,l}$, i.e., $\tau^{T,\star}_{m^\star(f),f,l} > \bar{\tau}^T_{m^\star(f),f,l}$, tax revenues will be zero, since traders would switch to another path. Hence, $\bar{\tau}^T_{m^\star(f),f,l}$ is directly linked to the indicator function:

$$
\mathcal{I}_{P^\star_{m^\star(f),f}}[l] = \begin{cases} 1 & \text{if} \quad \tau^{T,\star}_{m^\star(f),f,l} < \bar{\tau}^T_{m^\star(f),f,l}, \\ 0 & \text{else.} \end{cases}
\tag{D.22}
$$

Using equation (D.21), we can write the blockage costs from equation (D.20) as follows:

$$
B_l = \sum_{f\in\mathcal{F}\setminus\{l\}} \bar{\tau}^T_{m^\star(f),f,l} cM.
\tag{D.23}
$$

B_l therefore gives the maximum total tax revenue that a king in cell l can generate. However, there is a lower limit on the total tax revenue for a king in cell l to be sustainable, considering the fixed costs G, where G is greater than zero. As B_l is the maximum total tax revenue, it is greater than or equal to $R^{T,\star}_l$ given in equation (D.15). If kings are viable in cell l, $R^{T,\star}_l$ must be greater than or equal to G. Hence, B_l is an upper limit to sustain a king in cell l.

D.8.2 Blockage cost

We compute the blockage cost for a given grid cell l using the following procedure:

1. First, identify the tin and copper mine with the lowest transport cost to cell f in the unrestricted case, i.e., when transport is allowed through all cells and compute the overall costs of transport to cell f: $LC_f^\star = LC_{Sn^\star(f),f} + LC_{Cu^\star(f),f}$.
2. Then, for each farmland cell f:
   (a) Identify the tin and copper mine with the lowest transport cost to cell f when cell l is blocked.[66] Denote these mines as $Sn^{\setminus\{l\}\star}(f)$ and $Cu^{\setminus\{l\}\star}(f)$, and the cost of transport from these mines as $LC_{Sn^{\setminus\{l\}\star}(f),f}$ and $LC_{Cu^{\setminus\{l\}\star}(f),f}$. Then compute the sum of transport costs to cell f as: $LC_f^{\setminus\{l\}\star} = LC_{Sn^{\setminus\{l\}\star}(f),f} + LC_{Cu^{\setminus\{l\}\star}(f),f}$.
   (b) Compute the difference between the transport cost in the restricted and unrestricted cases.
   Formally: $B_{f,l} = \max\left\{LC_f^{\setminus\{l\}\star} - LC_f^\star, 0\right\}$, where $B_{f,l}$ represents the additional transport costs incurred by cell f when grid l is blocked. To proxy for the volume of the diverted trade, we weight this differential by cropland in the destination f.
3. Compute the total blockage cost resulting from blocking cell l as the sum of additional transport costs across all optimal paths from mines to farmlands. Formally: $B_l = \sum_{f \in \mathcal{F}\setminus\{l\}} B_{f,l}$, where B_l is the total blockage cost for l.

We disregard paths that end in the blocked cell when computing our blockage cost measure.

[66] Again, we operationalize the blocking of cells by setting the cost of transiting the cell very high (10,000).

D.8.3 Metal transit trade and blockage cost

Below, we first illustrate and discuss the relationship between metal transit trade and blockage cost in detail. We also show that the pattern of association is very similar across continents.

Illustration metal transit trade versus blockage cost

The scatterplot in Figure D.18 illustrates the relationship between blockage cost and the metal transit index. The two variables are clearly positively correlated. This positive relationship arises because the magnitude of the metal transit index is inherently embedded in the blockage cost measure.

As a reminder, the metal transit index of a grid cell captures the square kilometers of cropland that are connected to metal deposits via least-cost paths that pass through the cell. In contrast, the blockage cost measures the global increase in transportation costs that would occur if the cell were removed from the network—i.e., if it could no longer be traversed by any least-cost path connecting cropland to metal deposits. By construction, blockage costs can only be high if the transit index is also high: if no least-cost path crosses a cell, excluding that cell from the network will not affect global transport costs.

Crucially, however, high transit volume is a necessary but not sufficient condition for high blockage costs. In addition to having substantial trade volume, detouring around the cell must entail a significant increase in transport costs. This would occur, for example, if rerouting requires switching from relatively cheap transport modes (e.g., river or sea) to more expensive ones (e.g., overland), or if the area surrounding the cell is topographically challenging (e.g., due to mountain barriers). High blockage costs may also arise when bypassing a cell forces a shift to more distant metal sources, especially when a blocked cell hosts a mine.

To illustrate, Figure D.18 highlights two cells with very similar—and very high—levels of the metal transit index, but very different blockage costs.

In the first case (Case A), blockage costs are extremely high. This is due to two factors: (1) the cell is traversed by paths connecting a copper mine (Veshnaveh, Iran), located approximately 100 km to the east, with cropland in South Mesopotamia and Iran; and (2) it hosts the tin mine at Deh Hosein, which also supplies this cropland. Blocking this cell implies that copper-carrying paths must be rerouted overland—at greater expense—and that all cells previously sourcing tin from Deh Hosein must switch to alternative tin mines. Importantly, these alternative tin mines are located at much greater distances, resulting in significantly higher transport costs.

In contrast, blockage costs are low in the second case (Case B). This cell, located on the Yangtze River, is characterized by a high transit index due to its strategic position between metal sources and fertile lands, combined with its location on the river, which offers relatively cheap transport. However, circumventing this cell does not incur substantial additional transport costs. Only small portions of the cost-minimizing paths may need to be rerouted via land, while the majority is re-routed by river, partly due to the meandering course of the Yangtze River at this location. As a result, the impact of blocking this cell on overall transport costs is small.

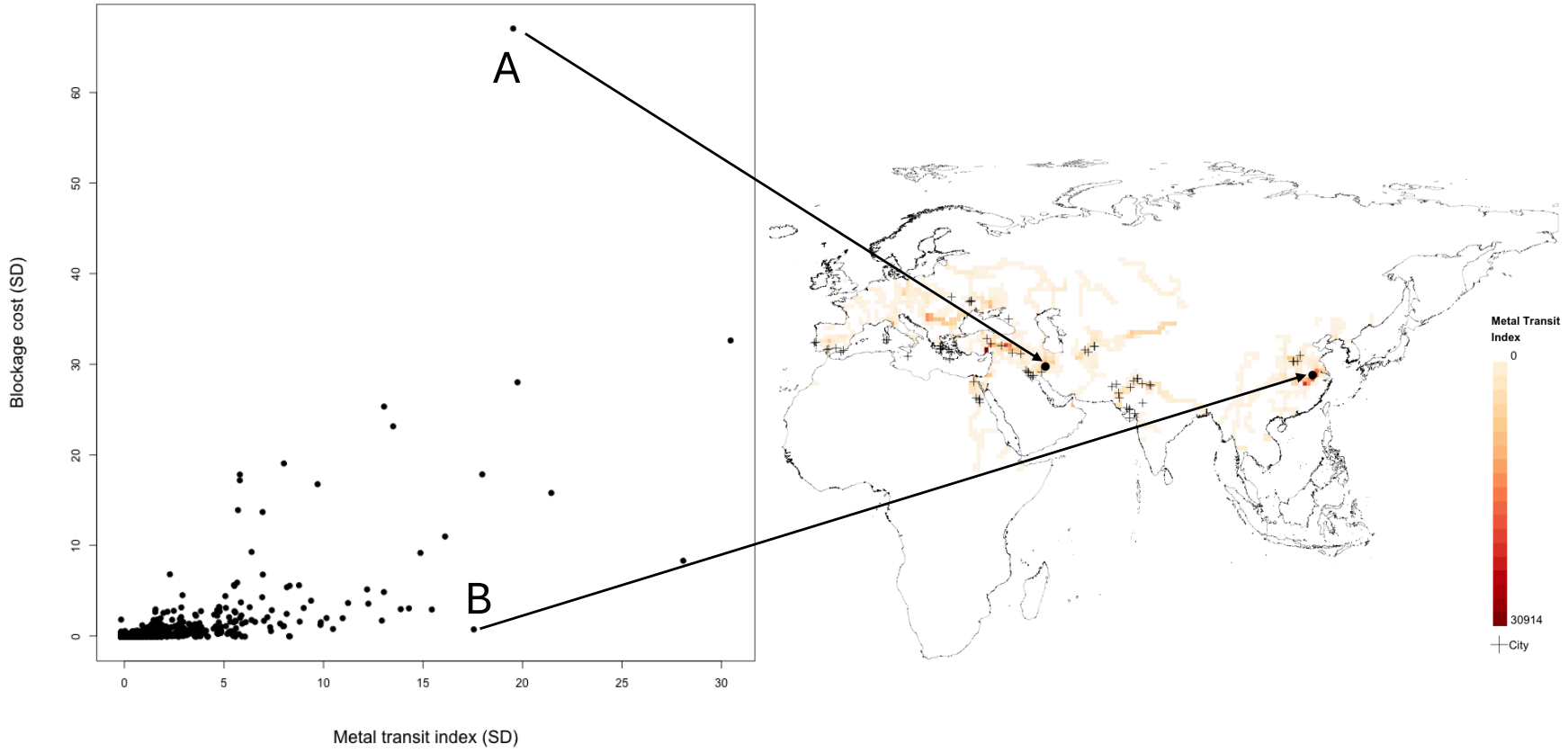


Figure D.18: Illustration metal transit index versus blockage cost

The figure shows a scatter plot of blockage cost versus the metal transit index (left subfigure), and links outliers in this relationship to their geographic locations on the map (right subfigure).

Scatterplots by continents

Figure D.19 shows the relationship between the metal transit index and blockage cost, separately for each continent. The scatterplots illustrate that, within all three continents included in our analysis—Asia, Europe, and Africa—there is a strong positive correlation between the two variables. However, the correlation is far from perfect, implying that we are able to empirically disentangle the effects of metal transit and blockage cost in our regression analysis.

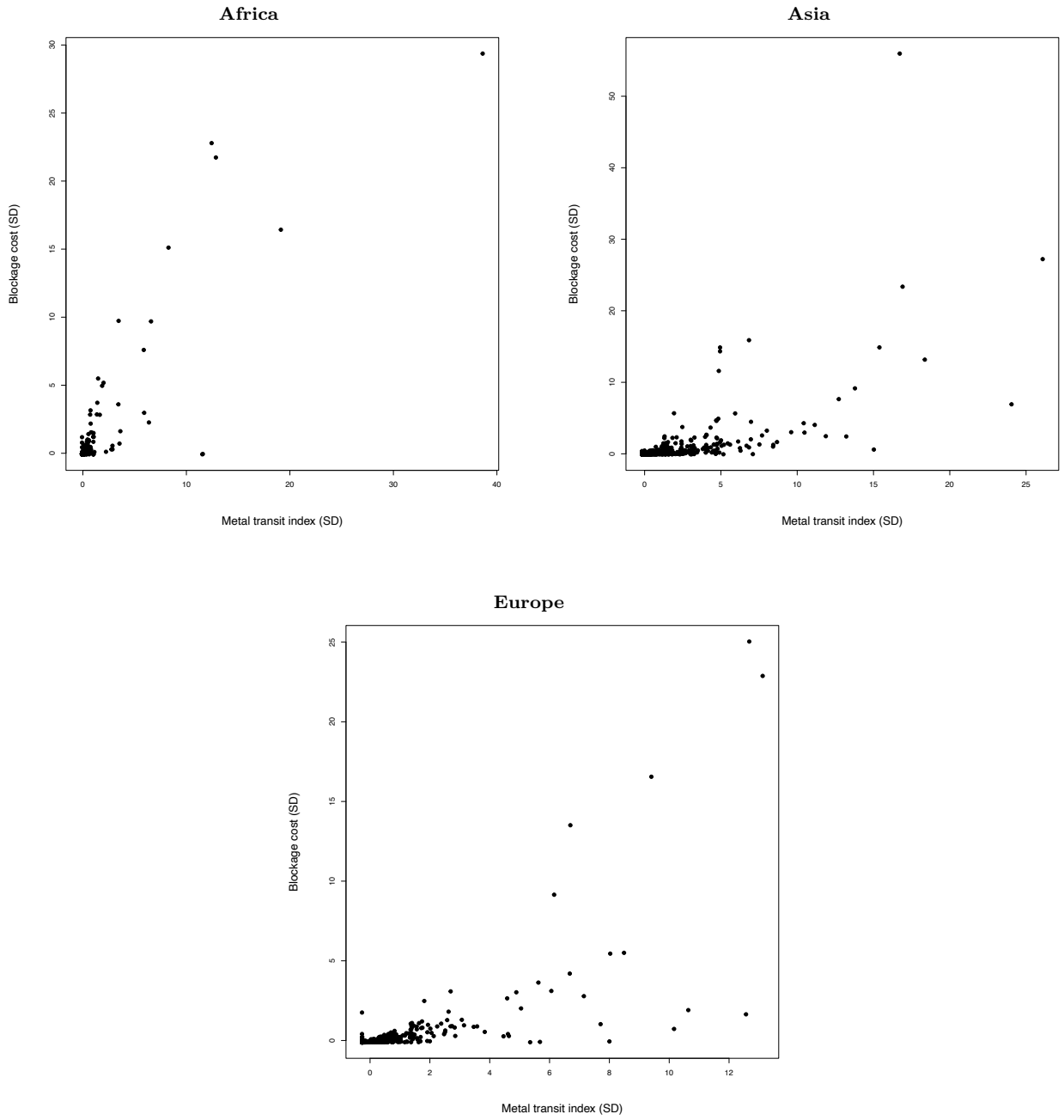


Figure D.19: Metal transit index versus blockage cost by continent
The figure shows scatterplots of blockage costs versus the metal transit index, separately for each continent.

Appendix E: Additional case studies

In this appendix, we focus on the Indus Valley, the city of Mari, the Aegean Sea, and China, and discuss the onset of the Urban Revolution in these regions.

E.1 The Harappan civilization in the Indus Valley (2600-1900 BC)

The second half of the third millennium BC marked the birth of the first urban civilization in southern Asia, in the Indus Valley. Rather than emerging from a slow period of gradual growth and modification, as in the Sumerian case, the Harappan civilization seems to have resulted from a very short period of transformation (Green and Petrie, 2018). During the Urban Phase (or Mature Harappan), within 100-150 years, both writing and a widely used system of weights and measures appeared, towns started displaying monumental buildings, signs of centralized urban planning (e.g., massive brick platforms, well-digging, drainage systems, grid plans) and unprecedented levels of social differentiation emerged (e.g., big/tiny houses, brick/mud houses, growth in the use of precious metals for personal adornments, etc.). Starting from the seminal work of Possehl (1990) and Ratnagar (1981), several scholars have suggested that transiting trade was a major factor in the rise and maintenance of the urban centers. Trade was facilitated by two major river systems, the Indus and the Ghaggar-Hakra (now dry), which connected metal-rich inland regions in Baluchistan and Afghanistan to the Indus urban centers and to coastal nodes, from which maritime routes through the Gulf of Oman linked this trade to the Persian Gulf and Mesopotamia.

In the words of Rita P. Wright (2010, p.231): *"The scale of the distribution system far outweighs anything known from previous periods and clearly was a catalyst in the growth of urbanism at mid-third millennium BC. Most revealing is the expansion of settlement into new territories located in regions strategically placed for long-distance trade linked to maritime routes."*

The foundation of some of the largest settlements in the Indus floodplains most likely reflected the growing importance of river transport. Jansen (2002) argues that this was the case for Mohenjo-daro, the largest settlement in the Indus valley and one of the world's earliest major cities. Its location was unsuitable for settlement, as it was at the constant risk of flooding by the nearby Indus. Still, *"this pristine settlement was founded in key central location midway between Harappa and the mountains on the one hand and Dholavira and the sea on the other, where the great highway of the Indus met a major routes into the mountains via the Kachi plain and the Bloan pass."* (McIntosh, 2007, p.389).

An appropriability mechanism behind the link between trade and civilization has been proposed by several scholars. For instance, Jane R. McIntosh (2007, p.394) writes: *"Towns developed at communications nodes or in locations well-placed to procure resources. [..] A managerial class emerged whose role was to facilitate and organize the circulation of goods and materials. [..] Artisans and state functionaries in the towns and cities may have been sustained by agricultural produce collected as taxes, probably at the city gate, where weights are often found, suggesting the weighing of goods or materials in order to deduct fixed proportions."*

Archaeological traces of the pivotal role of the Harappan civilization in moving raw materials from the center of Asia to Mesopotamia through the Persian Gulf can be found throughout the route. Several Harappan-related sites have been found in Southern Baluchistan and in Afghanistan: these were apparently trading colonies near major lapis lazuli, copper, and tin sources. Recent archaeological literature has used isotopic data from human tooth enamel in Harappan cemetery burials

to document an exceptional mobility of Harappan people, with mortuary populations composed almost exclusively of first-generation immigrants coming from resource-rich hinterlands (Kenoyer, Price and Burton, 2013; Valentine et al., 2015). Moreover, a series of archaeological findings points towards the presence of Harappan colonies or trade posts throughout the Persian Gulf. In Oman, archaeologists found a series of metal tools of clear Indus origin, several Indus trade tools used to normalize exchanges (e.g., the Indus-type stamp seals and cubical weights), and several Indus-type artifacts made in Oman by Indus or Indus-trained craftspeople using local raw materials. Also, Indus pottery is steadily being recognized at sites in Oman and the Persian Gulf, while there is some evidence of Indus products that were imitated in the Arabian coast (Edens, 1993, p. 354).

Mesopotamia was likely the final destination of the raw materials that were transiting through the Indus Valley. Although the tin sources in Mesopotamia are still not fully understood, several scholars have suggested that the Harappan civilization provided a major source. The supply of tin by this sea route is suggested, for instance, in a passage in one of the texts of Gudea, a priest-king reigning in Southern Mesopotamia, who describes the trove of objects reserved for the god and placed in the temple: *"Along with copper, tin, slabs of lapis lazuli, shining metal (and) spotless Meluhha cornelian"*. Another text describes the crossing of Meluhha: *"He crossed to the Kur Meluhha, Enki, the King of the Abzu, decrees its fate: [..] Your silver will be gold. Your copper will be bronze-tin."*

People of Meluhha are described as traders in the Sumerian texts, and there are frequent references to their ships. Harappan-style artifacts, including seals, beads, and shell objects, have been recovered from sites in Mesopotamia dating from 2550 BC (Chakrabarti, 1982; Gensheimer, 1984; Kenoyer, 2008). Conversely, there is no archaeological evidence of Mesopotamian goods in Indus cities. This has been interpreted as a sign that either imports from Mesopotamia were perishable goods, or that the Indus-Mesopotamia trade was mainly indirect, via Dilmun and Magan.

E.2 The city of Mari (2600-1760 BC)

Mari was an ancient Semitic city-state located in present-day Syria, strategically positioned on the Euphrates River, just downstream from its confluence with the Khabur River. Its prominence stemmed in large part from its geographic location at the intersection of major trade routes, enabling it to serve as a crucial entrepôt for interregional commerce (Kuhrt, 1995, p. 101, and Kristiansen and Larson, 2005, p. 93). Already by 2600 BC, Mari had emerged as a significant political and economic center.

The earliest expansion of Mari is described by Steinkeller (2021) as fundamentally commercial in nature, not territorial: *"Although I have repeatedly used the word "control" to describe Mari's dominance over the middle course of the Euphrates, it would be incorrect to think that this "control" involved territorial possession and the direct exploitation of natural resources, whatever they may have been. As far as our data permit to ascertain, Mari's sole objective in that regard was to maximise her profits from the Euphratean commerce. This she accomplished either directly, by establishing trading outposts at key traffic junctions or even by outright control of such places (and here the case of Tuttul comes to mind); or she did it indirectly, by forcing the various intermediaries to share their profits from duties on traded goods."*

While glimpses into Mari's early political and economic role emerge from inscriptions dated to ca. 2500–2350 BC (Charpin, 1987), as well as from the Royal Archives of Ebla, our most substantial knowledge of the city comes from a much later period, known as the Mari Age (ca. 1810–1760 BC).

The Mari archive, consisting of nearly 25,000 cuneiform tablets excavated from this phase, offers detailed insight into the city's administration, diplomacy, and commercial activity.

Central to Mari's political and economic organization was commerce, particularly trade in tin. A sequence of tablets deciphered by Dossin (1970) reveals that Mari functioned as a transshipment hub for tin moving from east to west. The metal originated from unspecified eastern sources—possibly via Babylon and Susa—and once it reached Mari, it was redistributed to centers in Syria and the Levant, including Ugarit, and from there further west to Crete (Morris, 1992, p. 102).[67]

The archive reveals the direct involvement of royal families across the region in the tin trade.[68] It also emphasizes the close connection between commerce and political diplomacy. The Mari texts show that royal journeys, while intended as occasions to visit other rulers, were regularly accompanied by trade caravans (Durand, 1983, p. 314). While the palace played a dominant role in long-distance commerce, it was not the sole actor. The texts document a thriving network of private merchants and brokers, some of whom operated independently, and others in parallel with the state apparatus.

Given Mari's control over key commercial routes, royal income derived from trading ventures was likely considerable. Moreover, although the precise mechanisms of taxation during the Mari Age remain only partially understood, as Kuhrt (1995) notes, *"state income was certainly derived from revenues levied on the transit trade, crossing-dues, tolls, boat taxes, and dues demanded in return for land grants."* These revenues were likely substantial, as reflected in the scale of state-sponsored construction, most notably the Royal Palace of Mari, one of the architectural marvels of the 18th century BC.

E.3 The Bronze Age Aegean

The Bronze Age Aegean in the eastern Mediterranean encompassed several powerful entities: the Minoans in Crete, the Mycenaeans in mainland Greece, and the Cypriots in Cyprus.

During the third millennium BC, the Minoans were already at the center of the Aegean trade network, with close contact with the Cyclades. This is testified by imports from these islands, trade in raw materials (e.g., obsidian, copper, lead, silver), the local production of material culture in Cycladic styles or technologies, and a relocation of Cycladic groups along the northern coast of Crete (Renfrew, 1964; Warren, 1984; Karantzali, 1996; Day, Wilson and Kiriatzi, 1998; Dimopoulou-Rethemniotaki, Wilson and Day, 2007). It is during the Middle Minoan period (1900-1800 BC), however, that the trade network of the Minoans starts expanding above the Cyclades: Minoan products and cultural influences start to be found in mainland Greece, Asia Minor, the entire Mediterranean coast of the Middle East, and even as far as Egypt. At the same time, the Minoans are becoming the most powerful European civilization. Several hallmarks testify to social development and economic growth. A state emerged together with writing, monumental burials, roads, and other public infrastructures. Towns such as Knossos, Malia, Gournia, and Palaikastro are often

[67] An interesting tablet, which dates back to the eighteenth century BC, is set up as a balanced account, listing the tin received and shipped in Mari. It describes the tin received from the kings of Babylon (Hammurabi) and Susa (Shephard), stocked in Mari, and then shipped to individuals residing in Ugarit and Caphtorite, a town presumably located in Crete.

[68] The political relevance of the tin trade and kings' involvement are illustrated in a letter from the King of Qatna to the King of Ekallate found in the Mari archive: "This matter is unspeakable, yet I must speak and relieve my feelings: you are a great king; you asked me for two horses, and I had them sent to you. And now you sent me (only) 20 minas (c. 10 kilos) of tin. Is it not the case that, without any quibbling and in full, you got (what you wanted) from me? And you dare to send me this paltry amount of tin! If you had sent nothing at all, by the god of my fathers, I could not have been so angry!"

described as the first urban settlements of Bronze Age Europe. These towns were centers of craft production (textile, pottery, and metalworking) and long-distance trade. They developed around royal "palaces", monumental buildings that, in some cases, had true Cyclopean size. These buildings were at the center of an economic system, which has often been referred to as "palace economy", in which a substantial share of wealth was flowing under the control of a centralized administration, centered in the palace. The palaces gathered up, manufactured, traded, and redistributed products and services needed in Crete. They were at the heart of an extensive network of intra-regional and interregional maritime trade of agricultural products in exchange for obsidian and metals (copper and tin). A long-standing fascinating hypothesis in the historical and archaeological literature is that the centrality of Crete in the metal trade network in the Mediterranean might go a long way in explaining the rise of the palaces and the Minoan civilization. The Minoan civilization has often been referred to as the first example in history of a thalassocracy[69], a polity that derives its power from its naval/commercial supremacy on the seas. Already in the fifth century BC, the Greek historian Thucydides wrote: *"Minos is the first to whom tradition ascribes the possession of a navy. He made himself master of a great part of what is now termed the Hellenic Sea; he conquered the Cyclades, and was the first colonizer of most of them, expelling the Carians and appointing his own sons to govern in them. Lastly, it was he who, from a natural desire to protect his growing revenues, sought, as far as he was able, to clear the sea of pirates."* More recently, Gordon Childe (1958) has emphasized the absolute centrality of the Minoans in the Mediterranean trade: *"In the Early Bronze Age peninsula Italy, central Europe, and the west Baltic coastlands, and the British Isles were united by a single system for the distribution of metalware, rooted in the Aegean market."*

Minoan vessels were the primary means of transportation of copper ingots in the Mediterranean (Muhly, 1985). In a shipwreck near present-day Israel, numerous tin ingots, with Minoan seals, have been found: trace-element analysis points towards Cornwall, present-day England, as the most likely provenance of the tin (Berger et al., 2019). This finding puts the Minoans at the center of a tin trade route connecting western and northern Europe with the Syrian civilizations.

The Mycenaean civilization emerged later, during the Middle and Late Bronze Age, roughly between 1750 and 1050 BC. As with the Minoans, the palace stood at the center of the Mycenaean economy. The production of manufactures, internal circulation, and long-distance exchange were to a significant extent organized under palatial authority. Tablets from the palace of Pylos suggest particularly tight palatial control of the metal industry. Bronze smiths were distributed throughout the kingdom, and the tablets indicate that they received raw materials and work assignments through palatial channels and were expected to return finished products. Chadwick (1994, p. 141) argues that the total number of smiths in the Pylian kingdom was nearly 400, implying a scale of production that may have exceeded purely local demand. This, together with the absence of local copper and especially tin deposits, suggests that Pylos was deeply involved in wider exchange networks. It has also been argued that long-distance trade became increasingly important as the quality of land suitable for cereal cultivation, already limited, declined under sustained intensive use (Ascherson, 2011).

From the mid-second millennium BC onward, Mycenaean material culture spread widely across the eastern and central Mediterranean, with especially strong evidence of contact in coastal Anatolia, Cyprus, southern Italy, and Sicily. The archaeological record suggests sustained commercial and

[69] Thalassokrateo means "to be master of the sea".

cultural interaction, supported in some cases by trading posts, migrant communities, and localized settlements. These connections likely facilitated exchange by creating relatively stable channels of contact, shared practices, and enduring relationships among elites and merchants across regions. Long-distance trade appears to have contributed to promote the rise of a political and administrative palatial elite that directly participated in trade voyages and would often engage in wars to crush their trade rivals. In the *Odyssey*, for example, Menelaus, the legendary Spartan *wanax*, describes the source of his wealth and power as the product of extensive maritime travel: *"But when it comes to men, I feel that few or none can rival me in wealth, for it took me seven years and great hardship to amass this fortune and bring it home in my ships. My travels took me to Cyprus, to Phoenicia, and to Egypt. Ethiopians, Sidonians, Erembians, I visited them all; and I saw Libya too ..."* (*Odyssey*, Book 4, 75–85)

Although there is little doubt that Mediterranean interregional trade was largely driven by the demand for the metals required for bronze production, it also facilitated the circulation of luxury and other less utilitarian goods that served as markers of status and power. This is especially evident in the Mycenaean world, where contacts with the eastern Mediterranean were particularly influential. The more advanced polities of Egypt, the Levant, Mesopotamia, and Anatolia supplied a wide range of valuable objects that not only circulated as prestige goods, but also provided important technological and artistic models for the development of Mycenaean craftsmanship and elite culture (Burns, 2010).

Another influential Aegean civilization rose in Cyprus. Starting from 1650 BC, the island experienced a rapid change from a somewhat isolated, village-oriented culture to an international, urban-centered, and highly complex society. It is generally agreed that the first urban developments and the gradual movement of population from rural hinterland to coastal towns were not merely an internal socioeconomic process, but rather the outcome of overseas demand for Cypriot copper (Knapp, 2013; Negbi, 2005). The development of metallurgy on Cyprus was driven by the local copper mines and the need to meet the increasing demand for copper in the Mediterranean basin. Eventually, the intensified production and trade of copper catapulted Cyprus into the role of the most important purveyor of this metal in the Mediterranean region, which lasted until the Roman Empire (the name Cyprus is directly related to the Latin word for copper, cuprum). A large number of documents of the second-millennium Egyptian, Syrian, Babylonian, Anatolian, and Mycenaean mention exchanges with Cyprus (Alashiya) and gifts of copper.

E.4 The Bronze Age in China and the Erlitou period (1900-1500 BC)

Bronze metallurgy in China originated in what is referred to as the Erlitou period, and it probably developed inside China separately from outside influence (Liu, 2005). The site of Erlitou is the largest among all its contemporary sites in China; several scholars have argued that it was the capital of the first state in China (Liu and Chen, 2003, 2012; Liu et al., 2004) [70].

Erlitou was nestled in an alluvial basin, positioned on the boundary between the Chinese lowlands and highlands, encircled by mountain ranges. Despite these natural barriers, the basin maintained effective connections to regions in all directions through an intricate network of rivers. Specifically,

[70] Some scholars believe Erlitou to be the capital of the mythical Xia Dynasty, China's first dynasty, although this is controversial (Wu et al., 2016).

Erlitou was situated at the point where two major rivers, the Yi and Luo, converged in a short canal, the Yiluo. The Yiluo, within a span of less than 30 kilometers, intersected with several smaller rivers, eventually discharging into the Yellow River. This interconnected river system, combined with its prime location, sandwiched between mountains and plains, made Erlitou an important road knot connecting the mineral-rich mountains with the fertile lowlands.

In the last four decades, more than 200 sites containing Erlitou material assemblages have been found over a very broad region from the middle Yellow River to the middle Yangzi River regions. The sites are distributed along several river systems, and the pattern of settlement distribution is indicative of the emergence of a highly integrated and centralized socio-political system (Liu, 2005, p. 226). The line expansion of this first state suggests a series of attempts to achieve political domination of metal-rich peripheries. One notable example is Panlongcheng, a site located at the intersection between the Han and the Yangzi River, and close to both copper and tin deposits. There is evidence that copper was melted at the mining sites, while the elite in Panlongcheng was likely playing a major role in forwarding copper ingots to the primary center at Erlitou (Liu and Chen, 2003). In the same site, there is also evidence of limited bronze-making dating from the Erlitou period. Another example of an outpost to control metal resources, set up by the Erlitou state, is the site of Donglongshan. Donglongshan is located on the north bank of the Dan River close to copper resources in Mt. Hongyan. Few pieces of metal slag were found at the site, suggesting that bronze metallurgy was carried out there (Yang, 2000).

The formation of the Erlitou state involved rapid territorial expansion by colonizing the surrounding regions, with the quest for bronze alloys as the main territorial driver. In the words of Li Liu (2005): *"The Erlitou state formed an inter-regional network focused on the production and distribution of prestige goods, especially bronze vessels. This network incorporated two interdependent sectors, core and periphery. The dominant core controlled the production of prestige items (bronze products, etc.), and the subordinate periphery provided raw material resources (e.g., metal ingots) [..] The Erlitou elite in the core achieved domination through military force by establishing outposts in the periphery to ensure the flow of material and information."*

References

Ankushev, Maksim N., A. M. Yuminov, Victor V. Zaykov, and V. V. Noskevich. 2018. "Copper Mines of the Bronze Age in the Southern Trans-urals." *Proceedings of Irkutsk State University. Series "Geoarcheology. Ethnology. Anthropology"* 23: 87–110.

Artioli, Gilberto, Caterina Canovaro, Paolo Nimis, and Ivana Angelini. 2020. "Lia of Prehistoric Metals in the Central Mediterranean Area: A Review." *Archaeometry* 62 (S1): 53–85.

Ascherson, Neal. 2011. *Black Sea: the Birthplace of Civilisation and Barbarism.* London: The Folio Society.

Avner, Uzi. 2014. "Egyptian Timna- Reconsidered." *Ancient Near Eastern Studies Supplement 45.*

Avner, Uzi, Hanan Ginat, Sariel Shalev, Sana Shilstine, Boaz Langford, Amos Frumkin, Rachamim Shem-Tov, Reuma Arav Sagi Filin and, Uri Basson, Omer Shamir, and Linda Scott-Cummings. 2018. "Ancient Copper Mines at Nahal 'amram, Southern Arabah." In *Mining for Ancient Copper: Essays in Memory of Beno Rothenberg*, The Institute of Archaeology of Tel Aviv University.

Bagnall, Roger. 2022. "Pleiades: A Gazetteer of Past Places." pleiades.stoa.org.

Bahn, Paul G. 2000. *The Atlas of World Archaeology.* New York: Checkmark Books.

Bakker, Jan David, Stephan Maurer, Jörn-Steffen Pischke, and Ferdinand Rauch. 2021. "Of Mice and Merchants: Trade and Growth in the Iron Age." *Review of Economics and Statistics* 103 (4): 652–665.

Bätscher, Fabrizio. 2020. "Rivers of Mesopotamia." *https://doi.org/10.5281/zenodo.3787264*, Accessed: 16 January 2025.

Beck, Curt W., Constance A. Fellows, and Audrey B. Adams. 1970. "Analysis and Provenience of Minoan and Mycenaean Amber, Iii. Kakovatos." *Greek, Roman, and Byzantine Studies* 11 (1): 5–22.

Beck, Curt W., Gretchen C. Southard, and Audrey B. Adams. 1972. "Analysis and Provenience of Minoan and Mycenaean Amber, Iv. Mycenae." *Greek, Roman, and Byzantine Studies* 13 (4): 359–385.

Begemann, Friedrich, Sigrid Schmitt-Strecker, Ernst Pernicka, and Fulvia Lo Schiavo. 2001. "Chemical Composition and Lead Isotopy of Copper and Bronze From Nuragic Sardinia." *European Journal of Archaeology* 4 (1): 43–85.

Bentzen, Jeanet Sinding, Nicolai Kaarsen, and Asger Moll Wingender. 2017. "Irrigation and Autocracy." *Journal of the European Economic Association* 15 (1): 1–53.

Benvenuti, Marco, Laura Charantini, L Norfini, A Casini, S Guideri, and Gisueppe Tanelli. 2003. "The "Etruscan Tin": A Preliminary Contribution From Researches at Monte Valerio and Baratti-populonia (southern Tuscany, Italy)." *BAR International Series* 1199: 55–66.

Berger, Daniel, et al. 2019. "Isotope Systematics and Chemical Composition of Tin Ingots From Mochlos (Crete) and Other Late Bronze Age Sites in the Eastern Mediterranean Sea: An Ultimate Key to Tin Provenance?" *PloS One* 14 (6): e0218326.

Bryce, Trevor. 2006. *The Kingdom of the Hittites.* Oxford: Oxford University Press.

Burgess, Colin, and Brendan O'Connor. 2008. "Iberia, the Atlantic Bronze Age and the Mediterranean." *Contacto Cultural entre el Mediterráneo y el Atlántico (siglos XII-VIII Ane). La*

Precolonización a Debate. Serie Arqueológica 11: 41–58.

Burns, Bryan E. 2010. *Mycenaean Greece, Mediterranean Commerce, and the Formation of Identity.* Cambridge: Cambridge University Press.

Cadet, Mélissa, Thongsa Sayavongkhamdy, Viengkeo Souksavatdy, Thonglith Luangkhoth, Philippe Dillmann, Christophe Cloquet, Justine Vernet, Paolo Piccardo, Nigel Chang, John Edgar, Eddy Foy, and T.O. Pryce. 2019. "Laos' Central Role in Southeast Asian Copper Exchange Networks: A Multi-method Study of Bronzes From the Vilabouly Complex." *Journal of Archaeological Science* 109: 104988.

Catapotis, Mihalis. 2007. "On the Spatial Organisation of Copper Smelting Activities in the Southern Aegean During the Early Bronze Age." In *Metallurgy in the Early Bronze Age Aegean*, edited by P.M. Day and R.C.P. Doonan. Oxford: Oxbow Books.

Chadwick, John. 1994. *The Mycenaean World, 8th Edition.* Cambridge: Cambridge University Press.

Chakrabarti, Dilip K. 1982. "Long-barrel Cylinder'beads and the Issue of Pre-sargonic Contact Between the Harappan Civilization and Mesopotamia." *Harappan Civilization: A Contemporary Perspective (ed. GL Possehl). New Delhi: Oxford & IBH Publishing* 265–70.

Charpin, Dominque. 1987. "Tablettes Presargoniques De Marie." *Mari: Annales de recherches interdisciplinaires* 5: 65–127.

Childe, Vere Gordon. 1958. *The Prehistory of European Society.* Pelican London.

Clark, William C. 1977. "Population Geography." *Progress in Human Geography* 1: 136–141.

Cleuziou, Serge. 1982. "Early Tin in the Near East." *Expedition Magazine* 25 (1).

Clift, Peter, Andrew Carter, Liviu Giosan, Julie Durcan, Geoff Duller, Mark Macklin, Anwar Alizai, Ali Tabrez, Mohammed Danish, Sam VanLaningham, and Dorian Fuller. 2012. "Pb Zircon Dating Evidence for a Pleistocene Sarasvati River and Capture of the Yamuna River." *Geology* 40: 212–215.

Cline, Eric H. 2013. *The Trojan War: A Very Short Introduction.* Oxford: Oxford University Press.

Conley, Timothy. 1999. "GMM Estimation with Cross Sectional Dependence." *Journal of Econometrics* 92 (1): 1–45.

Constantinou, George. 2012. "Late Bronze Age Copper Production on Cyprus From a Mining Geologist's Perspective." In *Eastern Mediterranean Metallurgy and Metalwork in the Second Millennium BC*, edited by V. Kassianidou and G. Papasavvas, 4–13. Oxford: Oxbow Books.

David M. Olson, Eric Dinerstein, Eric D. Wikramanayake Neil D. Burgess George V. N. Powell Emma C. Underwood Jennifer A. D'amico Illanga Itoua Holly E. Strand John C. Morrison Colby J. Loucks Thomas F. Allnutt Taylor H. Ricketts Yumiko Kura John F. Lamoreux Wesley W. Wettengel Prashant Hedao Kenneth R. Kassem. 2001. "Terrestrial Ecoregions of the World: A New Map of Life on Earth: A New Global Map of Terrestrial Ecoregions Provides an Innovative Tool for Conserving Biodiversity." *BioScience* 51 (11): 933–938.

Day, Peter M., David E. Wilson, and Evangelia Kiriatzi. 1998. "Pots, Labels, and People: Burying Ethnicity in the Cemetery at Aghia Photia, Siteias." In *Cemetery and Society in*

the Aegean Bronze Age, edited by Keith Branigan, 133–149. Sheffield: Continuum International Publishing Group.

Derikonjic, S., E. Pernicka, and T. Rehren. 2011. "The Vinca Culture Mining Complex in Jarmovac, Southwest Serbia." Vol. 4 of *Sonderheft*. Bochum.

Dijkstra, Edsger W. 1959. "A Note on Two Problems in Connexion with Graphs." *Numerische Mathematik* 1 (1): 269–271.

Dimopoulou-Rethemniotaki, Nota, David E. Wilson, and Peter M. Day. 2007. "The Earlier Prepalatial Settlement of Poros-Katsambas: Craft Production and Exchange at the Harbour Town of Knossos." In *Metallurgy in the Early Bronze Age Aegean*, Vol. 7 of *Sheffield Studies in Aegean Archaeology*, edited by Toby Wilkinson and Susan Sherratt, 84–97. Oxford: Oxbow Books.

D'Orazio, Mauro, Anna Gioncada, and Luca Bindi. 2018. "The ^{40}Ar–^{39}Ar dating and geochemistry of the Carpathian C1 obsidians (Zemplín, Slovakia)." *European Journal of Mineralogy* 30 (6): 947–959.

Dossin, Georges. 1970. "La Route De L'étain en Mésopotamie au temps de Zimri-Lim." *Revue d'Assyriologie* 64: 97–106.

Durand, Jean-Marie. 1983. "Archives Royales De Mari/21 Textes Administratifs Des Salles 134 Et 160 Du Palais De Mari/transcrits, Traduits Et Comm. Par Jean-marie Durand." *Archives royales de Mari*.

Earle, Timothy, Johan Ling, Claes Uhnér, Zofia Stos-Gale, and Lene Melheim. 2015. "The Political Economy and Metal Trade in Bronze Age Europe: Understanding Regional Variability in Terms of Comparative Advantages and Articulations." *European Journal of Archaeology* 18 (4): 633–657.

Edens, Christopher. 1993. "Indus-Arabian Interaction During the Bronze Age: A Review of Evidence." In *Harappan Civilization: A Recent Perspective*, Second revised edition, edited by Gregory L. Possehl, 335–363. New Delhi: Oxford: Oxford & IBH Publishers.

Esri. 2023. "World Continents." https://hub.arcgis.com/datasets/esri::world-continents/about, Accessed: 13 May 2024.

FAO and IIASA. 2021. "Global Agro-ecological Zones (gaez V4)." https://gaez.fao.org/, 15 May 2024.

Fink, Jonathan H. 1983. "Structure and Emplacement of a Rhyolitic Obsidian Flow: Little Glass Mountain, Medicine Lake Highland, Northern California." *GSA Bulletin* 94 (3): 362–380.

Flückiger, Matthias, Erik Hornung, Mario Larch, Markus Ludwig, and Allard Mees. 2022. "Roman Transport Network Connectivity and Economic Integration." *The Review of Economic Studies* 89 (2): 774–810.

Frahm, Ellery. 2025. "Archaeological Obsidian Sourcing: Looking From the First 60 Years to the Next." *Journal of Archaeological Science* 177: 106200.

Gale, Noel H. 2006. "Lead Isotope Studies-sardinia and the Mediterranean: Provenance Studies of Artefacts Found in Sardinia." *Instrumentum* 23: 29–34.

Gale, Noel H., and Zofia A. Stos-Gale. 1981. "Lead and Silver in the Ancient Aegean." *Scientific American* 244 (6): 176–193.

Gale, Noel H., and Zofia A. Stos-Gale. 2005. "Zur Herkunft Der Kupferbarren Aus Dem Schiffwrack Von Uluburun Und Der Spätbronzezeitliche Metallhandel im Mittelmeerraum." 117–132. Deutsches Bergbau-Museum.

Gale, Noel H., Zofia A. Stos-Gale, and Jack L. Davis. 1984. "The Provenance of Lead Used at Ayia Irini, Keos." *Hesperia: The Journal of the American School of Classical Studies at Athens* 53 (4): 389–406.

Gale, N., Zofia Anna Stos-Gale, Geoffrey Nowell, and R.E. Clay. 2002. "Archaeometallurgical Research in the Aegean." In *The Beginnings of Metallurgy in the Old World*, edited by Martin Bartelheim, Ernst Pernicka and Rüdiger Krause, 277–302. Rahden: Verlag Marie Leidorf GmbH.

Galor, Oded, and Ömer Özak. 2015. "Land Productivity and Economic Development: Caloric Suitability Vs. Agricultural Suitability,." Brown University Working Paper.

Galor, Oded, and Ömer Özak. 2016. "The Agricultural Origins of Time Preference." *American Economic Review* 106 (10): 3064–3103.

Garner, Jennifer. 2014. *Das Zinn Der Bronzezeit in Mittelasien II. Die Montanarchäologischen Forschungen an den Zinnlagerstätten.* Philipp von Zabern.

Garner, Jennifer. 2015. "Bronze Age Tin Mines in Central Asia." *Archaeometallurgy in Europe III. Bochum* 135–143.

Gensheimer, Thomas R. 1984. "The Role of Shell in Mesopotamia: Evidence for Trade Exchange with Oman and the Indus Valley." *Paléorient* 10 (1): 65–73.

GeologyBase.com. 2025. "Understanding Trachyte, a Fine-grained Volcanic Rock." Accessed: 17 June 2025.

Giardino, Claudio. 2019. *Magan - the Land of Copper: Prehistoric Metallurgy of Oman.* Oxford: Archaeopress.

Giumlia-Mair, Alessandra. 2005. "Handel und Rohstoffgewinnung im Italien der späten Bronzezeit." 415–430. Deutsches Bergbau-Museum.

Glatz, Claudia. 2020. "The Pontic Shatter Zone." *The Making of Empire in Bronze Age Anatolia: Hittite Sovereign Practice, Resistance, and Negotiation*, 125–151. Cambridge University Press.

Global Volcanism Program. 2025. "Volcanoes of the World (v. 5.2.7; 21 Feb 2025)." Distributed by Smithsonian Institution, compiled by Venzke, E.

Green, Adam S., and Cameron A. Petrie. 2018. "Landscapes of Urbanization and Deurbanization: A Large-scale Approach to Investigating the Indus Civilization's Settlement Distributions in Northwest India." *Journal of Field Archaeology* 43 (4): 284–299.

Green, Adam S., Toby C. Wilkinson, Darryl Wilkinson, Nancy Highcock, and Thomas Leppard. 2024. *Cities and Citadels: An Archaeology of Inequality and Economic Growth.* 1st Edition edition. London: Routledge.

Grigg, David B., ed. 1987. *The Industrial Revolution and Land Transformation.* New York: John Wiley.

Hahnekamp, Christine. 2011. "Vergleichende Untersuchung zum Fundkontext bronze- und urnenfelderzeitlicher Schwerter in Ostfrankreich und Süddeutschland." Diplomarbeit, Universität Wien.

Hauptmann, Andreas. 1997. "Feinan." In *The Oxford Encyclopedia of Archaeology in the Near East*, edited by Eric M. Meyers, 310–311. Oxford: Oxford University Press.

Hauptmann, Andreas. 2007. *The Archaeometallurgy of Copper: Evidence From Faynan, Jordan. Natural Science in Archaeology.* Berlin and Heidelberg: Springer.

Hauptmann, Andreas, Friedrich Begemann, and Sigrid Schmitt-Strecker. 1999. "Copper Objects From Arad: Their Composition and Provenance." *Bulletin of the American Schools of Oriental Research* 314 (1): 1–17.

Henderson, J. Vernon, Tim Squires, Adam Storeygard, and David Weil. 2018. "The Global Distribution of Economic Activity: Nature, History, and the Role of Trade1." *The Quarterly Journal of Economics* 133 (1): 357–406.

Higham, Thomas F. G., Andrew D. Weiss, Charles F. W. Higham, Christopher Bronk Ramsey, Jade d'Alpoim Guedes, Sydney Hanson, Steven A. Weber, Fiorella Rispoli, Roberto Ciarla, Thomas O. Pryce, and Vincent C. Pigott. 2020. "A Prehistoric Copper-production Centre in Central Thailand: Its Dating and Wider Implications." *Antiquity* 94 (376): 948–965.

Hosner, Dominic, Mayke Wagner, Pavel E Tarasov, Xiaocheng Chen, and Christian Leipe. 2016. "Spatiotemporal distribution patterns of archaeological sites in China during the Neolithic and Bronze Age: An overview." *The Holocene* 26 (10): 1576–1593.

Hughes, Simon J. S. 1981. "The Cwmystwyth Mines." *British Mining Monograph* 17.

Huska, Angela, Wayne Powell, Slobodan Mitrović, H. Arthur Bankoff, Aleksandar Bulatović, Vojislav Filipović, and Ruth Boger. 2014. "Placer Tin Ores From Mt. Cer, West Serbia, and Their Potential Exploitation During the Bronze Age." *Geoarchaeology* 29 (6): 477–493.

Jaang, Li. 2015. "The Landscape of China's Participation in the Bronze Age Eurasian Network." *Journal of World Prehistory* 28 (3): 179–213.

Jansen, Michael. 2002. "Settlement Networks of the Indus Civilization." *Indian Archaeology in Retrospect* 2: 105–128.

Kaptan, Ergun. 1990. "Findings Related to the History of Mining in Turkey." *Bulletin of the Mineral Research and Exploration* 111.

Karantzali, Efi. 1996. *Le Bronze Ancien Dans Les Cyclades Et En Crète: Les Relations Entre les Deux Regions—Influence de la Grèce Continentale. BAR-IS.* Oxford: Archaeopress.

Karger, Dirk Niklaus, Michael P. Nobis, Signe Normand, Catherine H. Graham, and Niklaus E. Zimmermann. 2021. "CHELSA-TraCE21k v1.0. Downscaled transient temperature and precipitation data since the last glacial maximum." *Climate of the Past Discussions* 2021: 1–27.

Kenoyer, J. Mark, T. Douglas Price, and James H. Burton. 2013. "A New Approach to Tracking Connections Between the Indus Valley and Mesopotamia: Initial Results of Strontium Isotope Analyses From Harappa and Ur." *Journal of Archaeological Science* 40 (5): 2286–2297.

Kenoyer, Jonathan Mark. 2008. "Indus and Mesopotamian Trade Networks: New Insights From Shell and Carnelian Artifacts." *Intercultural Relations between South and Southwest Asia: Studies in Commemoration of ECL During Caspers (1934–1996), E. Olijdam, RH Spoor, Eds.(Archaeopress, 2008)* 19–28.

Kiszewski, Andrew, Andrew Mellinger, A. Spielman, Pia Malaney, Sonia E. Sachs, and Jeffrey Sachs. 2004. "A Global Index Representing the Stability of Malaria Transmission." *American Journal of Tropical Medicine and Hygiene* 70 (5): 486–498.

Klassen, Lutz, Serge Cassen, and Pierre Pétrequin. 2012. "Alpine Axes and Early Metallurgy." 1280–1309. Centre de Recherche Archéologique de la Vallée de l'Ain.

Klein Goldewijk, Kees, Arthur Beusen, Gerard van Drecht, and Martine de Vos. 2011. "The HYDE 3.1 Spatially Explicit Database of Human-induced Global Land-use Change Over the Past 12,000 Years." *Global Ecology and Biogeography* 20 (1): 73–86.

Knapp, Arthur Bernard. 2013. *The Archaeology of Cyprus: From Earliest Prehistory Through the Bronze Age. Cambridge World Archaeology.* Cambridge University Press.

Kremer, Michael. 1993. "Population Growth and Technological Change: One Million B.C. to 1990." *The Quarterly Journal of Economics* 108 (3): 681–716.

Kristiansen, Kristian, and Christian Horn. 2018. "Warfare and the Political Economy: Europe 1500–1100 BC." In *Warfare in Bronze Age Society*, edited by Kristian Kristiansen and Rune Iversen, 23–46. Cambridge: Cambridge University Press.

Kristiansen, Kristian, and Paulina Suchowska-Ducke. 2015. "Connected Histories: The Dynamics of Bronze Age Interaction and Trade 1500–1100 BC." *Proceedings of the Prehistoric Society* 81: 361–392.

Kristiansen, Kristian, and Thomas Larson. 2005. *The Rise of Bronze Age Society: Travels, Transmissions and Transformations.* Cambridge: Cambridge University Press.

Kuhrt, Amelie. 1995. *The Ancient Near East, C. 3000-330 BC.* Vol. 2. Taylor & Francis US.

Kutterer, Johannes, Christina Neureiter, and Sabah Jasim. 2013. "Second Report on the Copper Smelting Site Hlo1 in Wādī al-Ḥilo (Sharjah, UAE)." *Proceedings of the Seminar for Arabian Studies* 43: 185–196.

Larreina-García, David. 2017. "Copper and Bloomery Iron Smelting in Central China: Technological Traditions in the Daye County (hubei)." PhD diss. University College London Institute of Archaeology.

Lawrence, Dan, Israel Hinojosa-Balino, and Francesca Chelazzi. 2025. "Persistence As Sustainability? Exploring Urban Longevity in Southwest Asia and Egypt." *Journal of Urban Archaeology* 11: 85–97.

Lehner, Joseph, and Kutlu Aslihan Yener. 2013. "Organization and Specialization of Early Mining and Metal Technologies in Anatolia." *Archaeometallurgy in Global Perspective: Methods and Syntheses* 529–557.

Lewis, Christopher Andrew. 1997. "Prehistoric Mining at the Great Orme-criteria for the Identification of Early Mining." PhD diss. MPhil. thesis, University of Wales, Bangor.

Lieth, Helmut. 1975. "Modeling the Primary Productivity of the World." *Primary Productivity of the Biosphere*, edited by Helmut Lieth and Robert H. Whittaker, 237–263. Berlin and Heidelberg: Springer.

Ling, Johan, Eva Hjärthner-Holdar, Lena Grandin, Zofia A. Stos-Gale, Kristian Kristiansen, Anne L. Melheim, Gilberto Artioli, Ivana Angelini, Rüdiger Krause, and Caterina Canovaro. 2019. "Moving Metals IV: Swords, Metal Sources and Trade Networks in

Bronze Age Europe." *Journal of Archaeological Science: Reports* 26: 1–34.

Ling, Johan, Zofia A. Stos-Gale, Lena Grandin, Kjell Billström, Eva Hjärthner-Holdar, and Per-Olof Persson. 2014. "Moving Metals II: Provenancing Scandinavian Bronze Age Artefacts by Lead Isotope and Elemental Analyses." *Journal of Archaeological Science* 41: 106–132.

Liu, Li. 2005. *The Chinese Neolithic: Trajectories to Early States.* Cambridge: Cambridge University Press.

Liu, Li, and Xingcan Chen. 2003. *State Formation in Early China.* London: Duckworth.

Liu, Li, and Xingcan Chen. 2012. *The Archaeology of China: From the Late Paleolithic to the Early Bronze Age.* Cambridge: Cambridge University Press.

Liu, Li, Xingcan Chen, Yun Kuen Lee, Henry Wright, and Arlene Rosen. 2004. "Settlement Patterns and Development of Social Complexity in the Yiluo Region, North China." *Journal of Field Archaeology* 29 (1-2): 75–100.

Liu, Ruiliang, A. Mark Pollard, Jessica Rawson, Xiaojia Tang, Peter Bray, and Changping Zhang. 2019. "Panlongcheng, Zhengzhou and the Movement of Metal in Early Bronze Age China." *Journal of World Prehistory* 32 (4): 393–428.

Liu, Ruiliang, Peter Bray, A. Mark Pollard, and Peter Hommel. 2015. "Chemical Analysis of Ancient Chinese Copper-based Objects: Past, Present and Future." *Archaeological Research in Asia* 3: 1–8.

Liu, Shuai, Kuang-Lin Chen, Thilo Rehren, Jianjun J. Mei, Junling L. Chen, Yue Liu, and David Killick. 2018. "Did China Import Metals From Africa in the Bronze Age?" *Archaeometry* 60 (1): 105–117.

Livi-Bacci, Massimo. 2007. *A Concise History of World Population.* 4th edition. Oxford, UK: Blackwell Publishing.

Lo Schiavo, Fulvia. 2005. "Metallhandel im zentralen Mittelmeer." 399–414. Deutsches Bergbau-Museum.

Mason, Andrea H. 2020. "Provenance of Tin in the Late Bronze Age Balkans: Preparation of Cassiterite for Sn Isotope Analysis and the Probabilistic and Spatial Analysis of Sn Isotopes." PhD diss. City University of New York.

Massoudi, Omara Khan. 2011. *Mes Aynak - Recent Discoveries Along the Silk Road.* Kabul: National Museum of Afghanistan.

Matthäus, Hartmut. 2005. "Kulturaustausch, Handel und Seefahrt im Mittelmeerraum während der späten Bronzezeit." 333–366. Deutsches Bergbau-Museum.

Mayshar, Joram, Omer Moav, and Luigi Pascali. 2022. "The Origin of the State: Land Productivity Or Appropriability?" *Journal of Political Economy* 130 (4): 1091–1144.

McEvedy, Colin, and Richard Jones. 1978. *World Atlas of Population History.* 1st edition. Hammondsworth, UK: Penguin Books Ltd.

McIntosh, Jane R. 2007. *The Ancient Indus Valley: New Perspectives.* Bloomsbury Publishing USA.

Melheim, Anne L., Lena Grandin, Per-Olof Persson, Kjell Billström, Zofia A. Stos-Gale, Johan Ling, Alan Williams, Ivana Angelini, Caterina Canovaro, Eva Hjärthner-Holdar, and Kristian Kristiansen. 2018. "Moving Metals Iii: Possible Origins for Copper

in Bronze Age Denmark Based on Lead Isotopes and Geochemistry." *Journal of Archaeological Science* 96: 85–105.

Montero Ruiz, Ignacio, Isabel Martínez Navarrete, and Eduardo Galán. 2016. "Objetos O Materia Prima: Problemas En La Interpretación de Procedencias con Análisis de Isotopos de Plomo." *Boletín del Museo Arqueológico Nacional* 34: 81–98.

Montero Ruiz, Ignacio, María R. Manunza, Fulvia Lo Schiavo, Paolo Valera, José I. Ibarguchi, Nuria Rafel Fontanals, and Pau Sureda. 2018. "The Funtana Coberta-ballao Hoard: New Copper Provenances in Nuragic Metallurgy." Vol. 56 of *Monographies Instrumentum*, 137–164. Éditions Mergoil.

Morris, Sarah. 1992. *Daidalos and the Origins of Greek Civilization.* Princeton: Princeton University Press.

Muhly, James D. 1985. "Sources of Tin and the Beginnings of Bronze Metallurgy." *American Journal of Archaeology* 89 (2): 275–291.

Murillo-Barroso, Mercedes, and Marcos Martinón-Torres. 2012. "Amber Sources and Trade in the Prehistory of the Iberian Peninsula." *European Journal of Archaeology* 15 (2): 187–216.

Murillo-Barroso, Mercedes, Enrique Peñalver, Primitiva Bueno, Rosa Barroso, Rodrigo de Balbín, and Marcos Martinon-Torres. 2018. "Amber in Prehistoric Iberia: New Data and a Review." *PLOS One* 13 (8): 1–36.

Needham, Stuart, and Claudio Giardino. 2008. "From Sicily to Salcombe: A Mediterranean Bronze Age Object from British Coastal Waters." *Antiquity* 82 (315): 60–72.

Negbi, Ora. 2005. "Urbanism on Late Bronze Age Cyprus: LC II in Retrospect." *Bulletin of the American Schools of Oriental Research* 337: 1–45.

Newman, Mark E. J. 2018. *Networks: An Introduction.* 2 edition. Oxford: Oxford University Press.

Nezafati, Nima, and Thomas Stöllner. 2018. "Economic Geology, Mining Archaeological and Archaeometric Investigations at the Veshnaveh Ancient Copper Mine, Central Iran." *Metalla* 23: 67–90.

NGA. 2019. *World Port Index.* 27th edition. Springfield, Virginia: National Geospatial-Intelligence Agency.

Northover, John P. N., William O'Brien, and Sabine Stos. 2001. "Lead Isotopes and Metal Circulation in Beaker/early Bronze Age Ireland." *The Journal of Irish Archaeology* 10: 25–47.

O'Brien, William. 1999. "Arsenical Copper in Early Irish Metallurgy." In *Metals in Antiquity*, edited by Suzanne M. M. Young, A. Mark Pollard, Paul Budd and Robert A. Ixer, Chapter 4, 33–42. Cambridge, United Kingdom: Proceedings of the 1995 Harvard Conference British Archaeological Reports, Archaeopress.

O'Brien, William. 2015. *Prehistoric Copper Mining in Europe: 5500-500 BC.* Oxford: Oxford University Press.

Ortiz, Mark A. Hunt, Bartomeu Llull Estarellas, Laura Perelló Mateo, and Bartomeu Salvà Simonet. 2014. "Bronze Age Copper Resources Procurement in Menorca: Sa Mitja Lluna Mine (illa Den Colom)." Vol. 24 of *Cuadernos de prehistoria y arqueología de la Universidad de Granada*, 85–109, Universidad de Granada.

Özbal, Hadi, Annemie Mieke Adriaens, and Bryan Earl. 1999. "Hacinebi Metal Production and Exchange." *Paléorient* 25 (1): 57–65.

Pernicka, Ernst, Bianka Nessel, Mathias Mehofer, and Elvira Safta. 2016. "Lead Isotope Analyses of Metal Objects From the Apa Hoard and Other Early and Middle Bronze Age Items From Romania." *Archaeologia Austriaca* 100: 57–86.

Pernicka, Ernst, Joachim Lutz, and Thomas Stöllner. 2016. "Bronze Age Copper Produced at Mitterberg, Austria, and Its Distribution." *Archaeologia Austriaca* 100: 19–55.

Pétrequin, Pierre, Serge Cassen, Michel Errera, Lutz Klassen, Alison Sheridan, and Anne Marie Pétrequin. 2012. *Jade: Grandes Haches Alpines Du Néolithique européen, Ve et IVe millénaires av. J.-C.* Centre de Recherche Archéologique de la Vallée de l'Ain.

Pinarelli, Laura. 2004. "Lead Isotope Characterization of Copper Ingots From Sardinia (Italy): Inferences on Their Origins." *Bulletin of the Geological Society of Greece* 36 (3): 1173–1180.

Pollard, A. Mark, Philip Bray, P. Hommel, Yi-Kuan Hsu, Ruiliang Liu, and Jessica Rawson. 2017. "Bronze Age Metal Circulation in China." *Antiquity* 91 (357): 674–687.

Possehl, Gregory L. 1990. "Revolution in the Urban Revolution: The Emergence of Indus Urbanization." *Annual Review of Anthropology* 19 (1): 261–282.

Pryce, Thomas O., Andrew H. Bevan, Roberto Ciarla, Fiorella Rispoli, Cristina Castillo, Brenna Hassett, and Jennifer L. Malakie. 2011*a*. "Intensive Archaeological Survey in Southeast Asia: Methodological and Metallurgical Insights From Khao Sai On, Central Thailand." *Asian Perspectives* 50 (1/2): 53–69.

Pryce, Thomas O., Marcos Pollard, M. Martinon-Torres, Vincent C. Pigott, and Ernst Pernicka. 2011*b*. "Southeast Asia's First Isotopically Defined Prehistoric Copper Proudction System: When Did Extractive Metallurgy Begin in the Khao Wong Prachan Valley of Central Thailand?" *Archaeometry* 53 (1): 146–163.

Quarta, Gianluca, Felice Larocca, Marisa D'Elia, Valentina Gaballo, Maria Macchia, Giuseppe Palestra, and Lucio Calcagnile. 2013. "Radiocarbon Dating the Exploitation Phases of the Grotta Della Monaca Cave in Calabria, Southern Italy: A Prehistoric Mine for the Extraction of Iron and Copper." *Radiocarbon* 55 (3): 1246–1251.

Radivojević, Miljana, Benjamin W. Roberts, Ernst Pernicka, Zofia Stos-Gale, Marcos Martinón-Torres, Thilo Rehren, Peter Bray, Dirk Brandherm, Johan Ling, Jianjun Mei, et al. 2019. "The Provenance, Use, and Circulation of Metals in the European Bronze Age: The State of Debate." *Journal of Archaeological Research* 27 (2): 131–185.

Radivojević, Miljana, Thilo Rehren, Ernst Pernicka, Dušan Šljivar, Michael Brauns, and Dušan Borić. 2010. "On the Origins of Extractive Metallurgy: New Evidence From Europe." *Journal of Archaeological Science* 37 (11): 2775–2787.

Rafel, Núria, Mark A. Hunt Ortiz, Ignacio Montero, Ignacio Soriano, Selina Delgado-Raack, and Dioscórides Marín. 2019. "New Bronze Age Absolute Datings for Solana Del Bepo Copper Mine (ulldemolins, Tarragona Province, Spain)." *Mediterranean Archaeology and Archaeometry* 19 (1): 9–24.

Ramankutty, Navin, Jonathan A. Foley, John Norman, and Kevin McSweeney. 2002. "The Global Distribution of Cultivable Lands: Current Patterns and Sensitivity to Possible Climate Change." *Global Ecology and Biogeography* 11 (5): 377–392.

Ratnagar, Shereen. 1981. *Encounters, the Westerly Trade of the Harappa Civilization.* Oxford: Oxford University Press.

Reba, Meredith, Femke Reitsma, and Karen C. Seto. 2016. "Spatializing 6,000 Years of Global Urbanization From 3700 BC to AD 2000." *Scientific Data* 3 (1): 160034.

Reguera-Galan, Aida, Tania Barreiro-Grille, Mariella Moldovan, Lara Lobo, Miguel A. de Blas Cortina, and José I. García Alonso. 2019. "A Provenance Study of Early Bronze Age Artefacts Found in Asturias (Spain) by Means of Metal Impurities and Lead, Copper and Antimony Isotopic Compositions." *Archaeometry* 61 (3): 683–700.

Reinhardt, Katrinka. 1997. "Mining and Smelting Technology and the Politics of Bronze in Shang and Western Zhou China : An Inquiry Into the Bronze Age Interaction Sphere." PhD diss. Department of East Asian Studies McGill University.

Reiter, Samantha, Karin Frei, Heide Nørgaard, and Flemming Kaul. 2019. "The ølby Woman." *Danish Journal of Archaeology* 8: 1–22.

Renfrew, Colin. 1964. "Crete and the Cyclades Before Rhadamanthus." *Kritika Chronika* 18: 107–141.

Renfrew, Colin. 1975. "Trade As Action at a Distance: Questions of Integration and Communication." In *Ancient Civilization and Trade*, edited by Jeremy A. Sabloff and C. C. Lamberg-Karlovsky, 3–59. University of New Mexico Press.

Renfrew, Colin, and Paul Bahn. 1996. *Archaeology: Theories, Methods, and Practice.* Thames & Hudson.

Renfrew, Colin, and Paul Bahn. 2016. *Archaeology: Theories, Methods and Practice, 11ed.* London: Thames & Hudson.

Rose, Charles Brian. 1998. "Troy and the Historical Imagination." *The Classical World* 91 (5): 405–413.

Sabatini, Serena, and Fulvia Lo Schiavo. 2020. "Late Bronze Age Metal Exploitation and Trade: Sardinia and Cyprus." *Materials and Manufacturing Processes* 35 (13): 1501–1518.

Schauer, Peter. 1971. *Die Schwerter in Süddeutschland, Österreich und der Schweiz I: Griffplatten-, Griffangel- und Griffzungenschwerter.* Vol. 2 of *Prähistorische Bronzefunde IV*. München: Beck.

Schauer, Peter, Andrew Bevan, Stephen Shennan, Kevan Edinborough, Tim Kerig, and Mike Parker Pearson. 2020. "British Neolithic Axehead Distributions and Their Implications." *Journal of Archaeological Method and Theory* 27: 836–859.

Schibler, Jörg, Elisabeth Breitenlechner, Sabine Deschler-Erb, Gert Goldenberg, Klaus Hanke, Gerald Hiebel, Heidemarie Plogmann, Kurt Nicolussi, Elisabeth Marti-Grädel, Sandra Pichler, Alexandra Schmidl, Anton Schwarz, Barbara Stopp, and Klaus Oeggl. 2011. "Miners and Mining in the Late Bronze Age: A Multidisciplinary Study From Austria." *Antiquity* 85: 1259–1278.

Schönholzer, David, and Pieter François. 2023. "The Origin of the Incentive Compatible State: Environmental Circumscription." Unpublished manuscript.

Sheppard, Peter J. 2008. "Obsidian Hydration Dating." In *Encyclopedia of Archaeology*, edited by Deborah M. Pearsall, 1695–1698. London: Academic Press.

Shorrocks, Anthony F. 2013. "Decomposition Procedures for Distributional Analysis: A Unified Framework Based on the Shapley Value." *The Journal of Economic Inequality* 11 (1): 99–126.

Singh, Ravindra N., and Dheerendra P. Singh. 2016. "A Note on Metallurgy at Khanan: An Indus Site in Tosham Mining Area, Haryana." *International Journal of Environmental. Chemical, Ecological, Geological, and Geophysical Engineering* 10: 847–856.

Steinkeller, Piotr. 2021. "International Trade in Greater Mesopotamia During Late Pre-sargonic Times." 173–197.

Stöllner, Thomas, Zeinolla Samaschev, Sergej Berdenov, Jan Cierny, Monika Doll, Jennifer Garner, Anton Gontscharov, Alexander Gorelik, Andreas Hauptmann, H Rainer, et al. 2011. "Tin From Kazakhstan: Steppe Tin for the West." *Anatolian Metal V Der Anschnitt Beiheft* 24: 231–251.

Stos-Gale, Zofia A. 2011. ""Biscuits with Ears": A Search for the Origin of the Earliest Oxhide Ingots." Vol. 9 of *Prehistory Monographs*, 221–229. INSTAP Academic Press.

Stos-Gale, Zofia A., and Noël H. Gale. 2009. "Metal Provenancing Using Isotopes and the Oxford Archaeological Lead Isotope Database (OXALID)." *Archaeological and Anthropological Sciences* 1 (3): 195–213.

Stos-Gale, Zofia A., and Noel H. Gale. 2010. "Bronze Age Metal Artefacts Found on Cyprus-metal From Anatolia and the Western Mediterranean." *Trabajos de Prehistoria* 67 (2): 389–403.

Thomlinson, Ralph. 1975. *Demographic Problems: Controversy Over Population Control.* Peacock Publishers.

Timberlake, Simon, and Peter Marshall. 2018. "Copper Mining and Smelting in the British Bronze Age: New Evidence of Mine Sites Including Some Reanlysis of Dates and Ore Sources." In *Mining for Ancient Copper: Essays in Memory of Beno Rothenberg*, edited by Erez Ben-Yosef, Chapter 29, 418–434. Tel Aviv: Eisenbrauns: Winona Lake, Indiana and Emery and Claire Yass Publications in Archaeology.

Tolksdorf, Johann Friedrich, Frank Schröder, Libor Petr, Christoph Herbig, Knut Kaiser, Petr Kočár, Alexander Fülling, Susann Heinrich, Heide Hönig, and Christiane Hemker. 2020. "Evidence for Bronze Age and Medieval Tin Placer Mining in the Erzgebirge Mountains, Saxony (Germany)." *Geoarchaeology* 35 (2): 198–216.

Tykot, Robert H. 2002. "Obsidian Studies in the Mediterranean and the Near East: A Review." *Journal of Archaeological Research* 10 (1): 1–44.

UNEP-WCMC. 2002. "Mountains and Tree Cover in Mountain Regions." Accessed: 2024-04-22.

U.S. Geological Survey. 2005. "Mineral Resources Data System." *https://mrdata.usgs.gov/mrds/.*

Valamoti, Soultana-Maria, and Glynis Jones. 2010. "Bronze and Oil: A Possible Link Between the Introduction of Tin and Lallemantia to Northern Greece." *The Annual of the British School at Athens* 105: 83–96.

Valentine, Benjamin, George D. Kamenov, Jonathan Kenoyer, Vasant Shinde, Veena Mushrif-Tripathy, Erik Otarola-Castillo, and John Krigbaum. 2015. "Evidence for Patterns of Selective Urban Migration in the Greater Indus Valley (2600-1900 BC): A Lead and Strontium Isotope Mortuary Analysis." *PLoS One* 10 (4): e0123103.

Valera, Rafael, and Paolo Valera. 2003. "Tin in the Mediterranean: History and Geology." *The*

Problem of Early Tin 3–14.

Wagner, Mayke, Pavel Tarasov, Dominic Hosner, Andreas Fleck, Richard Ehrich, Xiaocheng Chen, and Christian Leipe. 2013. "Mapping of the spatial and temporal distribution of archaeological sites of northern China during the Neolithic and Bronze Age." *Quaternary International* 290: 344–357.

Wang, Lu, Fan Chen, Yongqiang Wang, Wei Qian, Jianjun Mei, Marcos Martinón-Torres, and Kunlong Chen. 2019. "Copper Metallurgy in Prehistoric Upper Ili Valley, Xinjiang, China." *Archaeological and Anthropological Sciences* 11 (6): 2407–2417.

Wang, Shasha, Yuxian Du, and Yong Deng. 2017. "A New Measure of Identifying Influential Nodes: Efficiency Centrality." *Communications in Nonlinear Science and Numerical Simulation* 47: 151–163.

Wang, Yunchuan, Shasha Wang, and Yong Deng. 2019. "A Modified Efficiency Centrality to Identify Influential Nodes in Weighted Networks." *Pramana Journal of Physics* 92 (4).

Warren, Peter. 1984. "Early Minoan—Early Cycladic Chronological Correlations." In *Prehistoric Cyclades*, 55–62.

Williams, Ross A., and Cécile Le Carlier de Veslud. 2019. "Boom and Bust in Bronze Age Britain: Major Copper Production From the Great Orme Mine and European Trade, C. 1600-1400 BC." *Antiquity* 93 (371): 1178–1196.

Wilson, Margaret F. J., Brian O'Connell, Colin Brown, Janine C. Guinan, and Anthony J. Grehan. 2007. "Multiscale Terrain Analysis of Multibeam Bathymetry Data for Habitat Mapping on the Continental Slope." *Marine Geodesy* 30 (1-2): 3–35.

World Food Programme (UN Agency). 2022. "World Administrative Boundaries - Countries and Territories." *Opendatasoft*, Last modified: October 3, 2022.

Wright, Rita P. 2010. *The Ancient Indus: Urbanism, Economy, and Society.* Cambridge University Press Cambridge.

Wu, Qinglong, Zhijun Zhao, Li Liu, Darryl E. Granger, Hui Wang, David J. Cohen, Xiaohong Wu, Maolin Ye, Ofer Bar-Yosef, Bin Lu, et al. 2016. "Outburst Flood at 1920 BCE Supports Historicity of China's Great Flood and the Xia Dynasty." *Science* 353 (6299): 579–582.

Yalcın, Ünsal, and Alexander Maass. 2013. "Prähistorische Kupfergewinnung in Derekutugun." *Der Anschnitt* Beiheft 25: 153–194.

Yang, Yachang. 2000. "Shaanxi Xia Shiqi Kaogu De Xin Jinzhan (New Progress of the Xia Archaeology in Shaanxi)." *Gudai Wenming Yanjiu Tongxun* 5: 34–6.

Yener, Kutlu Aslihan, Fikri Kulakoğlu, Evren Yazgan, Ryoichi Kontani, Yuichi S. Hayakawa, Joseph W. Lehner, Gonca Dardeniz, Güzel Öztürk, Michael Johnson, Ergun Kaptan, and Abdullah Hacar. 2015. "New Tin Mines and Production Sites Near Kültepe in Turkey: A Third-Millennium BC Highland Production Model." *Antiquity* 89 (345): 596–612.

Yener, Kutlu Aslihan, Hadi Özbal, Ergun Kaptan, A. Necip Pehlivan, and Martha Goodway. 1989. "Kestel an Early Bronze Age Source of Tin Ore in the Taurus Mountains Turkey." *Science* 244 (4901): 200–203.

Zaks, David P. M., Navin Ramankutty, Carol C. Barford, and Jonathan A. Foley. 2007.

"From Miami to Madison: Investigating the Relationship Between Climate and Terrestrial Net Primary Production." *Global Biogeochemical Cycles* 21 (3).